INVESTIGATING THE SUITABILITY OF ELECTRIFIED POWERTRAIN ALTERNATIVES FOR REFUSE TRUCKS WITH EMPHASIS IN THE CITY OF HAMILTON

INVESTIGATING THE SUITABILITY OF ELECTRIFIED POWERTRAIN ALTERNATIVES FOR REFUSE TRUCKS WITH EMPHASIS IN THE CITY OF HAMILTON

BY

JACK TOLLER, B.Eng.

A THESIS
SUBMITTED TO THE DERPARTMENT OF MECHANICAL ENGINEERING
AND THE SCHOOL OF GRADUATE STUDIES
OF MCMASTER UNIVERSITY
IN PARTIAL FULFIMENT OF THE REQUIREMENTS
FOR THE DEGREE OF
MASTER OF APPLIED SCIENCE

Master of Applied Science
(Mechanical Engineering)

McMaster University
Hamilton, Ontario, Canada

TITLE: Investigating The Suitability of Electrified Powertrain Alternatives for Refuse Trucks with Emphasis in The City of Hamilton

AUTHOR: Jack Toller
B.Eng., (Mechanical Engineering)
McMaster University, Hamilton, Canada

SUPERVISOR: Dr. Ali Emadi

NUMBER OF PAGES: xix, 195

Abstract

Refuse trucks, commonly referred to as garbage trucks are a critical component of a municipality's waste management industry. Their primary purpose is to collect, transport and deposit waste from households or businesses to designated transfer sites or dumps. Historically, refuse trucks have been powered by diesel fuel. The consumption of diesel fuel paired with the frequent accelerations or decelerations between each residential household along a route attribute to high amounts of tailpipe emissions and noise pollution within neighbourhoods. There is significant opportunity to explore avenues of powertrain electrification in refuse trucks to reduce their emissions and improve energy efficiency.

To rapidly test promising powertrains, vehicle software models were developed. To accurately model the energy usage and power requirements of refuse trucks, environments for the models to operate were created. The environments were created using on-board diagnostic and positional data collected from refuse trucks in the City of Hamilton in Ontario, Canada. The data collection was done under a research collaboration between the City of Hamilton and the McMaster Automotive Resource Centre. The approaches used to develop the drive and duty cycles for the vehicle models offer some innovative approaches without the need for invasive devices to be installed.

The powertrains that were modelled includes an all-electric, ranged extended electric and conventional refuse trucks. A comparative analysis of the pump-to-wheel powertrain efficiencies were completed looking at metrics such as fuel economy, payload capacity and fuel costs. Lastly, a look at truck emissions from a well-to-wheel perspective were

completed to investigate the impact of each powertrain on greenhouse gasses and the effect on air quality of their immediate surroundings.

I dedicate this thesis to my family and close friends, who have provided me with never ending love and support.

Acknowledgements

This research was undertaken, in part, thanks to funding from the Canada Research Chair in Transportation Electrification and Smart Mobility and Natural Sciences and Engineering Research Council of Canada (NSERC).

The completion of my thesis would not be possible without the mentorship and support of people in my research department, past professors and family. I would like to thank Dr. Emadi for accepting me under his guidance as a master's student. The level of support and expertise at the McMaster Automotive Resource Centre (MARC) is empowering and nurturing for developing innovative ideas. Along the journey of completing my thesis, I have found passion in a field and have completed work I am proud of.

I would like to thank my mentors and friends from MARC. My primary mentor, Dr. Atriya Biswas offered valuable advice throughout my degree. His expertise from his doctoral degree assisted me in producing high quality publications and narrowing down a path towards quicker solutions for various inquiries.

I would like to thank my friend and colleague, Alexander Allca-Pekarovic for helping me navigate my master's degree amidst a global pandemic. I extend this thanks to my closer colleagues whom I had the pleasure to meet and work with while at MARC. Thank you to my knowledgeable friends Eduardo, Josimar, Pier and Alexander.

I appreciate the answers from Lucas Bruck to my many questions about my industry related project, as he helped ensure a smooth on-boarding during a time I knew very little. Fabricio

Machado gladly shared his extensive knowledge of engines with me. Yue Wang passed on valuable knowledge of *MATLAB* and *Simulink* to me, that I will continue to use well after my thesis work.

Dr. Phil Kollmeyer had completed similar work compared to my thesis. His repository of published papers, thesis and open-source databases have made integral contributions to my research. He helped me source the appropriate data logger which allowed me to make researched backed claims in my thesis.

Dr. Jennifer Bauman taught me how to approach vehicle modelling and structured her course to encourage me to take risks through trial and error.

Lastly, I would like to thank the City of Hamilton's Waste Division for their support in my data logging ventures. Thank you to Kim, Vince and Glenn for helping me on and off-site. I would also like to acknowledge the refuse truck operators for accommodating my data logging devices. Thank you to Maureen, the Ward One Councillor for facilitating the initial introductions to the Waste Division team.

Contents

List of Figures

List of Tables

Chapter 1

Introduction

Refuse Trucks

Refuse trucks, commonly referred to as garbage trucks are a critical component of a municipality's waste management industry. Their primary purpose is to collect, transport and deposit waste from households or businesses to designated transfer sites or dumps. An example of a refuse truck is shown below in Figure 1.1. Waste is typically stored in the rear of the truck where it will be compacted to allow the truck to carry a large volume of waste.

Figure 1.1: A side profile of a refuse truck [1].

The history of refuse trucks is fascinating, and modern-day refuse trucks have been servicing roadways for less than a century. Refuse truck innovation closely followed the industrial revolution and the introduction of the automobile. As cities became more industrialized and populated, more robust methods of managing waste became more apparent.

Cities like New York, US created a sanitization department in the early 20th century to develop methods of safely collecting, handling and disposing of waste, horse urine and

manure and other contaminants. Here, sanitization pioneers made efforts utilizing dump-truck like vehicles to collect roadside waste.

The first major advancement in refuse truck technology was the introduction of the *Dempster-Dumpster* by George Dempster in 1937 [2]. George utilized a wheeled waste container that could be tipped mechanically. His containers were called *dumpsters* which was the first introduction of this word to English vocabulary. The next technological breakthrough was in 1938 with the introduction of the *Garwood Load Packer* produced by Garwood Industries in Detroit, Michigan [3]. The addition of an on-board waste compaction system allowed the truck to more than double its capacity, using a hydraulic press.

Modern day refuse trucks operate using the same principles but in a much more efficient manner. These trucks vary drastically in size and function in different geological regions. This is predominately because waste collection requirements are unique to each municipality, regardless of being next to each other or on opposite sides of the world. First world countries usually have a well-defined waste collection operation where different types of waste are handled accordingly. Traditionally, waste from businesses, construction or demolition sites are handled by contracted waste disposal companies. Municipalities typically handle waste collection from residential properties, commonly referred to curb-waste. In some cases, municipalities will contract this work out in part or full to a waste disposal company. The techniques to handle different types of waste require specialized refuse trucks which are elaborated in Section 2.3.

To assist in defining the waste collection scope throughout this thesis, some considerations need to be set. Canadian municipal curb-side waste collected from residential properties will be studied. In Canada, this waste is commonly called municipal solid waste (MSW) and can be categorized into the following: garbage, leaf and yard (LYW), organic, recycling and other seasonal bulk items (Christmas trees, etc.). These types of waste are collected from households, businesses, institutions and construction and demolition sites [4]. MSW is defined as any material (non-hazardous or hazardous) that has no further use and can be managed at recycling, processing, or disposal sites [4]. This thesis will primarily focus on the collection of garbage and organic.

1.1 Background and Motivation

Heavy-duty applications such as refuse trucks are expected to remain primarily diesel-powered until 2030, when zero-emission vehicles such as battery electric vehicles (BEV's) and fuel cell vehicles (FCEV's) are projected to become cost-competitive to diesel alternatives [5]. The motivation for this thesis stems from this idea, to take a deep dive into electrifying refuse trucks to expedite this transition to zero-emission vehicles.

A significant portion of literature about powertrain electrification and different areas of powertrain optimization resides in the consumer-level light-duty vehicle area. With heavy-duty vehicles, there is a soft target for electrification, because the benefits are significant. Heavy-duty vehicles make up a wide array of applications ranging from long haul, short haul, construction and utility uses. These different use cases carry varying degrees of driver behaviour, different vehicle sizes and additional functionalities that convention light-duty

vehicles do not have. Additional functionalities can include things like a tipping function on a dump truck, a snowplow, a crane or a waste compactor on a refuse truck. All these added functionalities usually draw power parasitically from the truck's engine, thus adding a degree of complexity to powertrain electrification. Most of these functions are driven through hydraulics which mesh well with mechanically driven components. Electrified powertrains introduce the decision of continuing with conventional hydraulics or switching to an all-electric system to drive any additional functionalities.

To narrow down an area of heavy-duty truck application, refuse trucks were chosen due to their unique route characteristics, additional waste handling functionality and their integral need in municipalities worldwide. Their route characteristics include numerous stops and starts, changing in truck payload and back-to-base routine. Back-to-base means that refuse trucks typically return to a centralized yard at the end of the workday to park for the evening and night. These route characteristics are similar to delivery vehicles as well, except delivery vehicles do not have significant added functionalities that draw additional power from the engine.

Literature on refuse trucks sparsely populates certain areas of research. Little literature and open-source data exists to quantify refuse truck routes. This quantification includes drive cycles, which describes the vehicle's velocity profile over the day. Specific to refuse trucks, are the ability to load, compact and offload waste throughout the day. These actions use up fuel and add additional loading on the engine, that is documented in some key literature [6] [7] [8].

The waste collection efforts of refuse trucks contribute to around 40% of the total cost of waste collection in municipalities [9]. As such, investigating avenues to reduce fuel costs or move towards electrified powertrains is appealing from a business point of view, as fuel cost make up a significant portion of costs and can be very volatile in price. To investigate the usage of a refuse truck, is it convenient to do so in a software environment, to rapidly trial different powertrain use cases in a refuse truck. Before modelling can be completed, the refuse truck's operating environment must be quantified. This includes the truck's drive cycle, how steep or shallow the roadway grade is, how the payload of the truck changes throughout the day and the additional loading on the truck's engine from loading, compacting and unloading waste.

As previously mentioned, minimal data exists on the aforementioned quantifiables. Therefore, there is motivation to acquire this data directly from a source. The City of Hamilton in Ontario, Canada is a municipality that the McMaster Automotive Resource Centre (MARC) resides, where studies for this thesis were being completed. It was convenient to approach this municipality given the proximity and their usage of modern-day refuse trucks. Data was logged from Hamilton's refuse trucks and used to create an environment to simulate software models in.

Simulating different truck powertrains and analysing their efficiencies on real-life routes will aid in highlighting promising trends on where refuse truck technology might be headed, in the age of electrification.

1.2 Objectives and Contributions

The purpose of this thesis is to explore current literature contributions specific to refuse trucks and explore less established areas of refuse truck operational trends and powertrain modelling. Further, a streamlined and non-invasive approach to gathering refuse truck data will be explored, to help pave the way for easy access to municipal waste collection data. Lastly, promising trends of electrified powertrains will be trialled using data from real-world refuse trucks. The four objectives of the thesis are outlined as follows:

1. Complete a comprehensive literature review on current and state-of-the-art trends of refuse truck technology.
2. A comprehensive non-invasive data logging approach to gathering, processing and analysing refuse truck data will be outlined. This data will be used to help understand the waste collection requirements for the municipality of Hamilton.
3. Complete drive and duty cycles describing the kinematics and hydraulic loading on the refuse truck throughout the day will be presented. Macro-trends will be explored to highlight trends over many operation days and weeks on urban and rural routes.
4. Formulate and test vehicle software models of baseline as well as promising electrified powertrain trends that might be beneficial to the City of Hamilton and conduct a comparative analysis between these powertrains.

1.3 Summary of Thesis

A chapter breakdown of the thesis is provided in this section. Chapter 2 discusses the current state of refuse trucks with modern-day technology. The functionality of a refuse

truck is explained along with what options waste collection consumers have access to. The drawbacks of current heavy-duty trucking powertrain technology are addressed, setting up a transition to the following chapter. Chapter 3 explores the state-of-the-art technology trends where heavy-duty trucking and refuse trucks alike may be directed. Real-world products are discussed and quantified to help strengthen arguments towards each respective powertrain architecture.

Chapter 4 initiates the beginning of the contributions of this thesis to the refuse truck industry. Here, the methodology behind data logging real-world refuse truck data is explained and data processing techniques revealed. The data collected and processed from real refuse trucks was prepared to be used in the next chapter. Chapter 5 explains the workflow for developing refuse truck drive and duty cycles, to quantify the trucks operation on a day-to-day basis. The duty cycle of a refuse truck is composed of the power and mass cycles which quantify the hydraulic loading on the truck and the change in the truck's payload. Cycle results and macro-trends for weekly operational data are presented and discussed. Many derivatives from the collected data are provided, including stop estimation along routes, road grade and geo-referencing to differentiate different route characteristics. The different route characteristics are defined as whether the refuse truck is travelling between the collection zone, truck yard and transfer station or whether the truck is collecting waste in the collection zone.

Chapter 6 explains how the powertrains were modelled and simulated in the *MATLAB* and *Simulink* environment. The modelled powertrains include a conventional diesel truck with a 6-speed gear transmission, an all-electric truck and a range extended electric truck. The

parameterization and mass characterization of the refuse truck were completed using resources from the literature, manufacturer, physical truck and modelled environments. Once the mass profile and parameters of the truck were determined, information about route cycles from Chapter 5 were used as inputs into the vehicle models to simulate how each alternative powertrain would compare to a conventional diesel powered truck in the City of Hamilton.

The modelled powertrain efficiencies were compared in Chapter 7 in terms of fuel economy, payload capacity, emissions, and pump-to-wheel energy consumption cost. It was found that the all-electric truck can withstand the same payload demands as the conventional truck whereas the range extended electric truck had to sacrifice payload given the maximum load constraints on the chassis. The electrified powertrain alternatives offer significant savings in energy consumption costs, due to their better fuel economies and lower energy unit costs.

A summary of the completed work, conclusions and future work are covered in Chapter 8. Here, the contributions of this thesis to the literature are realized. Future work contains insightful trends developed from literature reviews, working with a waste collection team for a municipality and through vehicle software modelling environments. The thesis concludes with references.

Chapter 2

Current Refuse Truck Technology

This chapter introduces the current state of refuse truck technology that is present in most first world municipalities around the world, specifically in North America. Insight is offered into the near future for some municipalities, whereas other municipalities may already be pushing the state-of-the-art technology. The basics on how a conventional refuse truck uses its energy to function is explained in detail. In this case, conventional refuse trucks are defined as trucks that utilize current or near future technologies. In the field of heavy-duty trucks, these technologies consist of large engines that consume diesel or natural gas fuel. Lastly, types of commonly used refuse trucks will be explored.

2.1 Status of Refuse Trucks

The status of refuse truck technology largely remains unchanged since the development of the early day loader-packer trucks. Here, refuse trucks have traditionally used diesel engines to propel the vehicle around and utilized hydraulics to handle the on-board waste. What has changed over the years are refuse trucks have become larger, more fuel efficient and smarter at route optimization. They have also become more specialized for certain waste collection applications. Refuse trucks that have waste loaded into the rear or side or more commonly used on residential routes.

Trucks that have front or side automated loading arms typically service businesses and are more commonly being used in newer municipality waste programs to service their residential areas such as in the City of Mississauga located in Ontario, Canada. Roll-off refuse trucks primarily service construction areas or used in junk clearing services.

Refuse trucks are responsible for residential waste recovery, which can vary based on the province in Canada. Alberta and Saskatchewan have some of the highest amounts of waste generation at 1007 kg and 881 kg respectively per capita, whereas Nova Scotia and British Columbia have the lowest at 154 kg and 209 kg respectively in 2012 per capita [10].

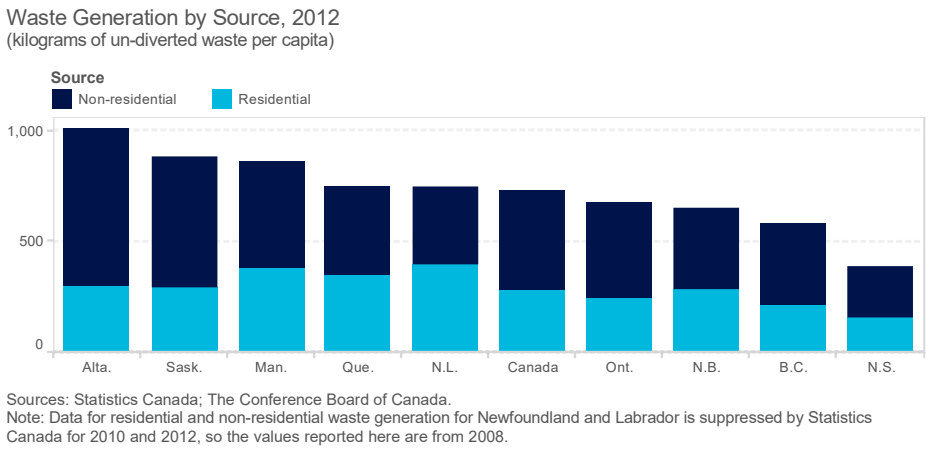

Figure 2.1: Residential and non-residential yearly waste generation per capita, for each province [10].

Canada's yearly average residential waster generation per capita, shown above, was 279 kg in 2012 and about one third of this waste is diverted to recycling and composting depots.

Refuse Trucks are commonly classified as heavy-duty vehicles in Canada as their gross vehicle weight rating (GVWR) typically falls within the class 6 to 8 categories, with class 8 trucks weighing over 14,969 kg [11]. As such, refuse trucks within the same classification of other heavy-duty vehicles such as long-haulers or short-hauler semi-trucks. Refuse trucks are part of a specialized group of heavy-duty vehicles that deal with demanding duty cycles. Other examples of trucks like refuse trucks are dump trucks, service vehicles and snowplows. These types of trucks are illustrated in Figure 2.2. A duty cycle defines additional functionality of a truck, like raising a crane or tiping an on-board container to

offload a payload. In the case of a refuse truck, the added functionality is loading, compacting and offloading waste.

Figure 2.2: Applications of a heavy-duty truck. Dump Truck (Left), Snowplow (Right) [12].

Since refuse trucks are part of the heavy-duty industry, they fall under common scrutiny of high emissions and the consequential direct and in-direct health impacts of these emissions. Almost all heavy-duty trucks in Canada (97.5%) are powered using diesel fuel, and as such are a particular interest in climate change policy making in Canada [5]. The consumption of diesel fuel paired with the frequent accelerations or decelerations between each residential household along a route lead to high amounts of tailpipe emissions and noise pollution within neighbourhoods. According to energy use in Canada, heavy-duty freight vehicles (which includes refuse trucks) contribute yearly between 16 – 19% of all greenhouse gas (GHG) emissions in the transportation sector [13]. This is a disproportional representation of road emissions caused by all vehicles on the road. The number of light-duty vehicles far outweigh the number of heavy-duty vehicles on the road, yet the amount of GHG emissions of heavy-duty vehicles is about half of light-duty vehicles [13] [14]

[15]. These yearly GHG emissions have steadily increased from 2000 to 2018 by 19.5% [13].

Further, because these trucks primarily use diesel fuel with compression-ignition (CI) internal combustion engines, emissions from these trucks contain particulate matter (PM) and Nitrogen Oxides (NO_z) which can directly impact the health of residents in the immediate environment. Short term exposure to NO_z is linked to adverse respiratory effects, especially in at-risk groups such as children, elderly, and those with asthma [16]. PM is also linked to respiratory as well as cardiovascular complications and has been classified as a carcinogenic in 2012 by the WHO [16]. Reducing emissions also benefits heavy duty trucking economically, as the cost of fuel is usually the largest operational cost of truck fleets, at around 30 – 40% of costs per kilometre [5]. Based on the factors discussed, improving the fuel efficiency of these vehicles will both benefit the economics and environmental impact of operating truck fleets.

Diesel powered heavy-duty trucks are expected to dominate the industry until 2030, when zero-emission vehicles such as BEV's and FCEV's are projected to become cost-competitive to diesel alternatives [5].

2.2 Anatomy of a Refuse Truck

The anatomy of a refuse truck can vary based on the model, application, and geographical location. At a high level, a refuse truck is composed of a chassis and a waste containment unit (WCU) that is installed onto a chassis, illustrated below.

Figure 2.3: The Anatomy of a refuse truck, including the chassis and waste collection unit [1].

The chassis includes the powertrain, energy storage, controls, and the driver's cab. For a conventional refuse truck, the powertrain is composed of a fuel tank, engine, torque converter, transmission, power take-off (PTO) and differential or final drive ratio. The PTO is responsible for powering the hydraulic pump. The powertrain for a conventional refuse truck is shown in Figure 2.4.

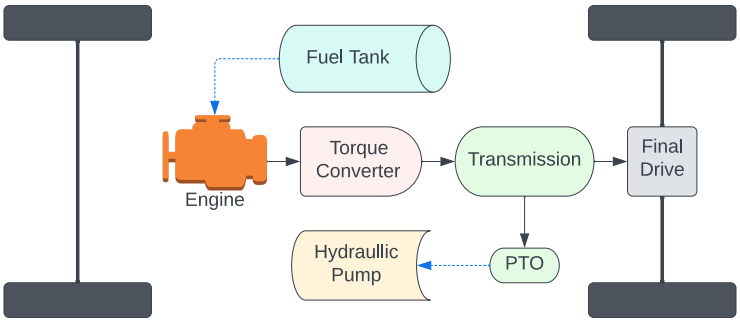

Figure 2.4: A conventional refuse truck powertrain.

During waste collection the WCU is responsible for storing waste, compacting waste from the hopper into the storage body and utilizing any loading arms that load waste into the collection hopper at each household.

The chassis and waste collection unit are typically produced in separate factories, owned by different companies. Established automotive companies such as Volvo, Peterbilt, Freightliner and more, produce the chassis which is used for a wide range of applications. The chassis can be used for refuse trucks but also dump trucks, mobile cranes, snowplows and other types of service vehicles.

The usage of a refuse truck during a day can be described by its drive and duty cycle. The duty cycle is composed of a mass cycle and power cycle. The drive cycle is a speed versus time profile that describes that kinematics and can be used with a complementary road grade profile to capture the changes in elevation of the route. The mass cycle describes the change in payload of the truck as it picks up and drops off waste. The mass cycle is important to consider as it significantly affects the road loads of the vehicle over the day. The power cycle includes all auxiliary power required to operate the vehicle including climate control of the cab and the power draw of the hydraulic compaction system. Together, the mass and power cycle describe the additional truck functionality and are used in tandem to define the truck's duty cycle. The creation of these duty cycles can come from previous literature or through in-field data collection.

An important aspect of refuse trucks is in the on-board WCU. WCU's are commonly powered using hydraulics or natural gas, with emerging state of the art technologies using all-electric units. Typically, the compaction and lifting sequences of the WCU are accomplished using hydraulics where the hydraulic pump is powered from the PTO. A PTO allows a subsystem to parasitically draw energy from the transmission of the vehicle, shown in Figure 2.5.

Figure 2.5: A schematic showing the power take-off connection on a multi-speed automatic transmission [17].

This means the pump drive shaft is mechanically connected to an additional output shaft of the transmission and the WCU has no internal energy storage. Usually there is a marginal gear ratio between the pump drive shaft and the transmission, where the pump will spin at a faster speed than the transmission. During a compaction, offloading or loading cycle, the hydraulic system usually requires the refuse truck to be idling as the high-power draw for this cycle will cause a decrease in vehicle drive performance. When the PTO is engaged, the engine speed will typically increase and remain at a target speed depending on the engine type and manufacturer's specification. Assisted hydraulic lifting can be used regardless of vehicle speed as the engine speed can remain close to idle, though the vehicle will mostly be stationary during this time as the operator will want to return the waste bin to the same location.

Understanding the fundamentals of waste compaction is a crucial part to this thesis, as the compaction process requires a very high amount of power to be drawn from the engine, or in the case of an all-electrical vehicle, power from the high voltage (HV) battery. Compaction capability in a refuse truck is important as it enables the truck to store more

waste in a smaller footprint allowing it to operate more economically. Sizing a WCU with its compaction unit can vary dramatically based on the country, as research has found the densities of waste can vary dramatically. Some factors affecting waste density can be the environment, as a more wet environment will lead to a higher water content amongst the waste or very sandy climates can lead to sand accumulation [18]. Further, studies have found that more industrialized and developed countries typically have lighter MSW densities ranging from 150 to 180 kg/m^3 [19] [20], whereas developing countries range from 300 to 600 kg/m^3, with an extreme example of Gaza, Palestine having up to 1040 kg/m^3 [18].

Apart from environmental differences between countries, other factors leading to high densities in developing countries could be the lack of separation between MSW and organic waste and less abundance of packaging materials such as carboards, plastics and paper [18]. The inability of some developing countries to adequately separate waste into different areas of disposal (garbage, LYW, organics, recycling and bulk items) puts more strain on refuse trucks compared to more developed countries as less locations can be serviced as the compaction chamber of the truck will fill rapidly with higher dense waste.

The compaction system of a refuse truck will vary slightly based on what model of truck is used, such as rear-loaded or front-loaded refuse trucks. The basic anatomy of the hydraulic compaction system is shown below for a rear loading refuse truck:

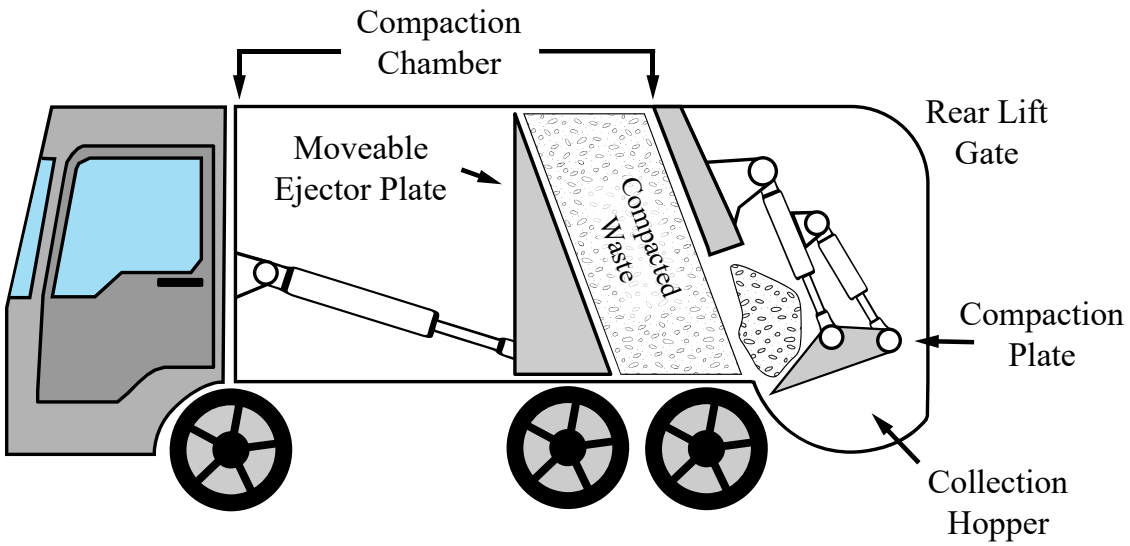

Figure 2.6: An illustration showing the basic system of a refuse truck hydraulic compaction system.

Overall, the hydraulic compaction system can be explained in the following steps:

1. Waste is loaded into a collection hopper by an operator or automated lifting arm
2. Waste will successively be added as the truck services a route, leading to the waste in the collection hopper to increase in volume
3. When the waste hopper is full, a compaction plate is hydraulically depressed against the collection hopper, sweeping the waste into the compaction chamber.
4. A moveable ejector plate provides an even amount of pressure against the waste as it is pushed into the compaction chamber and will move horizontally towards the front of the chassis as the chamber fills.
5. When the truck visits a landfill or transfer station after the route is complete or the compaction chamber is full, the compaction chamber is then tilted upwards and simultaneously the rear lift gate opens.

6. The moveable ejector plate then pushes all the waste out from the compaction chamber. Next, the compaction chamber is lowered and the rear lift gate closes, allowing the refuse truck to continue collecting more waste.

As mentioned earlier, the anatomy of a refuse trucks can vary significantly as sometimes a lighter and shorter vehicle is required to be more manoeuvrable in urban settings or a more robust vehicle is required for higher payloads. For the vast amount of refuse designs, they can be split into the following categories: Side Loader refuse trucks (SL-RT), Rear Loader refuse trucks (RL-RT), Front Loader refuse trucks (FL-RT) and Roll-Off refuse trucks (RO-RT). It is important to consider each type of vehicle as they are optimized at tackling specific jobs.

2.3 Types of Refuse Trucks

2.3.1 Front End Loader Refuse Truck

FL-RT's feature automated collection systems, where a lifting fork at the front of the vehicle lifts a bin and deposits it in a hopper located in the middle of the vehicle. These types of vehicles are usually used to collect waste for commercial and industrial businesses that use large dumpsters to collect waste. A front-end loader will collect more waste per stop compared to a rear or side loading refuse truck, averaging around 1.5 – 6.1 cubic meters or 180 – 280 kg per bin [21]. As a result of collecting more waste per stop, a front-end loader will make less stops per day as well, approximately 100 – 200 stops, and will need to visit a transfer station 2 – 4 times per day to offload waste [21]. Additionally, the compaction sequence in the WCU is usually deployed after a bin is collected, as the hopper

will be full. The fuel economy of models aged 4 – 6 years old was found to be 77 – 100 L/100km [21]. The fuel economy is slightly better than side or rear loaders due to the vehicle being more active on roadways and highways traveling between different pickup areas, as opposed to frequent pickups along residential routes.

Figure 2.7: A Heil front end loading refuse truck [1].

2.3.2 Side and Rear Loader Refuse Trucks

SL-RT and RL-RT are very similar in application as they are both used to service either commercial or residential properties. Rear loaders have a hopper at the rear of the vehicle where waste is collected. Side loaders have a hopper between the vehicle cab and waste reservoir, and waste is collected at the side of the vehicle. Each type of truck can also have its WCU split into two compartments which allows the collection of more than one type of MSW. A side-loader and rear-loader are illustrated in Figure 2.8.

Figure 2.8: Split rear-loader refuse truck (left). Heil automated side-loading refuse truck (right) [1].

The hoppers on rear loaders are commonly manually loaded or using a hydraulic assistive loading arm. Similar procedures are used for side loaders as well, but new models can feature an automated lifting arm that picks up waste bins and disposes them into the hopper, shown in Figure 2.8. This eliminates the need for an operator to be outside the truck and allows the driver to complete the route as a one-person crew. Because these types of trucks frequently visit residential properties, who accumulate less waste on a weekly or bi-weekly basis than commercial and industrial properties, the average bin mass ranged from 8 – 11 kg and up to 40 kg [22]. Also, the number of stops per workday is the highest compared to the other types of refuse trucks at around 500 – 1200 cans collected, resulting in the truck having to offload at a transfer station one to two times per day due to the high amount of waste collected. A study found the average fuel economy for trucks manufactured from 2009 – 2012 to be 60.3 – 130.7 L/100km for MSW [22], with newer models achieving better fuel economies.

2.3.3 Roll Off Refuse Truck

RO-RTs consist of a chassis and a detachable waste bin, shown in Figure 2.9. The rear of the chassis can tilt upwards to either drop-off or pick-up the waste bin. These trucks are commonly used for large scale commercial operations or removing waste from construction and demolition sites. It should be noted that these trucks can also transport MSW, such as when a homeowner is decluttering their household. The chassis features hydraulics to drop-off and pick-up the bins but does not have an on-board compaction system like the other types of refuse trucks have. The waste that is placed in the bin is left untouched and hauled off to a waste facility. Data on real world duty cycles are less known, as these trucks are typically operated by companies and not municipal governments. Typically, 5 – 10 bins are collected daily containing around 11 – 30 cubic meters of waste each [16]. When a truck collects a bin, it will visit a transfer station or landfill immediately after and as such will be present on the highway more often as opposed to more frequent accelerations or decelerations found in RL-RT and SL-RT's. For trucks manufactured from 2005 – 2012, the average fuel economy ranged from 41 – 67 L/100km [16]. This is the best fuel economy compared to the other types of refuse trucks and is mainly due to the drive patterns associated with this type of truck.

Figure 2.9: Roll off refuse vehicle and waste collection bin [23].

2.4 Current Fuel Options and Emissions

Current refuse trucks primarily run off diesel in CI-engines or compressed natural gas (CNG) and liquid natural gas (LNG) fuels in spark-ignition (SI) engines. The usage of diesel has been preferred in the past due to its greater energy efficiency compared to gasoline. This alternative comes at the cost of harmful emissions including carbon dioxide (CO_2), NO_x and PM. To mitigate some of these concerns, CNG or LNG powered refuse trucks trickled into newer alternative truck decisions when older diesel truck's service lives expired. CNG fuel is better suited for refuse applications over LNG as CNG is typically a cheaper fuel. Natural gas is decoupled from the price of oil and as such has a less volatile price. The stable price of natural gas allows fleet owners to more accurately account for their operational costs.

These types of fuels come from non-renewable sources, as they are extracted from the ground with a finite number of available resources. With today's technology, renewable alternatives exist for each in the form of renewable natural gas (RNG) and biodiesel. RNG is the resultant of biogas formed from decomposing organic matter, whereas biodiesel is

manufactured from vegetable oils or animal fats [24]. Biodiesel is available in a pure form known as B100. B5 and B20 also exist and are blends of diesel and biodiesel, containing up to 5% and 6 – 20% of biodiesel respectively [24]. RNG, B5 and B20 can be interchanged with their respective non-renewable counterparts with little to no vehicle powertrain alteration, though B100 requires modifications to the engine.

CNG has less energy density than LNG but because refuse trucks operate on a back-to-base route, the need for a higher energy dense fuel is usually not required. The density of CNG and LNG are between 180 – 215 kg/m^3 and 430 – 480 kg/m^3 respectively [25], based on the operating temperature and pressure. The fuel prices in the United States for gasoline, diesel, LNG and CNG in USD/GGE are displayed in Figure 2.10, where GGE represents the gasoline gallon equivalent. Historically in the past 10 years, CNG has usually been cheaper than diesel, gasoline and LNG. The price of LNG has been tracked since 2016 and is usually cheaper than gasoline and diesel. Blends of biodiesel such as B20 typically track the price of diesel.

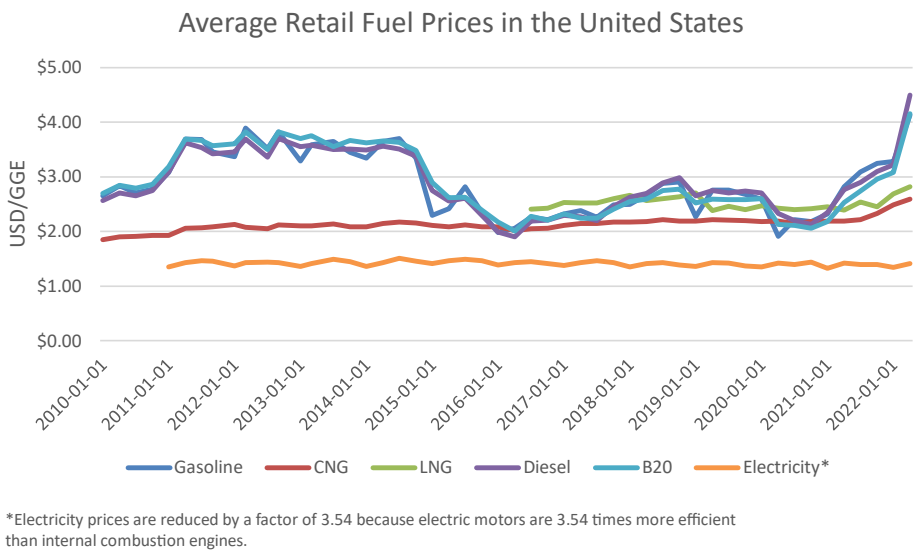

Figure 2.10: Average retail fuel prices in the United States [24].

An important factor to consider while comparing different types of fuels are the efficiency and emissions associated with extracting and delivering these fuels to vehicles. Indirect emissions and additional energy are required to extract fuels from their raw source and transport the refined fuels to a pump, where a vehicle can consume them. These indirect emissions and energy usage are defined as well-to-pump (WTP) [26]. The WTP η is defined as the percentage ratio of energy out versus energy in, to produce the fuel. The primary focus on emissions are CO_2, NO_x and methane (CH_4) as these types of emissions have the most impact on global warming [27]. In 2020, the U.S. GHG emissions were composed of 79% CO_2, 11% CH_4, 7% NO_x and 3% of fluoride gases [28], illustrated in Figure 2.11.

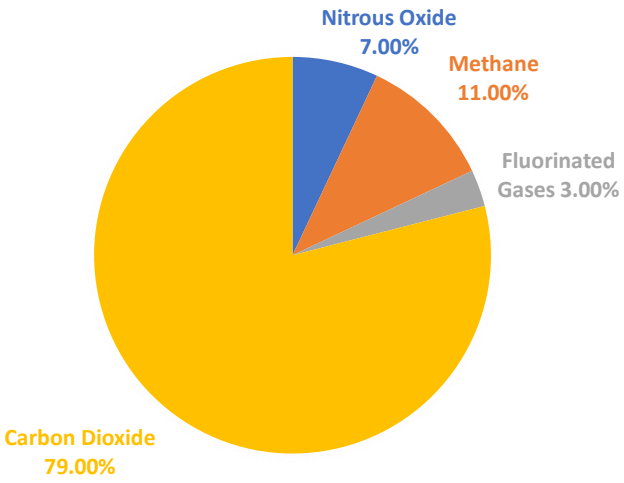

Figure 2.11: Overview of U.S. Greenhous Gas Emissions in 2020 [28].

Fluoride gases are a general term used to categorize hydrofluorocarbons, sulphur hexafluoride, nitrogen trifluoride and perfluorocarbons, which are synthetic and potent GHG's. These gases are typically emitted in small quantities but yield significant global warming potentials (GWP) factors in the tens of thousands. GWP describes how much of an effect a gas has on warming the atmosphere. The factors that affect how large or small a GWP value depends on the following [29]:

1. How strongly do they effect the atmosphere?
    - Different gases possess the ability to act as a stronger blanket to warm the earth's atmosphere. This is quantified by its radiative efficiency.
2. What is their lifetime in the atmosphere?
    - Each gas remains in the atmosphere for varying amounts of time once it has been emitted. This can range from a few years to thousands of years.

The lifetime and GWP for each type of GHG are shown in Table 2.1.

Table 2.1: Lifetime and Global Warming Potentials for various greenhouse gases.

GHG	Lifetime (years)	GWP (Average)
CO_2	300 - 1000[1] [30]	1 [31]
CH_4	10 [29]	28 [31]
NO_x	100 [29]	265 [31]
Fluoride Gases	3 weeks to 1000+ years [30]	1000 – 10000+ [29]

For the scope of emission analysis, fluoride gases will not be considered as the emission databases referred to throughout this thesis do not have information on the quantities of these gasses that are emitted from refuse truck operation.

NO_x and CH_4 can be quantified as carbon dioxide equivalents (CO_2e). CO_2e is a term used to define all GHG's under a common unit that is relative to CO_2. One unit of CO_2 is said to have a factor of one or a GWP of one. NO_x and CH_4 emissions can be converted to CO2e using the corresponding GWP factors in Table 2.1. CO_2e is calculated using the following formula:

$$CO_2e = \frac{GHG}{GWP} \qquad \text{Eq. 2.1}$$

For each type of fuel (diesel, biodiesel, CNG and LNG), the efficiencies of energy production and emissions associated with WTP per one MJ of energy were obtained from

[1] The lifetime of CO_2 can vary dramatically based on the natural process of carbon dioxide reabsorption by the environment.

the Argonne Greenhouse gases, Regulated Emissions, and Energy use in Technologies (GREET) model [32]. These metrics are displayed in Table 2.2.

Table 2.2: Comparison of different fuel types and their WTP impact per one MJ of energy consumed.

Criteria	Diesel	Biodiesel[2]	Gasoline	CNG	LNG
WTP η [32]	84%	91%	82%	86%	83%
WTP CO_2 Emissions (g) [32]	12.26	13.57	15.48	8.48	10.69
WTP Additional Emissions[3] - CO_2e (g) [32]	7.40	7.13	12.71	17.13	13.66
Fuel Cost (USD/GGE) [24]	2.89	2.90	2.89	2.13	2.52

2.5 Compressed Natural Gas Refuse Trucks

For all types of refuse trucks discussed in 2.3, CNG can be used as an alternative fuel type to diesel. The use of CNG powered refuse trucks have become more popular in recent years as they have a lower GHG emissions NO_x emissions and quieter operation compared to diesel power trucks. A study looked at the operational data of CNG refuse trucks where 70% of the sample size was composed of SL-RT and FL-RT, and the remaining percentage were RL-RT and RO-RT [33]. In this study, the real-world fuel use and tailpipe emissions were assessed. Like their diesel-powered counterparts, SL-RT and RL-RT have worse fuel consumption compared RO-RT due to the increased number of stops and lower sustained speeds.

Most new CNG trucks used SI-engines but are still regulated under the heavy-duty CI-engine standards [34]. CNG engines are usually less efficient than diesel due to the

[2] For B20 diesel blend. WTP efficiency does not include energy captured by plants through photosynthesis.

[3] CO_2 equivalence includes CH_4 and NO_x

volumetric efficiency of injecting gas with air, compared to injecting liquid diesel with air [33]. The volumetric efficiencies of diesel and CNG are approximately 0.70% and 0.62% respectively. Additionally, both engines have high compression ratios with CNG as 12:1 and diesel as 17:1. To summarize, diesel engines can generate the same amount of power as CNG with less fuel.

It was also found that the emissions of a loaded CNG refuse truck increased NO_x by 47%, CO by 31% and hydrocarbons (HC) by 300% on highway driving versus an unloaded truck [33]. A variety of CNG refuse trucks were considered, using a Cummins ISLG-320 235 kW engine. For an SL-RT, the fuel economy ranged from 138.4 – 180.9 DLE/100km, where DLE represents the diesel litre equivalent, or the amount of natural gas required to have the same energy content as diesel fuel. For an SL-RT the fuel economy ranged from 94.0 – 117.6 DLE/100km. The truck models were manufactured in 2012 and 2013.

2.6 Hydraulic Hybrid Refuse Truck

A type of hybrid powertrain more commonly found in heavy-duty trucks uses hydropneumatics accumulators that store some energy during braking. Hydraulic hybrids can be arranged in series, parallel or series-parallel, similar to electrified hybrid powertrains. During acceleration, this stored energy can be spent to assist the vehicle. The powertrain is shown in Figure 2.12, and has the following functionality:

1. When the vehicle is turned on, the engine and motor/pump charge the high-pressure accumulator

2. As the vehicle accelerates, the energy stored in the high-pressure accumulator is used. The high-pressure fluid flows from the high-pressure accumulator to the low-pressure accumulator, turning the motor/pump in the process. When the accumulator can no longer supply energy, the engine supplies energy to the powertrain.
3. When the vehicle brakes, some braking energy is routed through the pump into the high-pressure accumulator.
4. At high speeds, the engine supplies all tractive effort to the powertrain.

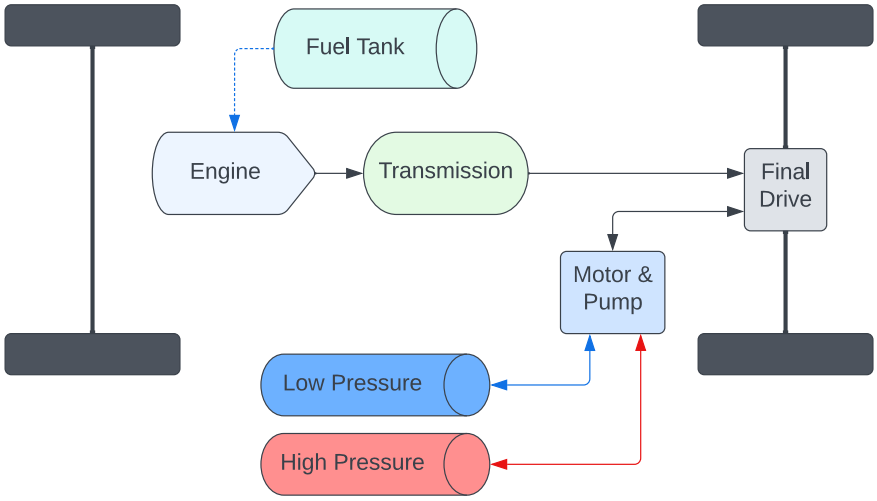

Figure 2.12: A parallel hydraulic hybrid powertrain.

In the case of a series hydraulic hybrid, the powertrain can recover up to 70% of energy that would be lost from braking [35]. This energy recovery paired with the hydrostatic drive assisting the mechanical drive, allows this powertrain to reduce fuel usage and in turn reduce emissions.

2.7 Summary

In conclusion, the current state of refuse truck technology was explored. The functionality of a refuse truck has been defined along with its accessory hydraulic systems that are responsible for loading, compacting and offloading waste. A review on the most popular types of refuse trucks including RL-RT, SL-RT, FL-RT and RO-RT was completed from available literature. The impact of conventional refuse trucks on the environment, as well as different fuel alternatives has been investigated to allow for comparisons to be made between electrified powertrain alternatives.

Chapter 3

State of the Art Refuse Truck Technology

In this chapter, state-of-the-art powertrain technology will be discussed as it applies to refuse truck applications. Vehicle electrification is rapidly accelerating in many avenues of vehicle uses, most popular in consumer level and light-duty vehicles. Some companies have started offering medium and heavy-duty electrified alternatives for many use cases such as buses, school buses, delivery vehicles and refuse trucks. Some of the discussed powertrain technologies in this section are theoretical, whereas some have been implemented into real world vehicles.

3.1 Battery Electric Refuse Trucks

BEVs offer an exciting alternative to the way traditional refuse trucks have operated in the past. The nature of refuse truck operation involves a large diesel engine that supplies power to the powertrain and hydraulic system to complete tasks such as waste compaction, offloading and loading. The large diesel engine must frequently operate in regions where it is less efficient. Due to high road loads and typical driving habits associated with a refuse truck, the diesel engine must be sized to provide high torque at low speeds. Consequently, when the truck is idling or operating the PTO, the engine is running in inefficient regions. Additionally, a refuse truck makes many stops and starts along its route which puts the diesel engine in inefficient regions as the vehicle is accelerating or a loss of kinetic energy to heat from the brake pads or air brakes being used to slow the truck down.

The scenario of high torque and slow speed operation, paired with frequent stops makes a refuse truck a perfect candidate for any sort of powertrain electrification. An electric motor

can operate in much higher efficiencies under the same conditions and can utilize regenerative braking. Regenerative braking is a term used to define diverting some or all braking energy into another form of energy rather than heat loss. In the application of electric motors, an electric motor can act as a generator which resists the motion of the vehicle, in turn slowing the vehicle down and converting some kinetic energy into electric. The advantages beyond regaining kinetic energy are that brake pads will experience less wear as they are used less often, or to provide lesser stopping forces.

A battery electric vehicle is also more mechanically simpler than a conventional or hybrid vehicle. The powertrain is composed of a battery, inverter, traction motor and an optional final drive ratio, visualized below in Figure 3.1.

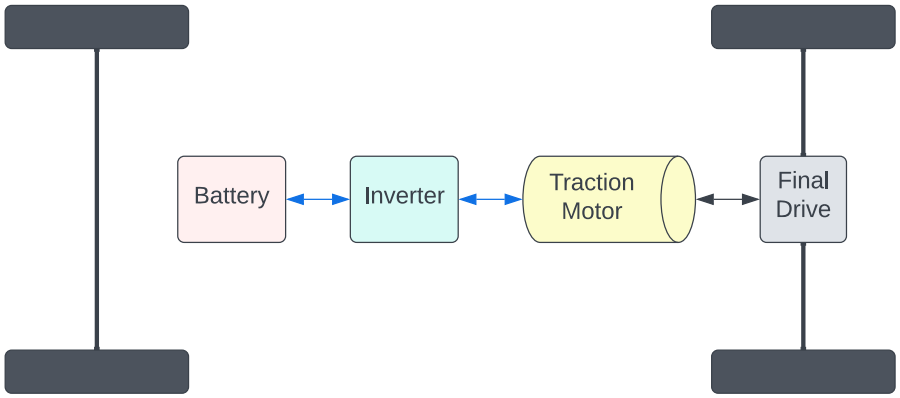

Figure 3.1: A battery electric vehicle powertrain.

The attractiveness of all-electric refuse trucks has begun to make sense to manufacturers as battery energy densities have risen and the cost per kWh of battery packs have dropped over the years. The battery pack can be viewed as a significant drawback to all-electric heavy-duty vehicles, as the volume, mass and cost can act as barriers for manufacturers to

enter the market. In the following sub-sections, two manufacturers who have entered the all-electric refuse truck market will be explored.

3.1.1 Mack LR Electric

The Mack LR Electric is an example of a class 8, fully electric refuse truck that integrates an all-electric chassis with a hydraulically powered WCU. The specifications of this truck model are displayed in Table 3.1 and were obtained from press releases and specification sheets [36] [37] [38].

Table 3.1: Mack LR Electric refuse truck specifications.

Specification	Value	Specification	Value
Curb Mass	Not Specified	Transmission	2-Speed
Battery Capacity / Range	376 kWh	Charging Time	120 min @ 150 kW
Range (on the job)	160 km	Waste Handling Unit	
Battery Chemistry	NMC	Manufacturer	Heil DuraPack 5000
Dual Traction Motor Model		Capacity	11500 kg
Power Rating	130 kW (each)		
Peak Torque	5500 Nm		

The Mack LR Electric can be used for both recycling and refuse collection. The on-board HV battery supplies energy to all HV components, as well as the accessory low voltage components. It features a two-stage regenerative braking system to help limit the wear on brake pads and regain kinetic energy that would otherwise be converted to heat. A side profile of the Mack LR Electric is shown in Figure 3.2.

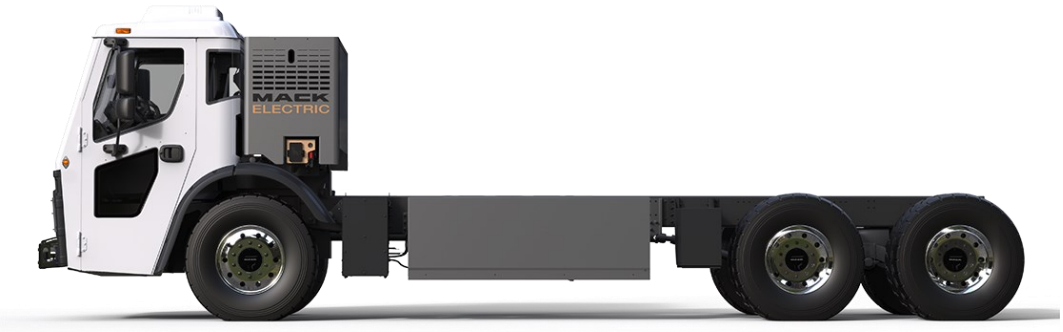

Figure 3.2: A side profile of the Mack LR Electric refuse truck.

3.1.2 Lion8 Electric

The Lion8 is an all-electric automated side loading refuse truck produced buy Lion Electric. Some important specifications of the vehicle are listed below [39] [40].

Table 3.2: Lion8 Electric refuse truck specifications.

Specification	Value
Tare Weight / Gross Weight	11 200 / 24 766 kg
Battery Capacity / Range	336 kWh / 274 km
Battery Chemistry	NMC
Maximum Power / Torque	350 kW / 3400 Nm
Traction Motor Model	Dana TM4 PMM
Waste Handling Unit	Boivin Evolution (Electric)

Figure 3.3: Lion8 refuse truck with a Boivin Electric waste containment unit installed.

The Lion8 truck is composed of a chassis made by Lion and a waste containment unit made by Boivin Electric. The vehicle can reduce operating energy costs by 80%, a reduction of 60% in maintenance costs and a further 50% reduction in energy consumption of the electric WCU compared to a hydraulic WCU [39]. Some benefits of an all-electric truck are the reduction of working fluids used, such as hydraulic fluid, oil and power steering fluid. Also, the presence of regenerative braking energy significantly prolongs the life of brake pads. Since less serviceable parts are in the vehicle, a reduction in possible downtime could be seen.

The Lion8 paired with the Boivin Electric WCU is capable of a 210 km range and the ability to service 1200 homes. Additionally, the Boivin Electric WCU can be paired with a diesel truck variant, replacing the traditional hydraulic powered WCU. This can lead to a fuel cost saving of 35%. The WCU capacity can range from 15 – 25 m^3.

This all-electric truck has zero tailpipe emissions and would be beneficial to municipalities seeking better emission initiatives. Traditional refuse trucks have a large diesel engine that

is responsible for both the acceleration of the vehicle and the hydraulic compaction cycles. This creates a very noisy environment compounded by use of the compaction cycle when the engine is idling, producing even more noise. Because of this, refuse trucks are usually limited to specific operating hours because if they ran too early in the morning or during the night, residents would be awoken by their noise.

All-electric trucks might be able to tap into different operating hours due to the elimination of most noise previously caused. Earlier morning operating hours could allow trucks to avoid heavier traffic during popular commuting times to work.

3.2 Hybrid Electric Refuse Trucks

3.2.1 Series Hybrid Powertrain

A type of hybrid powertrain that may be effective in heavy-duty applications are parallel hybrid architectures. An illustration of this powertrain architecture is shown in Figure 3.4. A series hybrid includes an engine that is mechanically decoupled from the vehicle's powertrain. The sole purpose of the engine is to provide mechanical power to a generator, that outputs electrical power in combination with an inverter. The truck is powered entirely by a main traction motor, like a BEV, which draws power from a HV battery. The series hybrid powertrain configuration is commonly referred to as a range extended electric vehicle (REEV). This is because the on-board engine and fuel tank provide extra range to the all-electric portion of the vehicle. Similar applications of series hybrid architectures for refuse trucks are available in the literature [41].

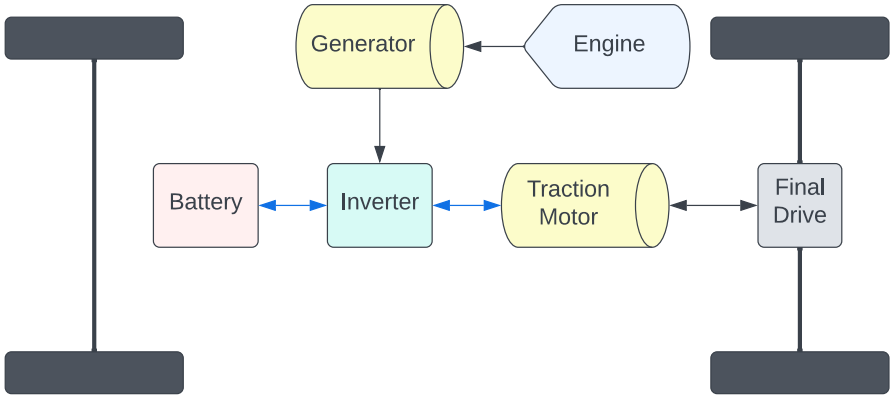

Figure 3.4: A range extended electric vehicle powertrain.

3.2.2 Wrightspeed

Wrightspeed is a company that specializes in retrofitting commercial heavy-duty trucks such as hauling trucks or refuse trucks with an electrified powertrain, instead of being solely mechanical. The electrified powertrain represents a series hybrid configuration, meaning the on-board engine is de-coupled from the traction wheels and one or more electric motors are solely responsible for traction efforts.

A REEV benefits in many ways like a BEV, as it can capture regeneration energy from braking and yields high traction efficiencies using electric machines. Further, a REEV can maintain desirable ranges as it can store a fuel such as gasoline or diesel which are significantly more energy dense than traditional lithium-ion batteries. Because a REEV has great range capabilities, the HV battery that is used to drive the traction motor can be designed with high power density battery cells that often have low energy densities. This means the battery will be able to provide a higher charging and discharging acceptance to the system, increasing the yield of regen energy or higher accelerations at the wheels. A

battery pack that suits these needs will often discharge quickly throughout a cycle and have range limitations, but these limitations will be offset by the energy supplied by the engine. The Route 1000 from Wrightspeed yields around 39 kilometres of pure EV energy [42].

Since the engine is no longer responsible for traction, the existing engine can be significantly downsized from a large diesel engine to a gasoline or compressed natural gas engine. The latter engines will result in reduced GHG emissions and other toxins such as NOx and PM compared to a diesel engine. It should be noted though that companies have the option to use a smaller diesel engine as well, if their existing infrastructure for their truck fleets favours diesel more heavily than other fuel types.

Wrightspeed supplies different powertrains to customers seeking a new life for their vehicles. Their Route 1000 which is used for refuse vehicles boasts a reduction of 60% in fuel consumption paired with around $40,000 in savings for annual maintenance and fuel costs [42]. Typically, these vehicles will be outfitted with an 80kW generator, 295 kW traction motor and a fuel economy of 5.5 MPGe [42] [43]. The total cost for a retrofit is estimated at $250,000 [44].

3.3 Hybrid Energy Storage Systems

A unique type of electrified powertrain architecture uses a hybrid energy storage system (HESS). A typical BEV utilizes one type of energy storage system (ESS), which is battery pack made up of identical cells. The benefit of using a single ESS includes a lower complexity and more simplistic EMS. A drawback of a single ESS is the inability to further optimize for the vehicle's application. Based on the vehicle requirements and powertrain

architecture, an ESS could be required to be more power dense or energy dense. A common trend amongst ESS techniques is to maximize the vehicle range by selecting battery cells that are more energy dense than power dense. In a refuse truck application, the vehicle would benefit from having an ESS that is power dense as well, to benefit from capturing more regenerative braking and higher power output due to the battery pack being able to supply a higher current during charge or discharge.

The ESS structure of a BEV is prone to high peak-to-average power ratios, and as such, the battery type and pack configuration selected for the vehicle must be oversized to account for either the lack of energy or power densities [45]. The effect of frequent high-power loads on the ESS has been found to result in reduced battery cycle life, as various literatures have reported findings of improved battery life when off-loading high power loads from the main ESS to an internal combustion engine or alternate ESS such as an ultracapacitor bank [46] [47] [48] [49].

To address the concern of high peak-to-average power ratios, the ESS can be hybridized into a HESS using two more types of energy storage. Some common combinations of different ESS's include:

1. Battery – Supercapacitor
2. Fuel Cell – Supercapacitor
3. Fuel Cell – Battery – Supercapacitor

This allows usage of both high energy and high power components to create a more robust ESS that can be tailored to a specific application. A common trend from the literature [50]

[45] [51] tends to pair batteries with ultracapacitors. This is because battery technologies traditionally have a high specific energy and suffer from cycle life limitations, whereas ultracapacitors have a high specific power and have extremely long cycle lives. The differences in specific power and energy are visualized below in Figure 3.5.

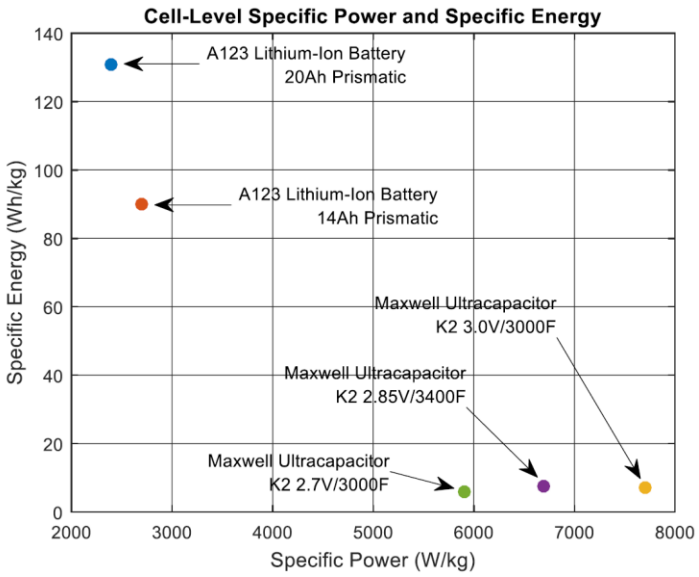

Figure 3.5: Various Batteries and ultracapacitors plotted by specific energy (Wh/kg) vs specific power (W/kg) [52].

Apart from reducing the high ratio of peak-to- average power loads, implementing a HESS has the potential to reduce the pack size of the main high energy battery ESS. Traditionally, BEV's utilize high energy batteries to maximize their range but the cost of doing so results in oversized battery packs to meet the high power requests of the vehicle. By offloading these high power requests to a secondary high power ESS, the HV energy battery can then be optimized to be smaller, while not sacrificing range or the vehicle's performance. As well as, by having a secondary high power ESS, the primary high energy ESS can be sized with a lower power rating, allowing for less expensive cell options to be explored [53].

3.3.1 Topologies

Different topologies of a HESS exist based on how the ESS components are arranged and controlled. If a battery (high energy component) and ultracapacitor (high power component) are considered, they can be arranged in the following ways with respect to the main DC bus of the vehicle:

1. A passive topology has both the battery and ultracapacitor directly coupled to the DC bus and is shown on the left in Figure 3.6. This is the simplest and lowest cost topology. As such, the battery and ultracapacitor must be sized to match the required DC bus voltage, and no control over the power-split between the battery or ultracapacitor. Also, utilization of the ultracapacitor voltage variation (ability to charge/discharge) is insignificant due to being directly connected with the battery ESS [51].
2. A semi-active topology had one ESS connected directly to the DC bus and the other connected through a uni-directional or bi-directional DC/DC converter. By connected the ultracapacitor through the DC/DC seen in the middle portion of Figure 3.6, the voltage requirements of the pack can be reduced, leading to a smaller pack size. Further, the DC/DC converter allows the ultracapacitor pack to have significantly greater variation in voltage compared to a passive topology, allowing for deeper discharge and charge cycles. Additional control strategies can be utilized to control the power that flows to or from the DC/DC converter, leading to a reduction in the ratio of average – to – peak power fluctuations in the battery [50].

The disadvantages of this topology are the added cost and complexity of the DC/DC converter and control scheme.

3. A fully active topology is a continuation of a semi-active topology in that both the battery and ultracapacitor are connected to the DC bus through a DC/DC converter, shown on the right of Figure 3.6. This allows both ESS's voltage ranges to be reduced, resulting in the reduction in the pack sizes of the battery and ultracapacitor. The complexity of this topology is increased compared to the semi-active HESS. Because of the addition of another DC/DC converter, the added weight of the HESS control system may begin to be a more significant disadvantage.

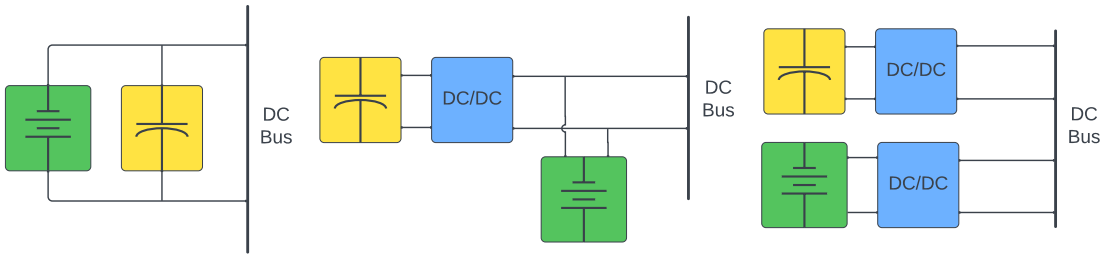

Figure 3.6: Left: A passive HESS topology. Middle: A semi-active HESS topology with the ultracapacitor connected to the DC Bus through a DC/DC converter. Right: A fully-active HESS, where both the battery and ultracapacitor are connected to the DC bus through DC/DC converters.

While considering the HESS topologies, it becomes apparent that each addition of DC/DC converters adds a level of flexibility for a control scheme and operating voltage range, at the expense of added cost and complexity. Most literatures have used one DC/DC converter, or a semi-active configuration, as it overs a good trade-off between flexibility and complexity [50] [54] [55].

3.3.2 Hybrid Energy Storage Configurations

Within a desired HESS topology, there exists various configurations of ESS's that can be used based on the application. Typically, two different ESS's are used in a HESS, where one is a high energy (HE) energy source, and the other is a high power (HP) energy source. Conventional BEV's utilize one type of energy source, usually a single type of HE battery connected in series and parallel to create a battery pack. Since only one type of battery cell is used in the pack, the power capability and energy storage are constrained to the cell type and cannot be modified independently [54]. By using a HESS inside a BEV, the power capabilities and energy storage can be considered separately as a HP energy source can be used to offload peak power demands from the HE energy source. This gives the opportunity for the HE energy source to be sized down accordingly by shifting more focus towards the energy storage requirements. Typical candidates for HE and HP energy sources are described below.

High Energy Sources

NCA (Nickle Cobalt Aluminium Oxide)

This battery cell has great energy density (250 Wh/kg) and a power density of 1.3 kW/kg. The lower power density is due to its high pulse resistance measured using the hybrid pulse power characterization test [54].

LG 18650HG2

This low weight and high energy capacity allow this cell to have an energy density of 240 Wh/kg. This is a significant amount of open-source data on this cell type which makes it useful for vehicle modelling [56].

Fuel Cell

Fuel cells are great high energy density sources and work similar to batteries, although the fuel cell itself does not deplete such as a battery cell does [57]. A fuel cell requires a fuel to operate continuously, such as hydrogen if the application is a hydrogen fuel cell. Fuel cells are like batteries because they convert chemical energy into electrical energy, except they cannot be recharged. As such, fuel cell electric vehicles (FCEV) are typically produced with an on-board HV battery to accept regenerative braking. The battery and fuel cell can be configured to work with each other in a HESS, allowing either component to be downsized in power capacity due to the use of a DC/DC converter. Fuel cells are a magnitude higher in energy density than traditional Li-ion battery cell technology, with some fuel cells having an energy density of over 1600 Wh/kg [58].

High Power Sources

Ultracapacitor

Ultracapacitors are like capacitors as they can discharge and charge rapidly, but ultracapacitors have much higher energy capacities compared to capacitors. They have very high power densities in the magnitude of many kW/kg and low energy densities, typically less than 10 Wh/kg as seen in Figure 3.5. The energy that an ultracapacitor can

store is a function of its voltage. Due to the low energy density of ultracapacitors, many are needed in a pack to have a meaningful impact on energy storage. Ultracapacitors can be utilized in a HESS through a DC/DC converter, allowing the ultracapacitor pack voltage to be lower than the HV DC bus voltage so less ultracapacitors are needed in a pack to reach a desired energy storage capacity.

LTO (Lithium Titanate Oxide)

This battery type has a lithium titanate oxide anode and a nickel cobalt manganese cathode [59]. The lower voltage of these battery cells is a stabilizing feature that eliminates the production of the solid electrolyte interface (SEI) film on the anode. This production of this film over time leads to decreasing battery capacity and thickening of the SEI film, which in turn increases the internal resistance of the battery [59]. As such, LTO cells are more resilient to aging, have excellent low temperature charging and high C-rate charge and discharge performance [59]. Due to the lower nominal voltage of the cells, the energy density is low but the power density is high, compared to other types of lithium-ion cell chemistries, at (60 – 75 Wh/kg) [53] and 3.2 kW/kg [54] respectively. Due to the resilience to aging, these cells typically have a much longer cycle life, in the range of >5000 cycles.

3.4 Summary

This chapter explored the current state-of-the-art powertrain alternatives to traditional internal combustion engine (ICE) vehicles. All-electric and a ranged extender electric vehicle were introduced as alternative powertrains to be the area of focus for the remainder

of the thesis. Real world examples of both powertrains were explored to verify their feasibility in a refuse truck application.

HESS's were explored as a theoretical alternative powertrain, as very little use case in heavy duty vehicles has been documented. The benefits of a HESS could become more prominent regarding fuel cell application in refuse trucks. The high energy density of fuel cells makes them an appealing ESS for refuse trucks over current battery pack technology, due to the significant weight of battery packs sized for heavy-duty applications. Fuel cells typically operate in only one direction, converting chemical potential energy into electrical energy. As such, pairing a fuel cell with a smaller battery pack in a HESS might make sense. The battery pack can act as buffer to current fluctuations on the HV DC bus and accept regenerative braking currents when the truck is braking.

Chapter 4

Data Collection for Refuse Trucks in Hamilton

This chapter introduces the waste collection requirements of Hamilton and the rationale behind the decision to implement a data logger device into select refuse trucks in the city's fleet. The data logger selection and set-up are introduced and explained. An in-depth review is conducted on how to log and decode recorded SAE J1939 on-board diagnostic (OBD) data in refuse trucks including time alignment between data streams, engine torque percentage conversions, truck payload and elevation data. Some data processing logic is shared to assist in streamlining a data decoding process for similar heavy-duty trucks that use the SAE J1939 protocol.

4.1 City of Hamilton Waste Collection Trends

Understanding the waste requirements of a region where a refuse truck will service is necessary to properly size a truck and assist in finding efficient powertrain alternatives. The city of Hamilton was selected because it is the local municipality to where research was being conducted. Hamilton, Ontario, Canada is located near Toronto on Lake Ontario. The city has been split up into three zones for the duration of this study. Zone one includes dense urban regions like the downtown core and surrounding tightly packed residential areas. The types of properties here are primarily industrial, apartment complexes, commercial and various types of dwellings. Zone two is comprised of Dundas and lower west Hamilton. These properties represent a more traditional suburban area with significantly fewer industrial properties than zone one. Flamborough is Zone three and is generally a more rural area composed of farmland with properties that are more spread out and clusters of suburban areas. These zones are illustrated below in Figure 4.1.

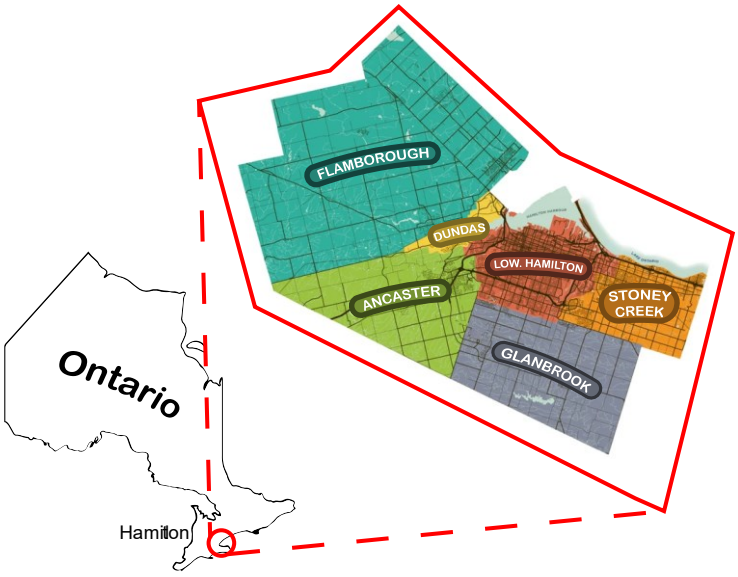

Figure 4.1: Map of Ontario, Canada with an enlarged map for the City of Hamilton. Notable areas include Zone one: Lower Hamilton, Zone two: Dundas and Lower West Hamilton, Zone three: Flamborough [60].

Hamilton has stark differences between its urban and rural communities due to different types of barriers including physical and socioeconomical. The Niagara Escarpment physically separates areas like Flamborough and Ancaster from the lower valley which includes Dundas and lower Hamilton. The escarpment acting as a barrier and the Ontario Green Belt above the valley act as driving factors which lead to dramatically different use of land. This leads to Dundas being mostly a suburban area but travel a few hundred meters to the other side of the escarpment to Flamborough and it is mostly farmland due to the Ontario Green Belt. Similar trends can be said between lower Hamilton and Ancaster where the escarpment acts a barrier between lower income communities in the downtown core in lower Hamilton compared with higher income communities in Ancaster. These differences between communities lead to a varying requirement in waste collection, and as

such the city must accommodate for these differences and ensure their truck fleet is up to the task.

Waste is collected weekly in each of the three zones in separated bins containing garbage, organic and recycling. Most waste is manually loaded into the municipally owned trucks, where some trucks have an assistive loading arm to help tip heavier bins into the collection hopper. Based on a collection route report completed by the city [20], the approximate number of properties of zones one to three are the following: 40,000 properties, 11,000 properties and 13,000 properties.

The garbage disposal needs for each of the three zones in Hamilton from May 2019 to April 2020 are shown in Figure 4.2. The trends here are important in determining the needs for each zone, as differences in the number of properties, geographic location and type of property can vary significantly. It can be seen that Lower Hamilton (zone 1) has the highest requirement for garbage collection whereas Dundas and West Lower Hamilton (zone 2) and Flamborough (zone 3) require comparable amounts of garbage collection. Overall, zone 1 produces approximately 0.57 tonnes per property on an annual basis, whereas zone 2 and 3 both produce around 0.41 tonnes.

The city handles collection of garbage and organics while contracting out recycling collection to a waste collection company. As such, the scope of data analysis includes garbage and organics and excludes recyclables. Compiling all MSW collection data for each zone [20], produces the following trends displayed in Figure 4.3. Trends seen from garbage collection have notable peaks occurring in May and October. A culture aspect in Canada that occurs in Hamilton is spring cleaning, which is an activity many residents

participate in after the winter season has subsided. This can involve decluttering of items in and around a household, contributing to a higher-than-normal disposal of garbage in May. Another trend is with LYW, where higher amounts are disposed of during the months of November, May and June. These months correspond with seasonal factors such as leaf fall during autumn or the start of gardening season in May and June. Another cultural factor in Hamilton is the disposal of Christmas trees where 40 tonnes (zones 1 through 3 have 17, 8 and 17 tonnes collected respectively) were collected from each of the zones during late December and into January.

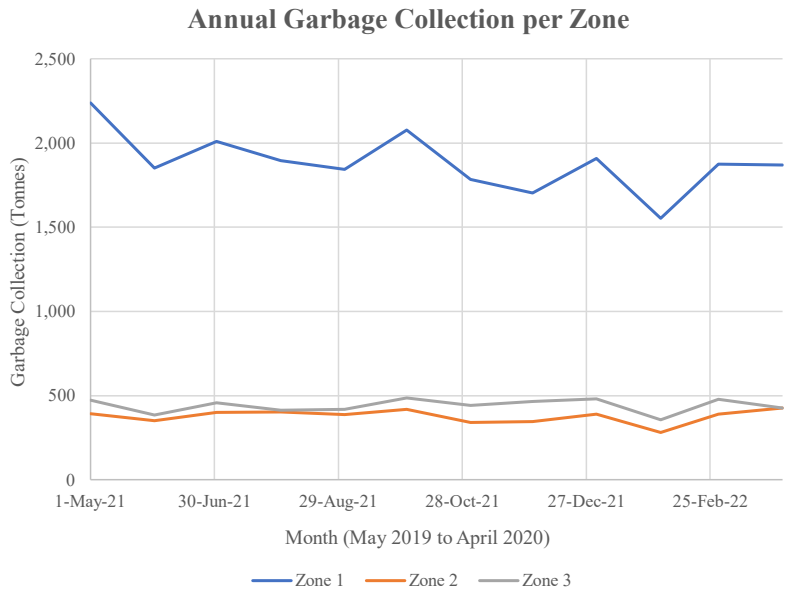

Figure 4.2: Annual garbage collection per zone. Zone 1: Lower Hamilton, Zone 2: Dundas and Lower West Hamilton, Zone 3: Flamborough.

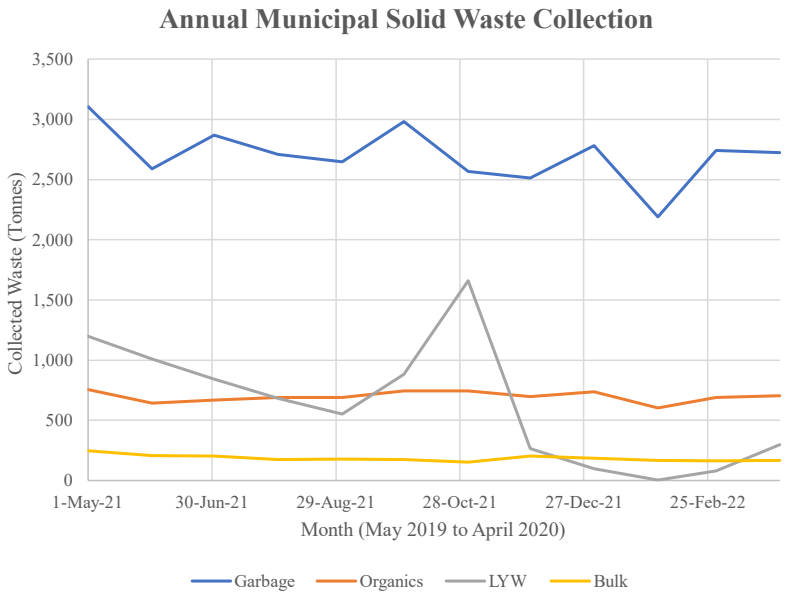

Figure 4.3: Annual municipal solid waste collection for zones 1 – 3, split into the following waste categories: Garbage, Organics, LYW and Bulk.

To service all these locations, the refuse trucks run on predetermined routes 5 days a week, reaching different areas within the zones each day. Most refuse trucks are rear or side-loading vehicles with some being a split bodies capable of collecting two types of waste. Two side-loading trucks are used in the Downtown Cleanliness Program, which is an initiative by the city to collect street-side public waste containers. The split bodies can either collect garbage and organics or LYW and organics. The number of trucks in the city's fleet are shown in Table 4.1 , with most of them being class 8 trucks.

Table 4.1: A breakdown of the City of Hamilton's refuse truck fleet.

Type of Collection	Number of Trucks
Garbage	8
Garbage & Organics	10
Organics & LYW	8
Bulk Waste	2
Downtown Cleanliness	4
Spare	6
Total	**38**

As discussed, the city has information on how much waste the city produces daily, approximate number of stops along some routes and general information on their truck fleet using fleet telematic software. The city does not keep high fidelity data on trucks in their fleet, which is required to approximate the energy and power demands that their trucks are exposed to daily. Understanding these energy and power demands is critical in determining what electric powertrain alternatives might meet the demands the city has on waste collection. High fidelity data for energy and power approximations typically requires a resolution of 1 Hz or less and examples of this data can include:

1. Vehicle speed and GPS location.
2. Truck controller area network (CAN) information.
3. Route information such as number of stops, incremental change in payload, the activation of the PTO.

Since this type of high-fidelity information is not available directly from the city, a method to capture this data in-situ had to be developed. A type of data logger that can record both GPS and CAN data

4.2 Data Logger Selection

To create a duty cycle that represents the functionality of a refuse truck in Hamilton, an OBD data logger with GPS was installed as a non-invasive approach to collecting data. The chosen data logger was the *CANedge2* with the CANmod.GPS add-on [61]. This device was chosen because of its small footprint and low power draw from the truck (~2 Watts). This means the data logger will not affect the operator's day to day routine and not require any additional sensors installed into the truck. The data logger plugs into the trucks J1939 OBD port and is capable of logging J1939 OBD and GPS data at a sampling rate of 1 Hz to an extractable memory card. Each day totalled approximately 100 MB of raw data. The logged parameters are displayed in Table 4.2.

Table 4.2 Logged parameters from the *CANedge2* data logger with CANmod.GPS attachment.

Device	Parameter	Unit	Device	Parameter	Unit
CANmod.GPS	Time	Epoch	CANedge2	Engine Speed	RPM
	Altitude	m		Engine Torque	%
	Vehicle speed	m/s		Fuel Consumption	L/h
	Latitude and Longitude	Degrees		Engine Air Mass Flow Rate	Kg/h
	Pitch	Degrees		Trip Distance	m
	Roll	Degrees		Ambient Temperature	ºC
				Transmission Gear	R, 1 – 6
				PTO Governor Switch	ON/OFF
				Brake Switch	ON/OFF

4.3 Data Logger Set-Up

The CANmod.GPS plugs into the *CANedge2*, and the *CANedge2* plugs into the CAN or J1939 port inside the driver's cabin by the steering column, shown in Figure 4.4. This port provides both raw CAN data and power to both units making this set up very easy to install.

This assembly is placed in an out of sight location to not interrupt the operators. The CANmod.GPS has an antenna with a magnet that can be affixed to a suitable location in the cab. It was identified that some components on-board the truck such as radio receivers disrupted the ability for the data logger antenna to receive GPS signals. An ideal location for the antenna is on a metal surface in the driver cab away from any instrumentation. The physical assembly of the entire data logging unit is shown in Figure 4.5. Not included in the photo is the 3-meter extension cable used between the J1939 connector and the data logger.

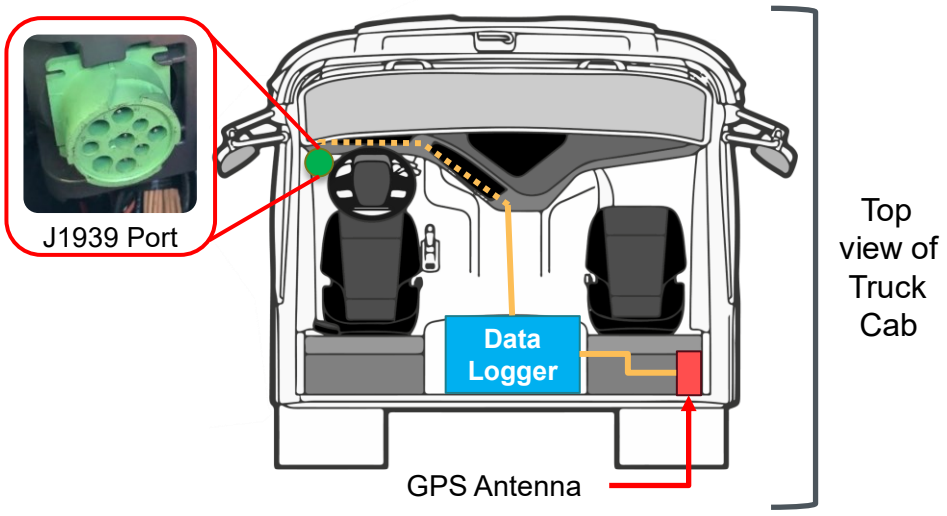

Figure 4.4: A J1939 port located by the steering column on a 2013 Freightliner 108SD model.

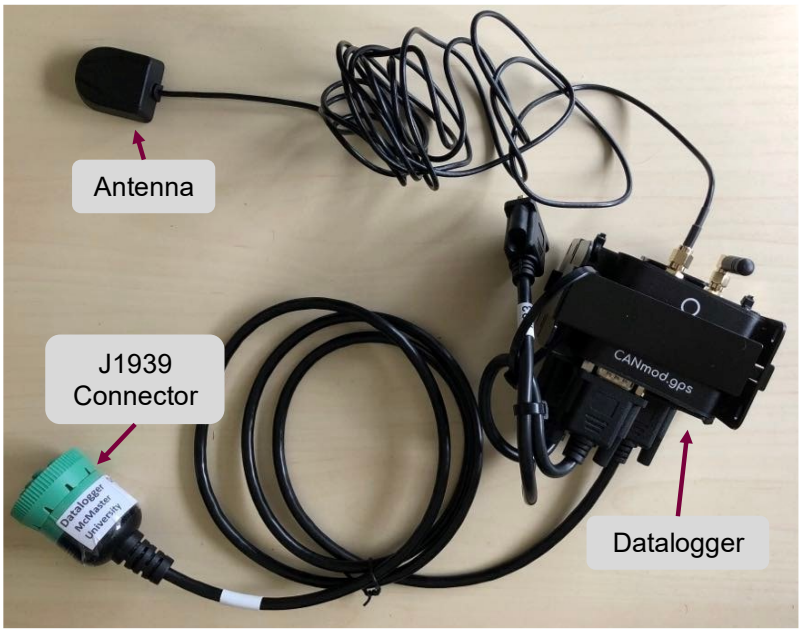

Figure 4.5: The physical data logger set-up, including the GPS antenna, data logger, GPS add-on and J1939 CAN connector.

Figure 4.6: The data logger installed into the split side-loading rural/urban truck. Left: The data logger unit was placed behind the driver's seat. Right: The J1939 connection is by the steering wheel column.

Other precautions were considered before installing the data logger into the truck. Sections of cable were exposed on the bottom of the cabin floor, creating the possibility of being stepped on or other objects being placed on the cables. To prevent any wear and tear, the J1939 connector cable and the extension cable were wrapped in a plastic cable protector, shown in Figure 4.6 (right). Also, in the refuse environment, there is a possibility of rodents chewing on wires, which the cable protector can help mitigate. No wear and tear issues were encountered while using the plastic cable protectors.

Another precaution was placing the data logger unit in a container, shown in Figure 4.6 (left). The data logger unit is not rated for a dusty or damp environment and the container helped mitigate some of the environmental effects. As well as the container acted as a barrier to prevent any foreign objects from hitting the unit. A concern with the J1939 connector was the possibility of it becoming disconnected from vehicle vibrations. Some electrical tape was used to secure the connector, which worked well. Lastly, extreme

weather rated zip ties (-40ºC to 80ºC) were used to secure cables and the data logger unit to secure points in the driver's cab. The trucks are either parked outside or in a warehouse and are subject to the outside elements, especially overnight. Typical zip ties were found to become too brittle in the wintertime and would break apart.

Before installation, it was unknown if the data logger would remain on while the truck was shut off. To adequately plan for unwanted power draw from the truck's low voltage battery, it was assumed that the data logger would draw power at all times of the day. The data logger and GPS add-in draw approximately 1 W each, for a combined power draw of 2 W. Over the span of a day, that is 48 Wh or 96 Wh per weekend. The chassis manufacturer of the truck specifies up to three 100 Ah can be installed, depending on the options selected by the customer. To assume the worst case, one 100 Ah battery was considered. A 100 Ah battery at an operating voltage of 12 V has a capacity of 1200 Wh. If the truck was not used for the span of one day while the data logger remained on, 4% of capacity would be drained. Over a weekend an 8% in capacity drain would be seen. These potential outcomes were deemed acceptable.

To further reduce the potential impact of the data logger on the truck's low voltage battery, the GPS add-on was configured to only be on from 6 AM to 6 PM, as this could be controlled from the data logger interface. Outside these hours, the potential power draw would be 1 W instead of 2 W. The typical operating time of the trucks ranged from morning to early afternoon. This time range allowed for adequate coverage of atypical schedules, if any.

After the initial trial was completed, referred to in Section 5.2 in Table 5.1, it was found that the data logger shuts off when the truck shuts off. This is because the operators turn off the truck's low voltage battery at the end of the day. It is still possible on other truck models that turning off the battery switch will still power some auxiliary components, like the data logger. As such, this is an important observation to make after an initial trial on a new truck. This was confirmed as no CAN data was logged outside of the truck's operating time.

Another consideration on the data logger set-up was how the data was logged to the extractable memory card. There are many configurations that the researcher can control such as logged file size which was set to a maximum size of 50 MB. Also, the files were split after midnight (00:00) if the file size of 50 MB was not reached. This ensures that one logged file does not include data from two different days. It was observed that with this set-up, two files were usually created for one day of operation. One file was 50 MB in size while the other was between 10 – 40 MB. To improve this set-up, the maximum size of the logged file before splitting should be increased to 150 MB. This would allow one file per day of operation, making data processing easier.

Lastly, the interface between the data logger and the truck's CAN port had to be configured. The data logger can receive, acknowledge and transmit signals to the truck's CAN. To avoid unseen communication between the truck and the data logger, the data logger was configured to only receive and acknowledge CAN signals. The remaining options are specific to the data logger manufacturer and the *CANedge2 Intro and Tools* guide was referenced to complete the set-up [62].

4.4 Extraction of Data and Decoding

The data logger records GPS and CAN J1939 data from the vehicle's controller area network (CAN) in a raw MF4 file format. The raw CAN data is communicated through the SAE J1939 protocol in heavy-duty trucks. This raw file format must then be decoded using a DBC file for the data to be interpreted in a practical sense. This process is outlined in the below figure.

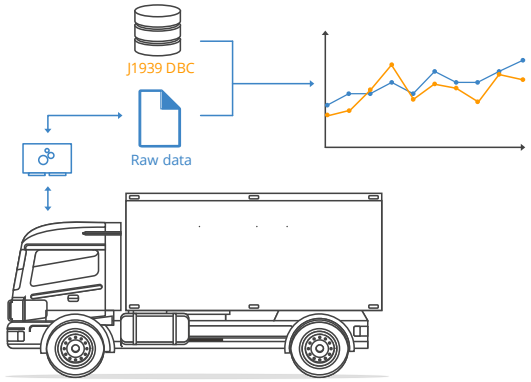

Figure 4.7: A simplified flow chart of how raw data is logged and decoded using a J1939 DBC file [61].

The raw J1939 data organizes CAN parameters through a series of suspect parameter numbers (SPNs) grouped into structures of parameter group numbers (PGNs). SPNs identify specific vehicle metrics such as engine speed or wheel speed. Most of the PGN's encoded structure are standardized across a wide range of truck manufactures, simplifying how the signals can be decoded. To decode the PGNs, the MF4 is first finalized into a format by ASAM measurement data format (MDF) standards, using the following MATLAB command:

```
mdfFinalize()
```

Finalizing the MF4 into MDF format allows proper sorting to be completed and enables compatibility with the Vehicle Network Toolbox™ in *MATLAB*. Next, the finalized MDF can be decoded by a database (DBC) file into readable parameters, which was obtained from *CSS Electronics* [61].

As previously mentioned, heavy duty trucks use the SAE J1939 standard protocol [63] and thus many CAN SPNs are shared across a wide range of truck manufacturers, meaning a generic J1939 DBC file can be used in this case. Similar to the data logger recording raw CAN data, the GPS unit records data in a raw .mf4 file format as well and must be decoded using the manufacturer's CANmod.GPS DBC file [61]. The process to extract the raw data into readable parameters for both GPS and CAN data are shown in Figure 4.8.

Line one formats an MDF file into a raw timetable using the read() function, where can_idx is equal 8 as this is the number of CAN channels considered while finalizing an MDF through MATLAB. Next, line two converts the existing CAN channels in the timetable from a flexible data (CAN FD) rate to a classical form by removing the extended data length (EDL) formatting from the indexed channels [64]. Line three converts the timetable into individual timetables of signal values captured over the J1939 protocol, using a DBC file to decode the signals.

```
1. rawTimeTable = read(m,can_idx,m.ChannelNames{can_idx});
2. rawTimeTable = removevars(rawTimeTable, "CAN_DataFrame_EDL");
3. msgTimetableJ1939 = j1939ParameterGroupTimetable(rawTimeTable, canDB);
4. msgEEC1 = j1939SignalTimetable(msgTimetableJ1939, "ParameterGroups","EEC1")
```

Figure 4.8: *MATLAB* code used to convert raw .MF4 files into readable J1939 timetable data.

Line four illustrates an example for extracting a certain PGN, *EEC1*, that contains information about some engine parameters. A sample of this PGN showing the individual SPN's of engine percentage torque and engine speed are shown in Table 4.3. There are many other SPN's in each channel message and the relevant ones can be extracted as needed. A similar process described for extracting CAN data can be used to extract the data from the GPS unit.

Table 4.3 A sample decoded J1939 timetable message

Time	EnginePercentTorqe	EngineSpeed	→
'2022-04-21 10:59:43.568000000'	39	140.75	
'2022-04-21 10:59:44.568250000'	25	723.375	
'2022-04-21 10:59:45.568349999'	28	729.25	⋮
'2022-04-21 10:59:46.568400000'	29	741.125	
'2022-04-21 10:59:47.568500000'	30	736.375	
⋮	⋮	⋮	

Usually, a manufacturer will have their own DBC file that contain instructions for decoding signals from their manufactured components. The user will know what parameters they have access to only after logging the available CAN SPNs and decoding them, as manufacturers do not release a list of SPNs available for each vehicle model.

4.4.1 Sampling Frequency

The sampling frequency of the GPS unit and data logger were set to a target of 1 Hz, but the sampling frequencies between these two devices fluctuated over time. For simplicity, the CAN data time was interpolated to match the internal real-time clock on the GPS unit

at a sampling frequency of 1 Hz. The sampling frequency of the GPS unit was consistently kept at 1 Hz, whereas the CAN data showed a higher variance in sampling frequencies.

4.4.2 GPS and CAN Signal Time Alignment

Aligning the GPS and CAN data allowed the location of the truck to be in sync with the measured CAN data to allow comparisons to be made. As such, it is important to verify the time occurrence of each GPS signal is aligned with the CAN data. Conveniently, the GPS add-on records vehicle speed in m/s and the data logger records wheel speed through the CAN port in km/h. These signal traces can be compared after interpolating to confirm whether the CAN data is time aligned with the GPS data. A sample comparison of these traces is shown below where both signals are in m/s. It should be noted that when the GPS antenna's signal is impeded by a physical barrier such as under a bridge, the measured speed from GPS is invalid.

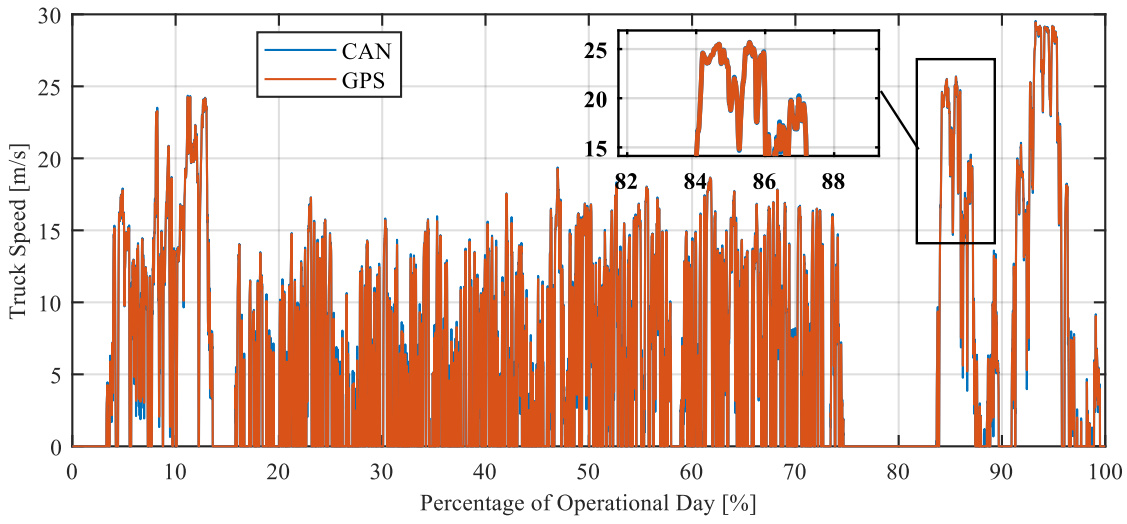

Figure 4.9: Vehicle speed signals captured from CAN and GPS, showing their alignment with respective to time.

Attention must also be directed towards the beginning and ending of daylight-saving time (DST), as the data logging period occurred during the transition to DST. In Canada and among other participating countries, DST is the practice of setting clocks one hour forward in warmer months, then bringing clocks back an hour in colder months. As a result, a day in March will be 23 hours whereas a day in November will be 25 hours, due to changing of clocks for DST. In Canada, Ontario which is in the eastern time zone, the colder months operate in eastern standard time (EST), and the warmer months operate in Eastern Daylight Time (EDT). Because the data logger's real-time clock is based on Universal Time Coordinated (UTC) and the refuse truck operates in EDT or EST, the conversion from UTC time must be adjusted accordingly. The following time zone differences are observed for both EDT and EST.

- EST (Autumn/Winter) is 5 hours behind UTC (UTC-05:00)
- EDT (Spring/Summer) is 4 hours behind UTC (UTC-04:00)

4.4.3 Conversion of Percentage Engine Torque

Some additional steps had to be considered after the data was decoded. Engine torque is recorded as a percentage of the engine torque-speed relationship. The engine torque percentage was converted to newton-meter using a torque-speed relationship of a similar sized diesel engine [65], that was calibrated using information from the manufacturer and illustrated in Figure 4.10. Additional proprietary information from the engine manufacturer may be needed to formally convert the engine torque percentage, but the engine torque is assumed to be a percentage of the below curve given an engine speed.

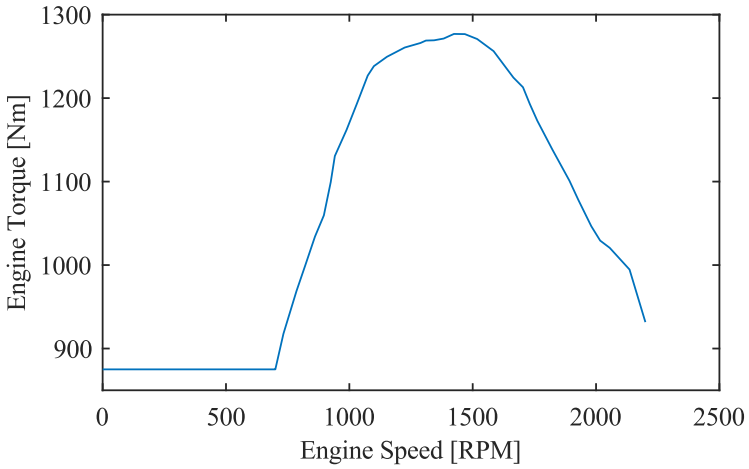

Figure 4.10: Diesel engine torque-speed performance curve.

4.4.4 Interpreting Elevation Data

By default, the GPS unit directly measures altitude using trilateration which approximates the truck's 3-D position on the earth's surface. This method of altitude approximation is not suitable for automotive applications due to a measured uncertainty of +/- 5 vertical meters which led to a root mean square error (RMSE) of over 400 each day. Instead, the digital elevation map from the United States Geological Survey called the National Elevation Dataset (NED) was used with an overall RMSE of 1.55 meters [66], that includes coverage of Canada. The NED has been compiled into a lookup dataset on *GPS Visualizer* [67], where pairs of latitude and longitude coordinates can be uploaded to find the corresponding elevation. This described method of aligning location data with elevation data works well for low amounts of individual trip data.

It became tedious when compiling large amounts of trip data across many separate days, as each day has a unique array of longitude and latitude coordinate pairs to be indexed with

elevation data. To work out this bottle neck in data processing, a local elevation profile of Hamilton was created, to reference for all refuse truck operation. Because the location of all refuse truck operation occurs within a set boundary, a digital elevation map (DEM) could be created for this specific area. A *MATLAB* function called *Terrain Elevation* [68] was used that enables a grid of elevation data from the USGS NED to be queried given a range of latitude and longitude bounds. This queried data is stored locally and is at a 1 arc-second resolution, or a resolution of 30 horizontal meters. The latitude and longitude coordinates of the truck over the span of the day can be used to interpolate the respective elevation using 2-D interpolation. This method is much quicker as it reduces a lot of human interaction of downloading sets of new elevation data for each day individually. The grid of elevation data representing a region of Hamilton, where the studied refuse trucks operated is shown below in Figure 4.11.

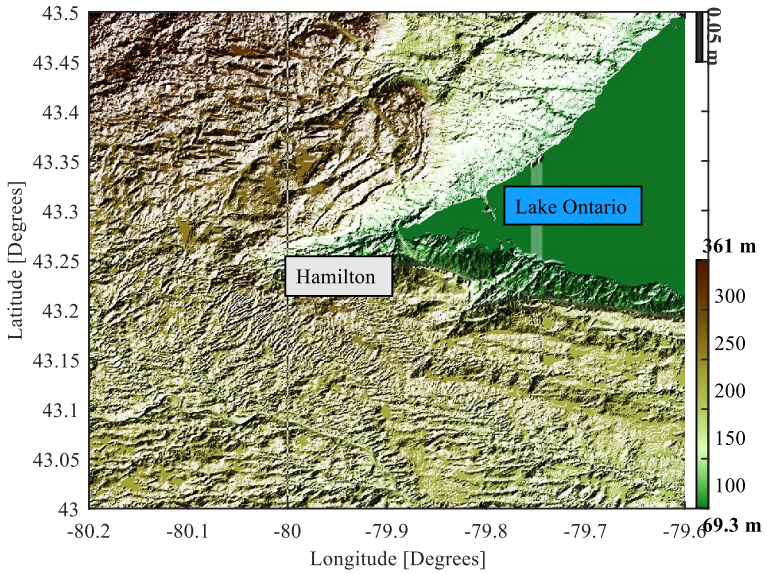

Figure 4.11: A digital elevation map of a region in Hamilton and some surrounding municipalities.

A comparative analysis between the interpolated elevation using the data from Figure 4.11 and data from *GPS Visualizer* was completed. The data from *GPS Visualizer* was assumed to be the best-in-class data available for the Hamilton region. The comparison between the two elevation traces are shown in Figure 4.12.

Overall, the interpolated elevation data from the USGS NED matches what *GPS Visualizer* outputs with an RMSE of 0.102 over an entire day. This should be expected as *GPS Visualizer* also queries from the USGS NED. There are some differences in peaks between the traces were the interpolated elevation data usually overshoots both below and above the peak values from *GPS Visualizer*. This means more caution should be considered when smoothing out noise due to bridges or other irregular changes in elevation.

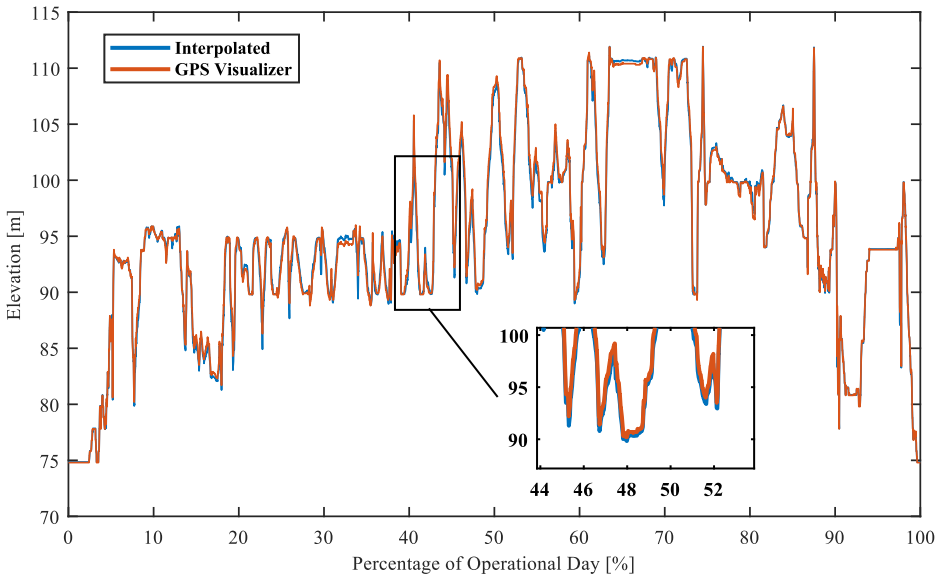

Figure 4.12: A comparative plot between queried elevation data from *GPS Visualizer* versus the developed DEM for Hamilton.

4.4.5 Estimating Truck Payload

The truck's mass could not be directly measured throughout the day due to lack of sensors and the cost and complexity of installing an appropriate sensor. The mass of the truck before and after the workday was recorded at the scale houses located at each offloading site. To approximate the gradual gain of truck mass while in the collection zone, a constant mass was added to the truck at each stopping event that reflected the overall gain of truck mass during the day. The techniques behind stop estimation are elaborated in Section 5.6.

Alternatively, it would be possible to approximate the truck's mass using Newton's second law given by Eq. 4.1.

$$F_{net} = ma \qquad \text{Eq. 4.1}$$

To understand the free-body diagram of a refuse truck, Figure 6.3 in Section 6.3 should be referred to. Given Eq. 4.1, as the trucks mass (m) increases, the net force (F_{net}) applied to the truck must also increase to sustain the same acceleration (a). Thus, it would be possible to measure the change in engine torque over the day to approximate the truck's mass. To minimize the error in this approximation, only route segments where the roadway is flat should be considered to reduce the impact of road grade estimation. An additional driving factor that was not measured during this study is wind speed. Depending on the aerodynamic coefficient of the vehicle, wind speed can significantly affect the road loads.

4.5 Summary

This chapter introduced the waste requirements for the City of Hamilton to assist in outlining what a refuse truck should be capable of to successfully collect all the

municipality's waste. The selection criteria in determining the data logger were discussed and the chosen data logger was presented. Framework was created to assist in setting up the data logger and successfully capturing data and decoding it to be meaningful for data analysis. A walk-through example for decoding a CAN PGN is explained, allowing a similar process to be completed for other PGN's of interest. Some limitations were discussed such as the errors involved with approximating the elevation at each time instance as well as estimating the truck's payload within the collection zone.

Chapter 5

Developing Refuse Truck Drive and Duty Cycles

This chapter introduces what a drive and duty cycle are and how it relates to modelling of refuse trucks in a software environment. This chapter also contains additional data processing that was done on-top of the work completed in Chapter 4 to obtain trends such as the number of stops the truck made in the collection zone or defining the road grade. A notable topic discussed in this chapter is differentiating when a refuse truck is in the collection zone or off-route in the form of geo-referencing. This vehicle specific route characteristic could allow better control on how energy is utilized in the powertrain, as different driving habits are present along the trucks route. Geo-referencing can also be applicable to other vehicles that operate on a back-to-base route style and a specific purpose along their route such as delivery vehicles, buses and more. Finally, the chapter concludes with general operating trends for both refuse trucks that were studied using the data logger.

5.1 Defining Drive and Duty Cycles

Drive cycles are critical inputs to vehicle models as they describe the vehicles velocity with respect to time, giving the model an idea on how the vehicle must accelerate or decelerate to account for the powertrain's spent energy. Since a refuse truck has added functionality compared to a typical car, a duty cycle can be used to compliment the drive cycle. For the application of a refuse truck, the duty cycle is composed of a mass cycle and a power cycle, or a hydraulic load cycle. Together, these cycles can be used as an input to a vehicle model to accurately track the energy and power requirements of a refuse truck, illustrated in Figure 5.1.

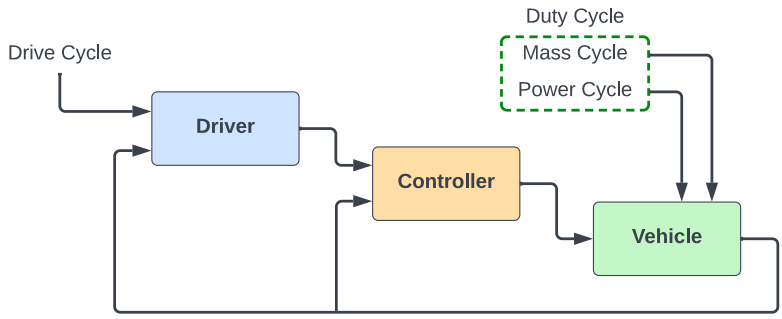

Figure 5.1: An illustration showing how a drive and duty cycle are used as inputs in a top-level view of a vehicle model.

Generic duty cycles can be developed from online resources such as the Nation Renewable Energy Laboratory (NREL) or more tailored duty cycles can be created for a specific municipal region with measured data [69]. Some in-depth literature has been published in partnership with the NREL on important considerations needed to create an accurate refuse truck driving and duty cycles [7], with other authors also contributing to this field of study.

One study investigated a deep look into the engine loading from hydraulic system through the PTO [6], for a truck in Poland. The investigation looked at a twin-flow fixed displacement hydraulic pump that powers an assistive loading arm (ALA) or compaction operation, where the ALA and compaction are on separate hydraulic circuits. The data was collected using pressure transducers installed into the hydraulic circuit, and truck data through the CAN bus. Some key findings are that the engine operates at inefficient operating regions while the PTO is engaged, as the PTO is usually active when the truck engine is idling. It should be noted that the PTO can run when the truck is in first or second gear as well, but typically operators use the PTO when the truck is idling.

Further, it was determined that driver habits have less of a significant impact on fuel consumption in refuse trucks compared to other heavy-duty trucks without a PTO such as long-haul trucks. Since refuse trucks have a PTO, reducing fuel consumption is more largely driven by appropriate truck powertrain optimization for its intended purpose.

Another study looked at urban refuse truck operation across various cities in the United States, across varying ambient temperatures, road grade and waste collection requirements [7]. Data was collected using a CAN bus data logger, GPS antenna, truck scale houses and pressure transducers installed in the hydraulic circuit. This data was used to analyse operation trends and construct drive and duty cycles, where the duty cycle is composed of a mass and power cycle. These cycles will be defined in the subsequent sections of this chapter. This was the first documented drive and duty cycle study that was found and provided the framework to construct the data collection, processing and analysing portions of this thesis.

These efforts to accurately model the energy and power requirements of refuse trucks are to provide more data on the current state of refuse truck operation, and how they can be hybridized, electrified or run off alternative fuels rather than the traditional diesel fuelled trucks. There are other clear distinctions of refuse truck drive and duty cycles versus other heavy-duty vehicles such as, the number of frequent stops and starts that occur, the need to handle variations in road grade and the consistency in predetermined routes that a specific truck will travel each day.

As mentioned previously, drive and duty cycles have been developed in literature, but the open access to complete drive and duty cycles of realistic truck usage is limited. Further,

the representation of refuse truck operation for rural routes is underrepresented. Studying refuse truck operation first-hand in the City of Hamilton will provide answers to these gaps in research.

5.2 Research Collaboration with the City of Hamilton

The City of Hamilton in Ontario, Canada was approached to form a research collaboration with the McMaster Automotive Resource Centre (MARC) to allow data collection from their refuse truck fleet. This collaboration allowed two different trucks to be studied, one that serviced urban areas and another that serviced a mixture between urban and rural areas. The data logging took place over 5 operating days per week for a span of 15 weeks, totalling approximately 500 hours of operation. Details about each week of logged data are displayed below in Table 5.1.

Table 5.1: The sequence of data logging trials in an urban and urban/rural refuse truck.

Week	Month	Area Type	Type of Data Collected
1	January 31 – February 4	Urban	CAN/GPS
2	March 7 – 11	Urban/Rural	CAN/GPS
3	March 14 – 18		
4	March 21 – 25		
5	March 28 – April 1		
6	April 4 – 8	Urban	CAN[4]
7	April 11 – 15		
8	April 18 – 22		
9	April 25 – 29		
10	May 2 – 6		
11	March 31 – June 3[5]	Urban	CAN/GPS
12	June 6 – 10		
13	June 13 –17		
14	June 20 – 24		
15	June 27 – 29[5]		

The two trucks are both categorized as class 8 vehicles and have similar vehicle components. These components are displayed in Table 5.2.

The major differences between these trucks are how MSW is loaded into the truck, illustrated in Figure 5.2. The RL-RT has a rear compaction chamber, whereas the split SL-RT gives the operator the ability to load garbage and organics into the side, into separate chambers.

[4] GPS data was not recorded for this duration as the signal to the GPS antenna was disrupted by an on-board communication radio and will not be included in the analysis of this paper.

[5] Indicates that data was not collected for the entire week.

Table 5.2: The parameters for the refuse trucks of interest at the City of Hamilton,

Component	Description	
Truck Type	Rear-Loader	Split Side-Loader
Engine Type	8.3 L Diesel Engine	8.9 L Diesel Engine
Advertised Engine Power at 2000 RPM	223 kW	223 kW
Curb Mass	14400 kg	16000 kg
WCU Type	Manual Rear-Loader	Split Side-Loader with Assistive Loading Arm
WCU Capacity	19 m^3	10 m^3 | 15 m^3 split
Wheel Specification	315/80R22.5	315/80R22.5
Service Area	Urban	Urban and Rural
Final Drive Ratio	5.29	5.29
Transmission	6 Speed Automatic	6 Speed Automatic

Figure 5.2: The rear-loading compaction chamber (left). The split side-loading compaction chambers (right).

5.3 Route Characteristics Review

The truck fleet is stationed at a truck yard in Lower Hamilton, where trucks leave for predetermined routes around the city and pick up MSW in a collection zone. An example route for the split SL-RT urban/rural refuse truck is shown in Figure 5.3. Once the trucks have serviced the entire area, garbage is offloaded at one of three transfer stations and organics are offloaded at a processing building at the truck yard. In this case, the truck offloads garbage at the Dundas transfer station. Over the duration of this study, the trucks serviced the same routes on each day of the week. There are a few instances where a truck will go off its predetermined route to collect MSW in other areas, perhaps to cover the load for another truck.

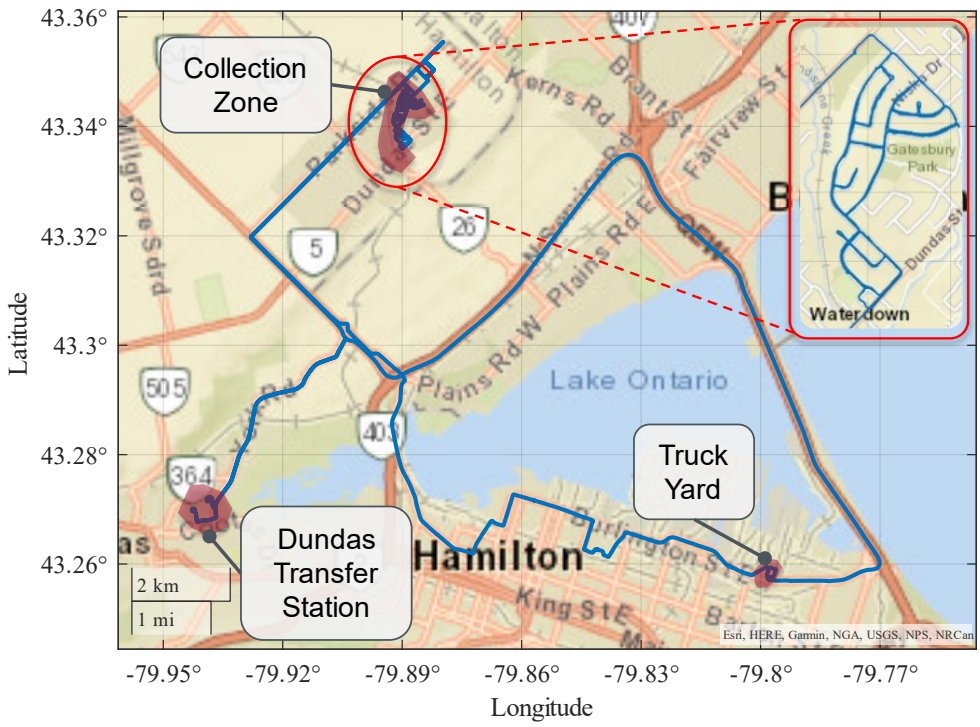

Figure 5.3: A route overview of a typical urban refuse truck operational day in Flamborough, where the GPS location of the truck is shown in blue.

5.4 Collection Zone Geo-Referencing

The operation of the truck was split into collection zone and off-route segments. The collection zone refers to when the truck is picking up curb side MSW from residential properties. Off-route refers to when the truck is travelling between the truck yard, collection zone and offloading sites. Each segment was georeferenced by constructing a perimeter of latitude and longitude coordinates. Since the latitude and longitude of the truck was known at sampling frequency of 1 Hz, this could be tracked accurately.

Some aspects of data processing such as estimating the number of stops the truck collected MSW at, or the change in truck payload, required isolating the truck while it was in a collection zone. Additionally, the isolation of the truck in the offloading sites was required to observe the hydraulic power required while offloading MSW. To identify when the truck was within these areas along a route, each area's perimeter was geo-referenced using latitude and longitude coordinates in decimal degree ($\pm°$) units. An example collection zone for a route is shown in Figure 5.3, illustrating how the geo-referenced perimeter was set-up.

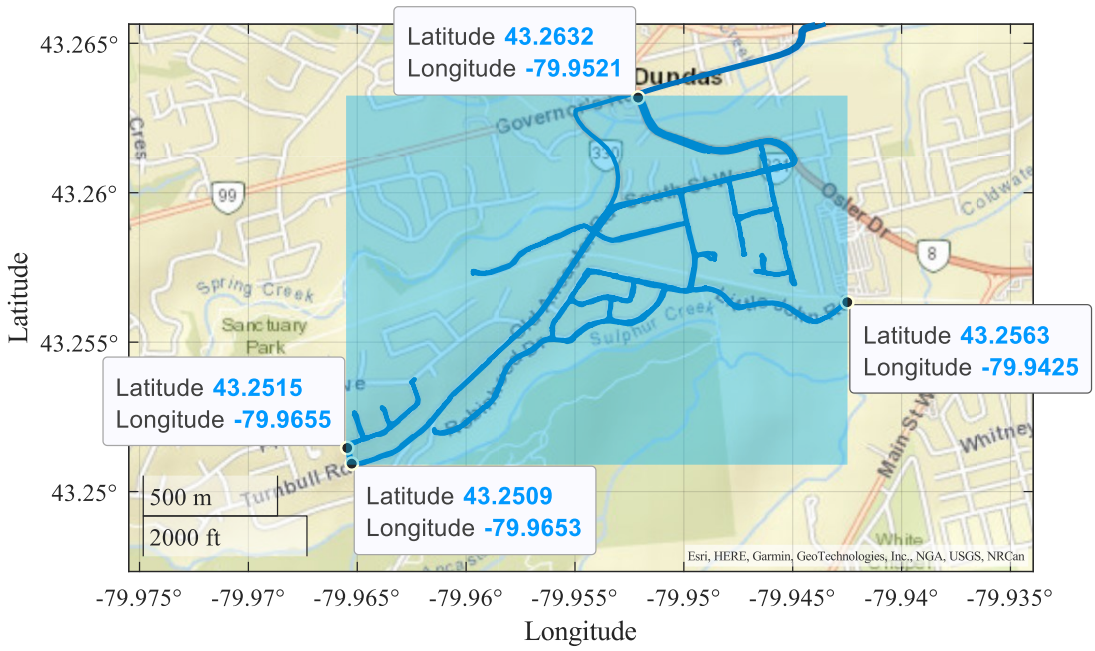

Figure 5.4: Geo-referencing a sample collection zone of a refuse truck's route.

For the collection zone in Figure 5.4, a pair of latitude and longitude coordinates are defined for the outer edges of the truck movement within the zone, creating a bounded area shown in light blue. A buffer of 0.0005º was used to enlarge the bounded area to account for human error in marking the upper and lower bounds of latitude and longitude coordinates. The buffer value was calculated through trial and error where it is large enough to account for human error but small enough to not include significant area outside the bounded zone. This method can be repeated to identify when the truck is in other key areas such as the truck yard or transfer station.

5.5 Driving Cycle

The drive cycle is a time series of the truck's velocity profile at a time-step of 1 second and provides instructions on how the vehicle needs to accelerate or decelerate. Samples of

urban and rural drive cycles are shown in Figure 5.5 and Figure 5.6 respectively with collection zone and off-route segments visually identified. As mentioned previously in this chapter, the GPS location of the truck was used to characterize when the truck was in the collection zone or off-route. The collection zone is when the refuse truck is travelling between each household along its designated route, consisting of frequent accelerations and decelerations during numerous stops and starts where the payload is estimated. The off-route segments consist of higher sustained speeds and simulates the refuse truck traveling between the truck yard, transfer station and collection zone where the payload is known.

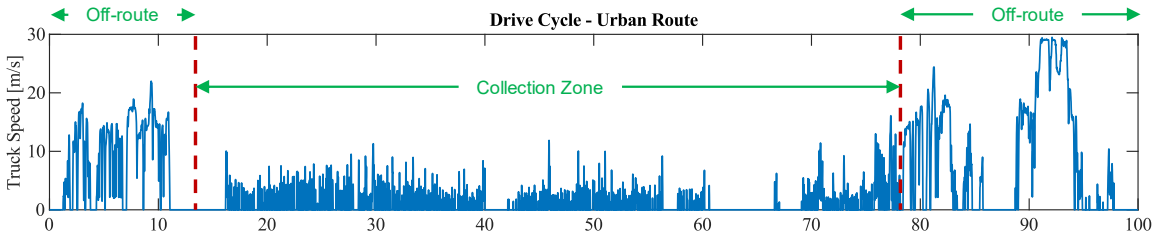

Figure 5.5: An urban refuse drive cycle route that services the downtown Hamilton Region.

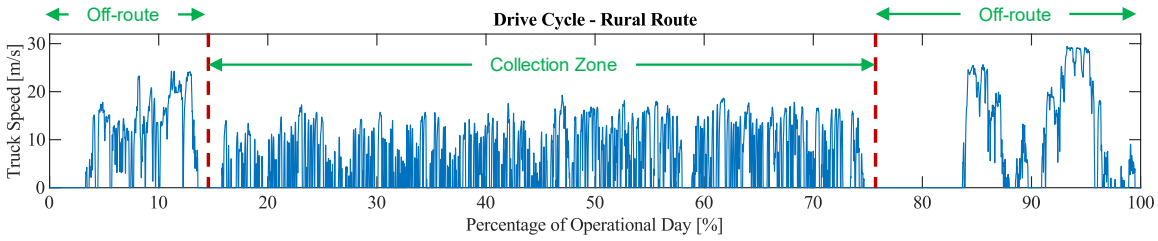

Figure 5.6: A rural refuse drive cycle route that services the Flamborough region in Hamilton.

5.6 Estimating the Number of Household Stops

The speed of the truck was used to estimate the amount of household stops while in the collection zone. To achieve this estimation, a *MATLAB* script was used to identify instances when the consecutive truck speed was 0 m/s. If the speed was 0 m/s for 3 consecutive seconds or more, a stop was added to the accumulated number of households stops for that day. This number was determined from the literature as the lowest average stop time at a household [70], as any stop longer than 3 seconds would be included as well. Because the vehicle speed is determined using the on-board wheel speed sensor of the truck, the speed accuracy is assumed to be acceptable.

The function shown in Figure 5.7 has the following workflow, where (v_veh) is the speed of the vehicle and (N_stops) is the number of stops on a route. Line one defines the minimum duration in seconds required for the threshold to be true. Line two defines the threshold (v_veh = 0) and the sign change between when the threshold is true for the minimum duration or false. When the threshold and minimum duration conditions are true, *runedges* increases from 0 to 1. When the conditions are no longer met, *runedges* will equal -1, then return to 0. Line three extracts indices when *runedges* is equal to 1 or -1. Line four calculates the *runlength* (stop duration) for each stop occurrence. Line five filters and keeps stops with a stop duration greater than or equal to the minimum duration. Line six calculates the total number of stops that meet the threshold and minimum duration conditions.

Function (Find Consecutive Instances for a Minimum Duration and Threshold):

```
1.  min_duration = 3;
2.  runedges=diff([false(1,size(v_veh,2));v_veh==0;false(1,size(v_veh,2))]);
3.  [edgerow, edgecol] = find(runedges);
4.  runlengths = edgerow(2:2:end) - edgerow(1:2:end);
5.  longruns = runlengths >= min_duration;
6.  N_stops = accumarray(edgecol(2:2:end), longruns)';
```

Figure 5.7: The *MATLAB* function used to estimate the number of stops along a route.

Using the above function, each stop can be defined. A sample route for the rear-loading refuse truck is shown below in Figure 5.8, with the GPS location of the estimated stops along the route shown in the collection zone.

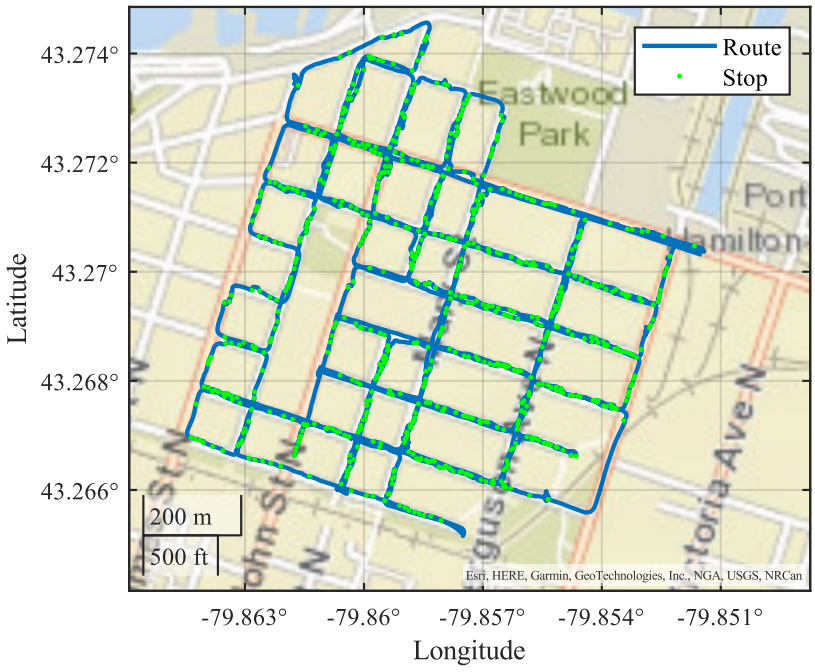

Figure 5.8: The dispersion of stops illustrated for the rear-loader refuse truck on a route.

5.7 Road Grade

Road grade (α) describes the incline or decline of a roadway and is defined by the ratio of change in vertical distance (Δh) to the change in horizontal distance (Δd), shown in Figure 5.9. Positive values of road grade indicate an incline on the roadway, whereas negative values indicate a negative slope or a decline. Including road grade is recommended as it has a significant effect on road loads, as authors have found fuel rate increases of 40-90% and emission rate increases for NO_x, CO and HC by 60 – 450% for light duty gasoline vehicles on flat road surfaces compared to greater than +5% road grades.

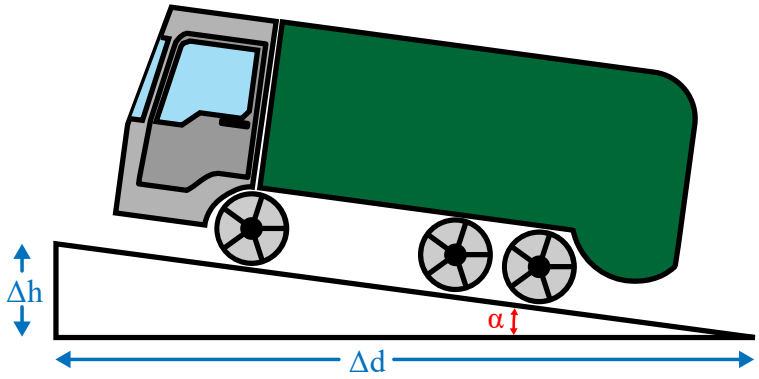

Figure 5.9: An illustration of a positive road grade.

Road grade cannot be directly measured from the data logging equipment or from a sensor on the truck and thus must be estimated. To estimate the road grade, a relationship between the vehicle velocity (V_{veh}) and vertical velocity (V_{vert}) of the truck at each time step must be determined. It should be noted that V_{veh} represents the hypotenuse component in Figure 5.9. The NED elevation data was used to estimate the corresponding elevation of the truck given the GPS coordinates. The elevation was treated using processes described in [71]. Here, the elevation data was uniformly down-sampled to 1/20 Hz with the median value

being calculated for each point. This is to help eliminate the effect of bridges and other irregularities in the elevation data that deviate from how a typical roadway would appear. It is important to note that the NED dataset returns elevation data that represents the ground surface. In the event of a bridge, the elevation data would show a sharp decrease in elevation, whereas the actual roadway would be flat. To compute the median at each down-sampled point, a for-loop was used, shown in Figure 5.10.

```
for i = 2:length(Time_downsampled)
   Signal_downsampled(i,1) = median(Signal(Time_downsampled(i-1):Time_downsampled(i),1));
end
```

Figure 5.10: A for-loop used to compute the median at each point of a down-sampled signal.

Where Signal is the elevation data at 1 Hz, Signal_downsampled is the elevation data at 1/20 Hz and Time_downsampled is the down sampled time array

Next, noise in the elevation was smoothed using the *MATLAB* Savitzky-Golay filter function in Figure 5.11.

```
Signal_filtered = sgolayfilt(Signal_downsampled, order, framelen)
```

Figure 5.11: A Savitzky-Golay filter function used to smooth and filter elevation data.

Where Signal_filtered is the filtered altitude.

After the altitude was filtered and smoothed, the gradient of the altitude was computed to obtain the vertical velocity with respect to time in Eq. 5.1:

$$\mathrm{V_{vert}} = \nabla A = \frac{\partial A}{\partial t} \qquad \text{Eq. 5.1}$$

Road grade (α) was then estimated using V_{veh} and V_{vert} in Eq. 5.2:

$$sin\ (\alpha) = {}^{V_{vert}}/_{V_{veh}} \qquad \text{Eq. 5.2}$$

Additional filtering based on conditions was implemented to prevent divisions by zero while calculating road grade. If the truck velocity or vertical velocity was zero, it was assumed that the road grade was zero as well. With the given data logger and available elevation data, accurate road grade estimation at very low speeds or stationary speeds was deemed too complicated and not within the scope of this study.

Finally, a Savitzky-Golay filter and lowpass filter were implemented on the road grade array to smooth the final result and eliminate infrequent and high magnitude signa characteristics.

The described workflow is illustrated in Figure 5.12. In this scenario, the truck is gaining about 170 meters of elevation while traveling at speeds of 80 km/h or more.

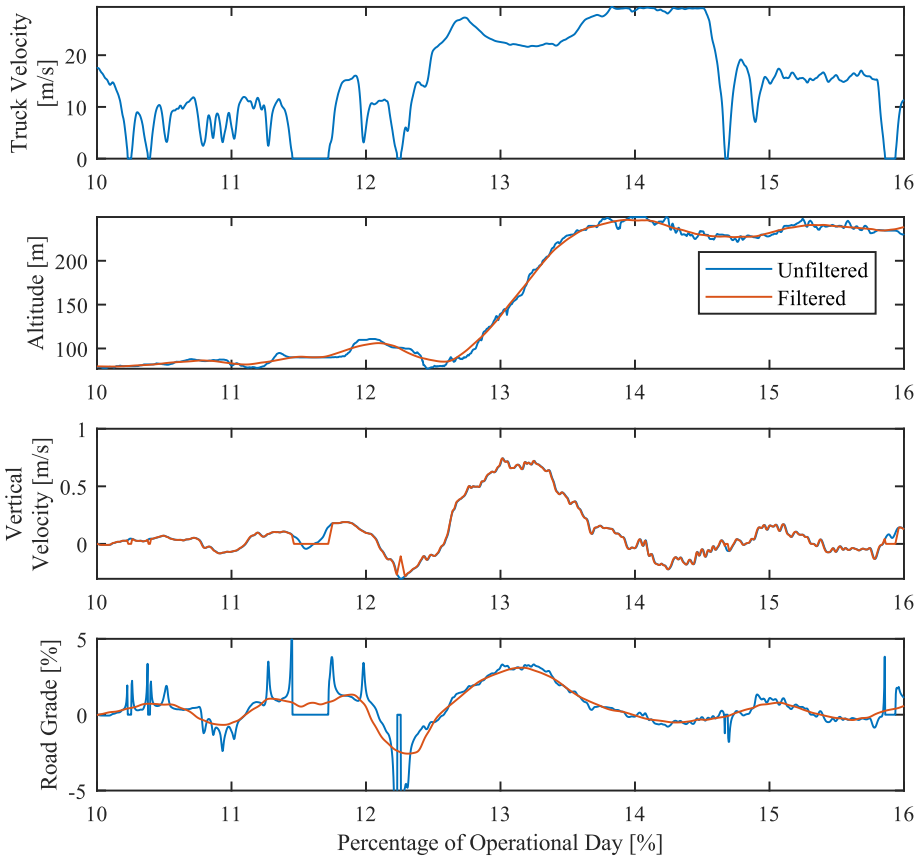

Figure 5.12: The process of filtering altitude signals to calculate the respective road grade.

5.8 Mass Cycle

A mass cycle gives information on how the truck's payload changes over the operational day. Within the collection zone, a refuse truck collects MSW on each household stop and was found to collect up to 3 – 11 tonnes per day. The mass cycle will allow a model to account for changes in road loads more accurately as the wheel rolling friction ($F_{rolling\ friction}$) and grade (F_{grade}) loads are a function of vehicle mass, shown in Eq. 5.3 and Eq. 5.4 respectively. The variables are denoted as vehicle mass (m), gravity (g), road grade

(α), vehicle velocity (v_{veh}), c_{r0} and c_{r2} are the zero and second coefficients of rolling friction force.

$$F_{grade} = mgsin(\alpha) \quad \text{Eq. 5.3}$$

$$F_{rolling\ friction} = (c_{r0} + c_{r2}{v_{veh}}^2)\,\text{mgcos}(\alpha) \quad \text{Eq. 5.4}$$

The truck's mass could not be directly measured throughout the day due to lack of sensors and the cost and complexity of installing an appropriate sensor. As mentioned previously, to approximate the gradual gain of payload while in the collection zone, a constant mass was added to the truck at each stopping event that reflected the overall gain of truck mass during the day.

Stopping events were tracked based on the collected GPS data. When the truck was stationary for more than 3 second, a counter was triggered for the total number of stops for MSW pickup. It should be mentioned that if the truck were stationary at a stop sign or traffic light for longer than 3 seconds in the collection zone, this stop would be counted as well, adding some error to the estimated number of stops. The city does not currently have a record for the number of stops along a route, so a sensitivity analysis on the accuracy of stop estimation cannot be completed at this time.

To approximate the decrease of mass during offloads, the truck was identified when it was in a transfer station or the truck yard area, and a decrease in mass occurred when the offloading PTO cycle was initiated. A sample mass cycle is shown below.

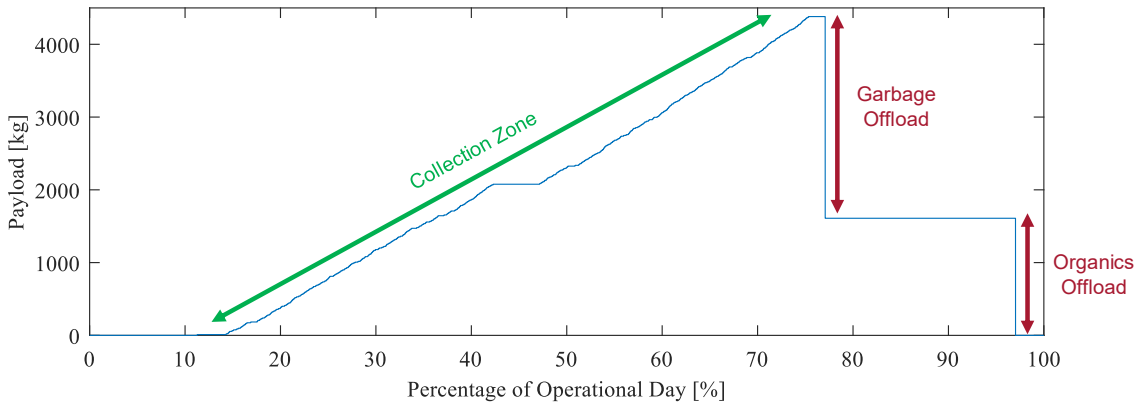

Figure 5.13: A sample mass cycle for the urban/rural split side-loading refuse truck.

In Figure 5.13, the payload of the truck does not change while the truck is off-route and traveling from the truck yard to the collection zone. While in the collection zone, the payload will increase at each household where MSW is picked up. During the off-route segment proceeding the collection zone portion, the payload of the truck decreases when the truck off-loads garbage at designated transfer stations and organics at the truck yard. Typically, the split-body SL-RT truck will offload twice per day whereas the single-body RL-RT truck will offload garbage once per day.

5.9 Power Cycle

Throughout an operational day, a refuse truck utilizes an on-board hydraulic circuit to compact and offload MSW. Some trucks have an assisted or fully automated lifting arm (ALA) that is also run off the on-board hydraulic circuit. This hydraulic circuit is powered through a PTO, allowing power from the engine to be transferred to the hydraulic pump instead of the powertrain. The power and energy consumption of this hydraulic circuit must be considered to accurately model a refuse truck.

As mentioned previously, authors in past literature have investigated methods to isolate the power required by the hydraulic circuit using pressure transducers. These methods involve installing a pressure transducer into the areas along the hydraulic circuit, usually near the hydraulic pump outlet. It should be mentioned that some hydraulic pumps in these applications have two inlets for a primary and secondary hydraulic circuit. The primary circuit will usually handle higher loads such as compaction and offloading MSW. The secondary circuit will handle lesser loads such as the ALA. This results in having to install many pressure transducers, as a transducer is required at the pump outlet and at the load location on the truck. These transducers require additional expertise to appropriately install and are a more invasive approach compared to studying the trucks CAN data.

To avoid using invasive sensors, the hydraulic system's power and energy requirements were considered from the engine's point of view. A schematic of the truck's mechanical connection to the hydraulic system is shown below.

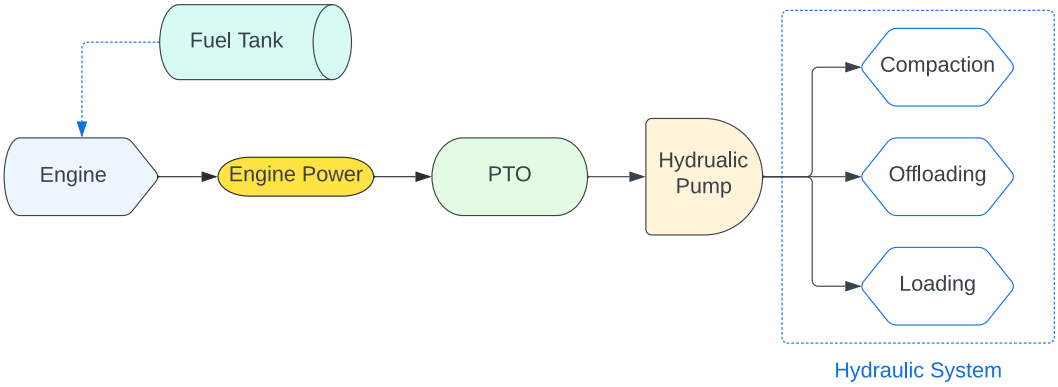

Figure 5.14: A schematic illustrating the mechanical connection between the refuse truck's powertrain and the hydraulic system.

The logged CAN from the *CANedge2* includes engine speed, torque and a PTO activation switch. The PTO activation switch is active when the driver is using the primary hydraulic circuit for compaction or offloading. During this activation, the engine speed is set to a target of 1200 RPM. During this scenario, the generated engine power (P_{eng}) is equal to the power required to idle the engine (P_{idle}) and the required power from the PTO pump (P_{PTO}), as the truck is stationary during this time. As such, P_{eng} can be calculated using Eq. 5.5.

$$P_{eng} = P_{idle} + P_{PTO} \quad \text{Eq. 5.5}$$

The ALA that runs on the secondary hydraulic circuit does not have an explicit indicator of its usage, as the truck's idle state remains consistent with normal driving conditions and the target engine idle speed remains at 700 RPM. Engine torque and engine air mass flow rate fluctuations at collection zone stops were analysed to determine if the ALA was used or not.

An example of a compaction and offloading cycle with respect to engine power consumed by the hydraulic system and engine speed are displayed below for the split SL-RT in Figure 5.15 and Figure 5.16 respectively.

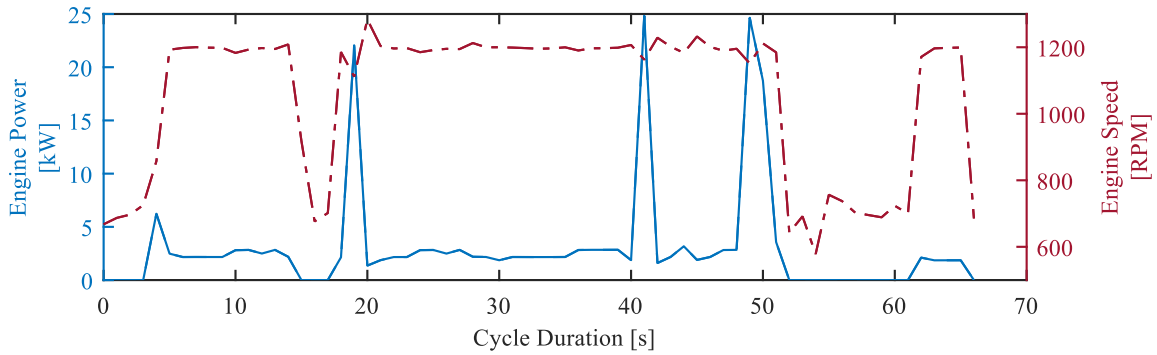

Figure 5.15: A sample compaction cycle, where engine power is the amount of power consumed by the hydraulic system.

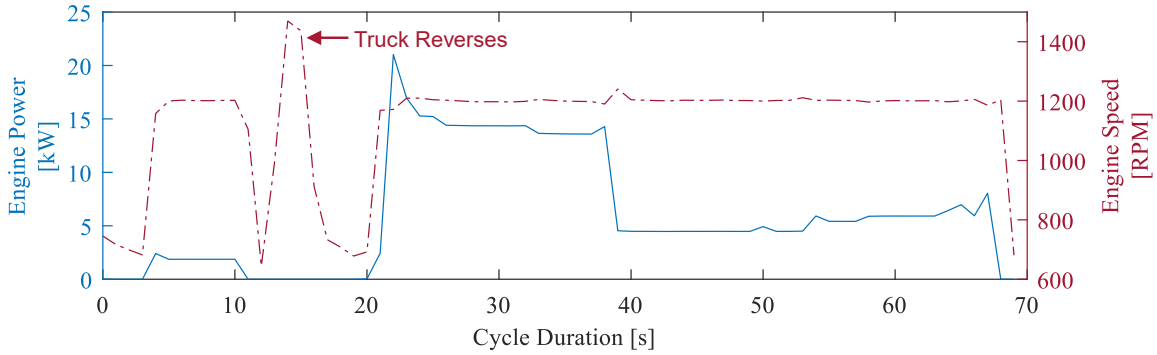

Figure 5.16: A sample off-loading cycle, where the truck reverses between 10 and 20 seconds during the cycle duration. Engine power is the amount of power consumed by the hydraulic system.

5.10 Split Side-Loader Operating Trends

A split SLRT was studied over a period of 4 weeks that serviced the Flamborough and Dundas in Hamilton, containing a mixture of urban and rural areas. A side profile of the truck that was studied is shown below in Figure 5.17. The split SLRT has a split hopper that the operator can load both garbage and organics into, located on the side of the truck. There is an ALA to help load the organic bins. The driver cabin has two steering wheels, allowing the driver to sit on the side of the truck nearest to the curb.

Figure 5.17: A side profile of the urban/rural split side-loading refuse truck, parked inside a warehouse.

This truck operated 5 days a week, servicing a rural area Monday and urban areas Tuesday to Friday. Based on the logged data and post data processing, operating trends of the SLRT could be determine, shown in Table 5.3. It was found that the truck regularly collects more garbage than organic, collecting more of each in the urban areas compared to the rural areas. Rural routes are longer, consume more fuel, and have more highway driving than urban. These driving conditions are reflected in better fuel usage on rural routes where the truck, on average, had a 35 % better fuel economy.

Using densities for MSW garbage and organic found in the U.S. Volume-to-Weight Conversion Factors [19], the capacity utilization of the split side-loader could be determined. For rural and urban routes, the garbage capacity utilized ranged from 33 – 55% and 56 – 77% respectively. The organic capacity utilized for rural and urban ranged from 10 – 11% and 23 – 35% respectively.

The number of stops the truck collected MSW at while in the collection zone was estimated using a combination of vehicle speed and georeferencing analysis. Each route's collection

zone on each workday were identified and a perimeter of latitude and longitude coordinates were constructed around each. These collection zones are shown in Figure 5.18:

Table 5.3: Split side-loader refuse truck operating trends for rural and urban routes.

Quartile	Metric	Mon	Tues	Wed	Thurs	Fri	Metric	Mon	Tues	Wed	Thurs	Fri
Upper Quartile	Garbage Collected [kg]	2643	3678	3315	3310	3305	Fuel Economy [100L/km]	58.2	83.6	95.1	92.0	85.6
Median		2260	3280	3270	3075	3125		56.3	83.6	92.0	91.2	84.5
Lower Quartile		1570	2673	2735	2770	2895		55.6	80.8	88.8	90.2	83.6
Upper Quartile	Organic Collected [kg]	558	1575	1650	1670	1715	Idling [%]	49%	66%	62%	65%	64%
Median		520	1505	1475	1425	1635		41%	62%	62%	63%	64%
Lower Quartile		468	1425	1295	1135	1500		38%	61%	61%	61%	62%
Upper Quartile	Number of Stops	249	404	474	427	407	Trip Distance [km]	183	75	70	67	67
Median		238	395	461	412	397		165	75	69	63	67
Lower Quartile		192	341	431	388	385		154	73	69	61	66
Upper Quartile	Distance Between Stop [m]	565	93	80	63	80	Fuel Usage [L]	106	63	65	62	57
Median		310	35	35	30	30		96	61	64	58	56
Lower Quartile		120	15	15	15	15		86	59	62	55	56
Upper Quartile	Garbage Mass Per Stop [kg]	10.7	9.5	7.2	8.0	8.1	Garbage Capacity Utilized	55%	77%	69%	69%	69%
Median		9.8	8.4	6.9	7.5	7.9		47%	69%	68%	64%	65%
Lower Quartile		9.0	8.2	6.1	6.9	7.5		33%	56%	57%	58%	61%
Upper Quartile	Organic Mass Per Stop [kg]	3.1	4.7	3.5	4.1	4.4	Organic Capacity Utilized	11%	32%	34%	34%	35%
Median		2.3	3.8	3.4	3.5	4.1		11%	31%	30%	29%	33%
Lower Quartile		2.0	3.5	3.0	2.8	3.8		10%	29%	26%	23%	31%
		Rural	Urban					Rural	Urban			

This allows stops outside the collection zone segment to be excluded which might include stops for stop-signs, traffic lights and stops in traffic. Within the collection zone, it is still possible for the truck to stop for reasons other than servicing a household, but georeferencing lowers the possibility of including traffic related stops.

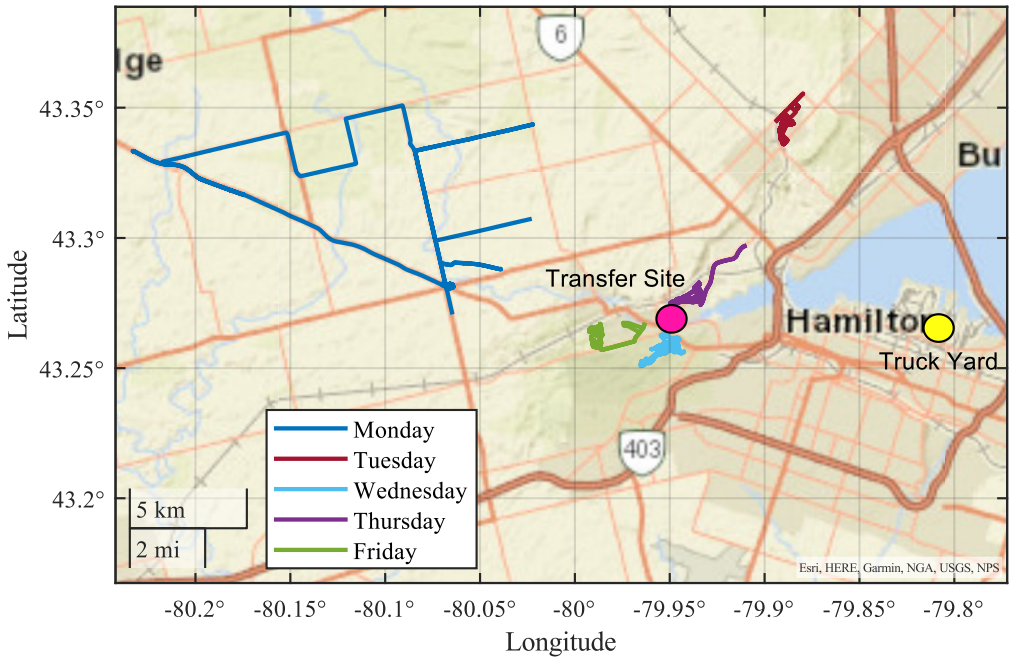

Figure 5.18: The locations of the collection zones, truck yard and transfer site for the split side-loader refuse truck.

The number of stops the truck collected MSW at while in the collection zone is lower for the rural route and higher for the urban route. The rural route is more likely to have households spaced further apart which limits the number of households the truck can visit per day, compared to an urban area.

In terms of the power cycle, the number of compaction cycles throughout the study ranged from 6 to 22 cycles each day, whereas the number of ALA cycles ranged from 50 to 170 cycles each day. Typically, the truck would offload MSW twice a day for organics and garbage separately. Occasionally higher amounts of collected MSW resulted in up to 3 offloads per day. Compaction and offloading required the highest peak powers ranging from 10 to 40 kW and 20 to 35 kW respectively.

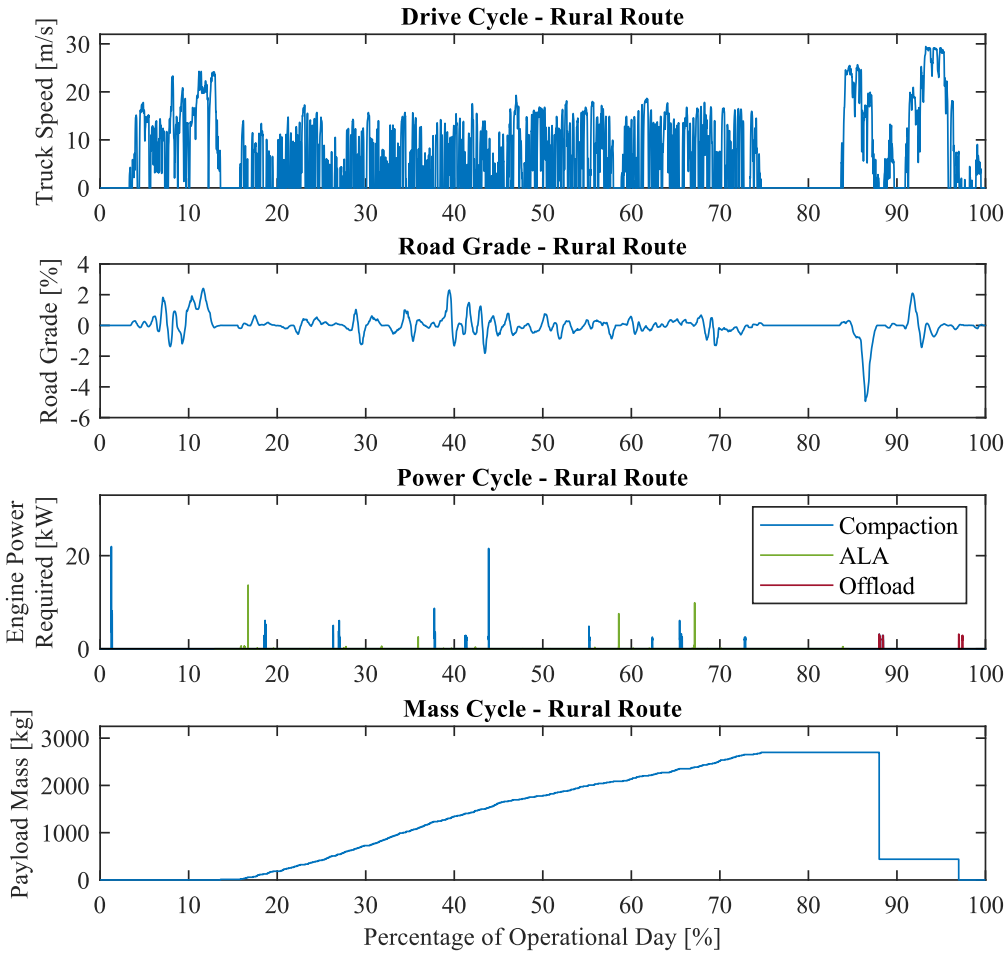

Figure 5.19: A complete drive and duty cycle sample of the split-side loader refuse truck for a rural route.

5.11 Rear-Loader Operating Trends

Logged data from the RE-RT was compiled into operating trends to illustrate a general overview of the truck's daily routes over 5 weeks of operation. A side profile of the truck that was surveyed is shown in Figure 5.20. This truck operates with a crew of two operators. This truck only collects garbage and offloads its payload at a transfer station, then returns to the truck yard to park for the evening and night.

Figure 5.20: A side profile of the urban rear-loader refuse truck.

The daily operating trends are shown in Table 5.4. This truck collects more combined waste than the SL-RT at over 11 tonnes at its heaviest and 7.5 tonnes at its lightest. Along with the higher payload, the number of stops and waste per stop is higher as well. This is more than likely due the denser urban routes this truck completes. All routes are within the lower Hamilton region which includes densely packed dwellings of various sizes, shown in Figure 5.21. The higher density of stops along a route makes the estimation of individual stops harder to distinguish and could lead to the possibility of the operator collecting more than one household's waste at one stop, contributing to a higher waste per stop value. The number of estimated stops typically ranged from 485 – 735.

The collection zones for each route were in close proximity to the truck yard and transfer site, seen in Figure 5.21. This resulted in shorter trip distances ranging from 43 to 62 kilometres. These shorter trip distances paired with a high number of stops equated to truck spending about 50 – 66% of its operational time idling.

Table 5.4: Rear-loader refuse truck operating trends for urban routes.

Quartile	Metric	Mon	Tues	Wed	Thurs	Fri	Metric	Mon	Tues	Wed	Thurs	Fri
Upper Quartile	Garbage Collected [kg]	10528	9780	11130	10600	8150	Fuel Economy [100L/km]	107.6	103.6	110.7	117.6	97.5
Median		10040	9135	10105	9775	7805		88.0	94.8	96.5	109.0	82.4
Lower Quartile		8720	8355	8975	8875	7475		87.6	92.9	89.9	98.9	81.0
Upper Quartile	Number of Stops	735	742	556	707	664	Idling [%]	54%	61%	66%	63%	52%
Median		723	697	545	664	638		53%	58%	64%	60%	52%
Lower Quartile		667	656	486	637	627		53%	55%	61%	60%	50%
Upper Quartile	Distance Between Stop [m]	55	45	55	45	60	Trip Distance [km]	60	57	61	55	62
Median		25	25	25	25	30		56	53	55	49	59
Lower Quartile		15	15	15	15	15		56	52	43	46	57
Upper Quartile	Garbage Mass Per Stop [kg]	14.3	14.0	20.1	15.7	12.8	Fuel Usage [L]	62	56	54	58	58
Median		13.9	13.4	19.2	14.0	12.3		53	53	51	54	51
Lower Quartile		13.1	12.0	18.5	13.4	11.4		50	51	47	50	48
Upper Quartile	Garbage Capacity Utilized	88%	82%	93%	88%	68%		Urban				
Median		84%	76%	84%	81%	65%						
Lower Quartile		73%	70%	75%	74%	62%						
		Urban										

The idle percentage ($idle_{\%}$) is calculated as the following:

$$idle_{\%} = \frac{length\big(find(V_{veh} = 0 \;\&\; \omega_{eng} > 0)\big)}{length\left(find\big(\omega_{eng} > 0\big)\right)} \qquad \text{Eq. 5.6}$$

Where ω_{eng} is the engine speed and both find() and length() are *MATLAB* functions. Find() finds the indices of an array where a certain condition is met. Length() returns the length of an array. As a result, idling percentage is a ratio of when the vehicle is stationary with the engine on compared to the total duration that the engine is on.

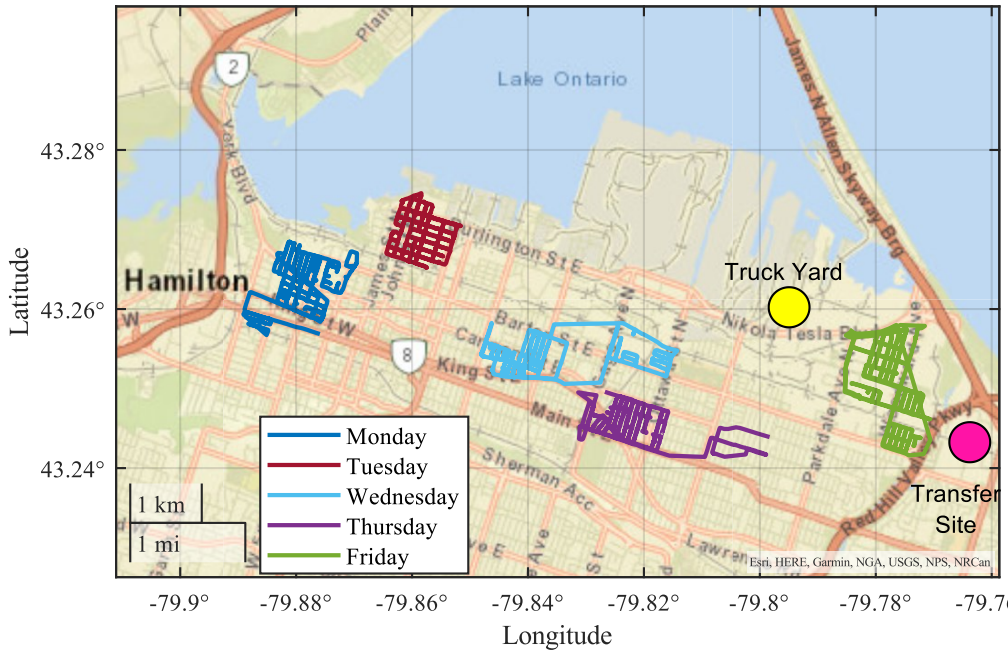

Figure 5.21: The location of the collection zones, truck yard and transfer site for the rear-loading refuse truck.

Ideally, engine idle percentage is determined when the vehicle is stationary with the engine at its idle speed. Due to fluctuation in idling speed, an engine speed greater than zero was used instead. Idling percentage will also include when the truck is stationary with its PTO active while compacting or offloading MSW.

The idle percentage calculation is mostly likely over-estimating the idling time of the truck due to how it is calculated with the available data. Because each dataset of vehicle speed and engine speed corresponding to a specific day is used in the calculation, there is typically a time constant involved in the truck's on-board computer during changes in speed. A change in engine speed will result in a new vehicle speed with some delay between the previous vehicle speed and the current reading. This time delay in vehicle speed from the

wheel speed sensor is shown in Figure 5.22, where the orange line represents the change in engine speed and the blue line represents the response from the wheel speed sensor. This time delay may result in a few seconds during vehicle acceleration, where the truck would be moving in real life, even those the wheel speed sensor is still returning a zero speed, contributing to a longer time spent idling compared to reality.

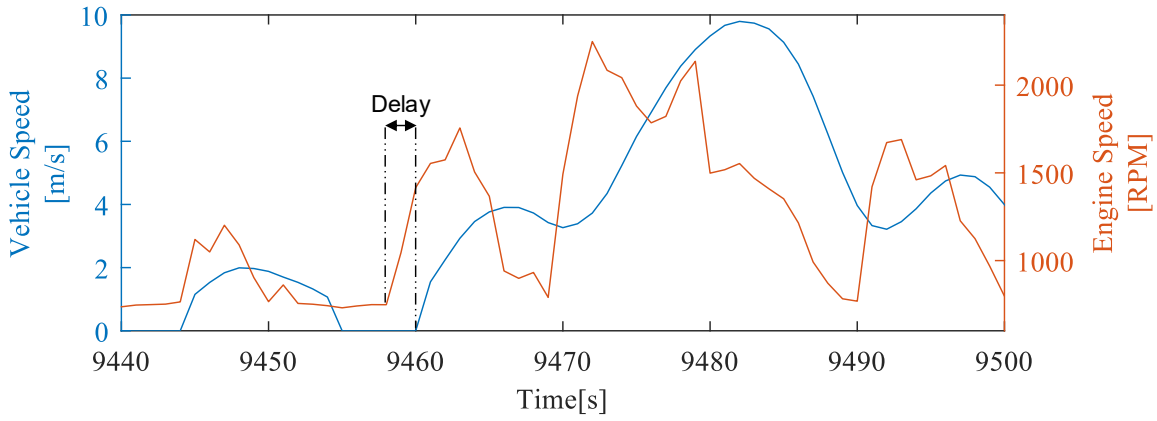

Figure 5.22: Vehicle speed measured from the truck's wheel speed sensor and the recorded engine speed.

Figure 5.23 summarizes the trends discussed in sample drive and duty cycle plot for a particular operating day. As mentioned previously, refuse trucks operating in urban areas will experience lower sustained speeds in the collection zone. Also, downtown Hamilton is a rather flat area, so the road grade variation over the day is typically small. Since waste is loaded manually into the RE-RT, there is no ALA drawing additional engine power in the power cycle.

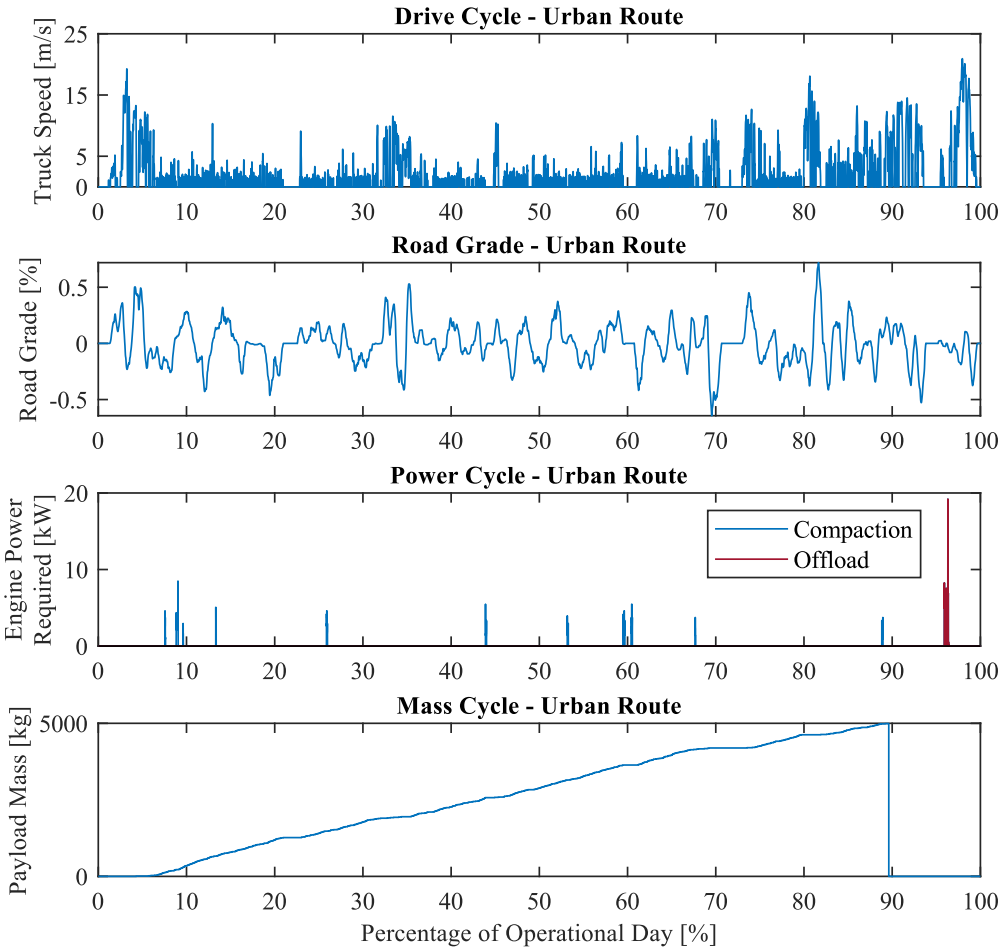

Figure 5.23: A sample drive and duty cycle for the rear-loading refuse truck.

5.12 Summary

This chapter covered the techniques and insights that were used to analyse the collected CAN and GPS data in a meaningful way. Some data is useful after decoding, but other presented data such as road grade and the number of households stops rely heavily on the correct data processing techniques. Each data processing technique was developed to accept data for any truck from the fleet, meaning that theoretically, any logged data from a traditional refuse truck could be analysed.

The definitions of a drive and duty cycle have been explained, allowing the operational environment of a refuse tuck to be quantified. Samples of each cycle are shown, with the significance of each cycle explained as it relates to the refuse's energy usage.

Trends that were computed using collected data were shown for the urban RL-RT and urban and rural SL-RT. The routes of both trucks for each day were illustrated to give the reader a visual on what the trucks accomplish on a day-to-day basis as well as how far each collection zone is from the truck yard and transfer site.

Chapter 6

Refuse Truck Powertrain Modelling

This chapter covers a comprehensive overview of how each powertrain of interest was modelled. The powertrains included in this chapter are a conventional truck, an all-electric truck and a range extended electric truck. A walk through of the top-level model structure, down to the finer detail of sub-models and the vehicle plant is shown, with important equations to describe how the model's function.

The parameters and mass of a refuse truck are sourced and validated using the conventional vehicle model to create a foundation for the other powertrains to be built on. For the all-electric and range extended truck, the models are simulated for each operational day that logged data from the refuse truck fleet was obtained for, to verify whether either powertrain could meet the demands that the City of Hamilton has for waste collection.

A study into a real time controller developed in *StateFlow* for the range extended electric truck is investigated using solutions found from an off-line control technique called dynamic programming.

6.1 Top-Level Model Structure

For each vehicle case, the same top-level forward looking model structure was used, illustrated in Figure 6.1. Here, the inputs to the model are the drive cycle and for a refuse application, there is the duty cycle composed of the power and mass cycle inputs. The model is forward looking as it evaluates each time-step of the inputs given no prior knowledge of the drive or duty cycle. In this case, the model must react on-the-go and cannot be optimized in an off-line manner beforehand.

A top-level view of the model structure is shown in Figure 6.1 and includes a driver, controller and vehicle block. The driver block receives input from the drive cycle and vehicle plant, and outputs torque commands to the controller block using a PI controller. The controller block outputs propelling and braking torque commands to the vehicle block, deciding decisions such as whether regenerative braking can occur, if the requested torque is achievable or whether the engine should be on or off if the vehicle is a hybrid. The vehicle block contains all vehicle plants that are controlled by the previous controller and driver blocks. The output from the vehicle block can vary but usually contains the vehicle plant speed, plant road loads and any other vehicle information required by controller logic.

An important consideration is the memory block (grey) which delays the output from the vehicle block by one time step. This block ensures that algebraic loops are prevented and assigns an initial condition of zero to all signals that pass through it. As the model simulates through each time step, the feedback from the vehicle block will be delayed by one time-step, meaning the driver and controller blocks make decisions based on the next known input, compared with the previous output from the vehicle block.

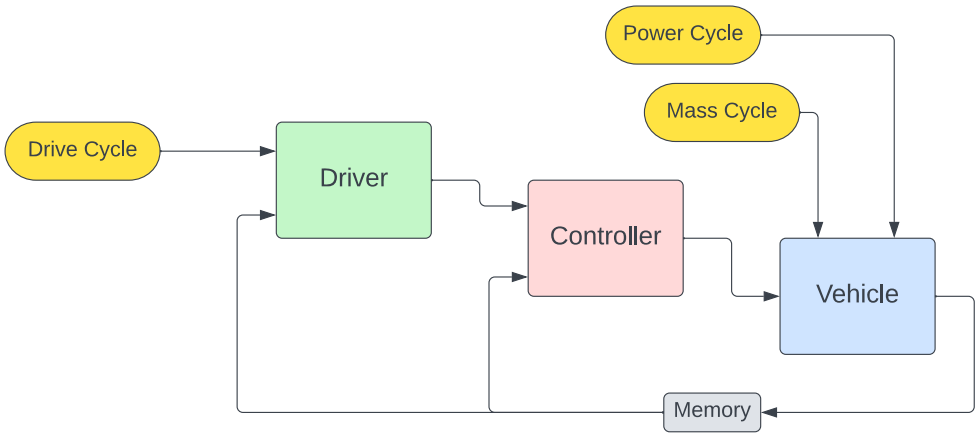

Figure 6.1: A top level overview of the model including the driver, controller and vehicle blocks.

6.2 Driver Model

The driver sub-model is responsible for sending positive or negative torque requests to the controller block based on the reference vehicle speed and the calculated chassis vehicle speed, shown in Figure 6.2.

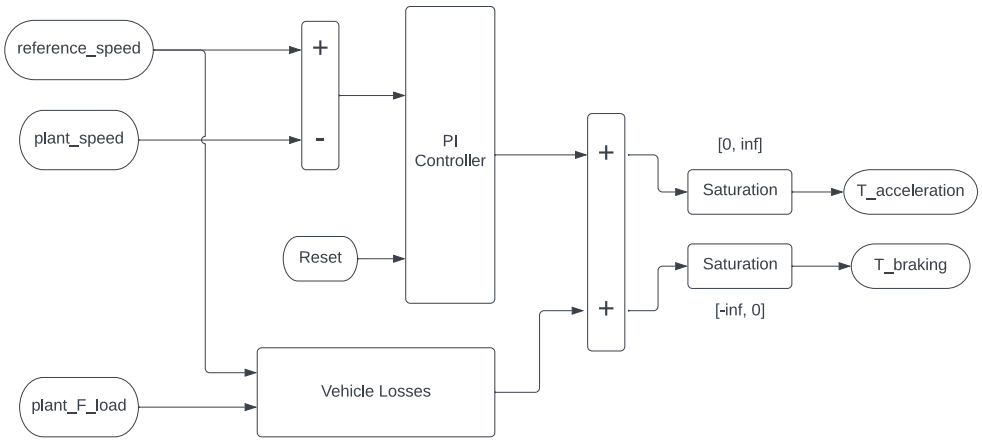

Figure 6.2: The PI Controller block layout in the driver model.

Within the driver block, a PI controller is used to calculate a torque (τ_{PI}) to tune the torque demanded, defined by Eq. 6.1 and Eq. 6.2, where K_p and K_i represent the proportional and integration constants.

$$\tau_{PI} = K_p \left(e(t) + \frac{1}{T_i} \int_o^t e(\tau) d\tau \right) \quad \text{Eq. 6.1}$$

$$K_i = K_p \frac{1}{T_i} \quad \text{Eq. 6.2}$$

The e(t) term represents the error between the reference speed and the calculated chassis speed. The torque calculated from the PI controller (τ_{PI}) is added to the torque required to overcome the road loads (τ_{lost}), defined by Eq. 6.3.

$$\tau_{lost} = \left(m \frac{dV}{dt} + F_{load} \right) r_{whl} \quad \text{Eq. 6.3}$$

Accounting for the road loads and the torque from the PI controller, the torque demand from the driver is calculated by Eq. 6.4.

$$\tau_{demand} = \tau_{PI} + \tau_{lost} \quad \text{Eq. 6.4}$$

The torque demand can be further segregated into positive and negative values, representing the torque required to propel or brake the vehicle respectively, shown in Eq. 6.5 and Eq. 6.6.

$$\tau_{demand\ propel} = \max \{0, \tau_{demand}\} \quad \text{Eq. 6.5}$$

$$\tau_{demand\ brake} = \min \{0, \tau_{demand}\} \quad \text{Eq. 6.6}$$

6.3 Chassis and Wheel Sub-Model

An accurate vehicle model relies on a strong kinematics model as the foundation. The kinematics model is what determines the load the vehicle will experience as it is follows a drive cycle, shown in Figure 6.3. As previously mentioned, vehicle models can operate in either a forward or backward-looking mode. A forward-looking model involves studying the powertrain from the wheels to the engine/motor, where the only input would be a drive cycle that the vehicle must follow. With the application of a refuse truck and the extra functions performed alongside driving, a mass and power cycle must be included as well.

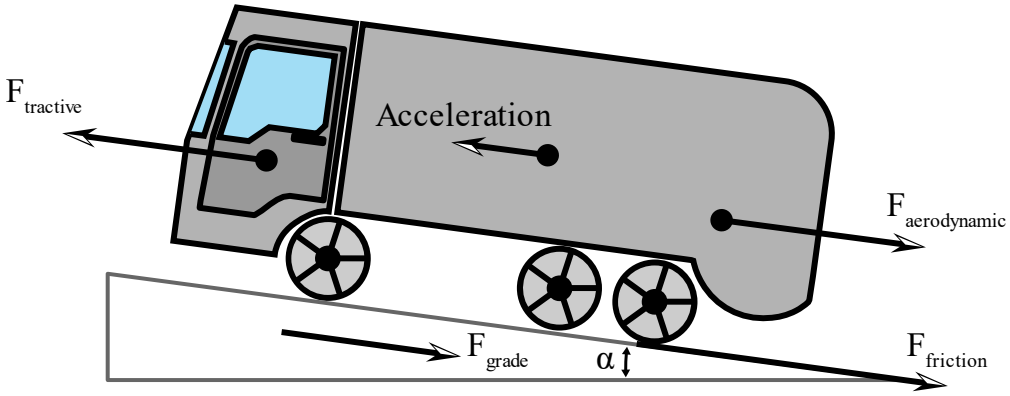

Figure 6.3: The road loads acting of a vehicle while on a roadway.

As the refuse truck navigates its route, it is exposed to a variety of forces that the engine or motor must overcome to accelerate the vehicle. Acting against the tractive force are friction due to rolling resistances of the wheels ($F_{rolling\ friction}$), aerodynamic drag ($F_{areodynamics}$), force due to road grade (F_{grade}) and the force required to accelerate the truck. As such, the force of the road loads (F_{load}) the truck must overcome are defined by Eq. 6.7 to Eq. 6.11.

$$F_{load} = F_{rolling\ friction} + F_{aerodynamics} + F_{grade} + F_{acceleration} \quad \text{Eq. 6.7}$$

$$F_{grade} = mgsin(\alpha) \quad \text{Eq. 6.8}$$

$$F_{rolling\ friction} = mg(c_{r0} + c_{r2}v)\cos(\alpha) \quad \text{Eq. 6.9}$$

$$F_{areodynamics} = 0.5 * C_d A_f \rho_{air} v^2 \quad \text{Eq. 6.10}$$

$$F_{load} = mg(c_{r0} + c_{r2}v^2)\cos(\alpha) + 0.5 * C_d A_f \rho_{air} v^2 + m_{eq} g sin(\alpha) + m_{eq} a \quad \text{Eq. 6.11}$$

Where m is the truck mass, g is gravity, c_{r0} and c_{r2} are the zero and second coefficients of rolling friction force, α is the angle of road grade relative to the horizon, C_d is the coefficient of drag, A_f is the frontal area of the truck, ρ_{air} is the density of air, a is vehicle acceleration and m_{eq} is the equivalent mass taking into account the mass of any rotating objects on-board the truck (i.e.: wheels, engine rotor, drive shaft, etc). Throughout this thesis, gravity and the density of air is assumed to be 9.81 m/s^2 and 1.21 kg/m^3 respectively.

6.4 Refuse Truck Parameterization

Determining accurate truck parameters is important to calculate the correct energy and power requirements of vehicle models. Each truck parameter was chosen carefully with preference to what could be determined from the truck itself or from a manufacturer. When a parameter could not be determined using these avenues, a creditable source was referenced. Information about the engine size, wheel size and fuel capacity were determined from the physical truck. Information about refuse storage capacity and truck mass was obtained from the respective manufacturers. The logged CAN data revealed the

transmission gear ratios. The parameters for each studied refuse truck are displayed in Table 6.1.

Effort was directed towards accurately accounting for accessory loads the refuse truck powertrain. The type of accessory loads and overall impact on power draw for conventional, hybrid electric and electric refuse trucks are displayed in Table 6.2.

A conventional vehicle does not need to regulate the temperature for a HV battery pack or the cabin during winter, whereas an electric or hybrid electric vehicle must take these additional loads into consideration. The heat exhaust from the conventional truck's engine is adequate to heat the cabin during colder months and operate the defroster. During warm months, the loading of the air conditioner compressor for all types of powertrains can significantly impact range and fuel consumption.

Table 6.1: Parameters for each refuse truck that were studied.

Parameter	Value	Unit	Parameter	Value	Unit
Curb Mass			6-Speed Transmission		
SL-RT	16000	kg	Gear Ratios	4.99, 4.59, 2.25, 1.53, 1.00, 0.749	-
RL-RT	14400	kg			
Chassis Capacity			Final Drive Ratio	5.29 [72]	-
SL-RT	25	m^3	Wheel Specification	315/80R22.5	-
RL-RT	19	m^3	Rolling Coefficients		
Height, Width	3.30, 2.5	m	Zero Order Coefficient	0.007 [73]	-
Diesel Engine			Second Order Coefficient	0 [74]	-
Max Power	223	kW	Drag Coefficient	0.85 [74]	-
Peak Torque	1166	Nm			
Max Speed	2200	RPM			

Table 6.2: Accessory Loads on a Refuse Truck.

Accessory Type	Load	Conventional	Hybrid Electric	Electric
Power Steering	High			
Air Brake Compressor	High			
Cooling Fans	Medium			
Air Conditioning	High			
Electrical Accessories	Low			
Heating	High			
Defroster	Medium			
HV Cooling	Low			

Based on past literature [75] [76] [77], a conventional heavy-duty vehicle's average accessory load can range from 6.5 – 8.5 kW, a hybrid electric 11 – 14 kW and an electric vehicle from 7 – 10 kW. These ranges are affected by whether air conditioning is active or whether the vehicle is driving on the highway or urban roadways.

6.5 Conventional Model Validation

To validate the chosen vehicle parameters, a simplified version of a conventional vehicle model was created. The purpose of this model is to evaluate the loading on the model's engine from the estimated road loads from the chassis and wheel model. If the model's engine loading is like that of the real-world truck for the same drive and duty cycle, then it can be concluded that the chosen truck parameters are similar to the actual truck. When referring to the engine's load, engine torque and speed will be compared in the form of consumed engine energy. Comparing the fuel usage of the truck and model would be a good metric. Although, the fuel consumption map of the truck's engine was not available and using an alternative fuel consumption map would introduce more error to the

comparison. Engine load is a function of fuel consumption and therefore comparable engine loads should result in comparable fuel consumptions, given the same fuel consumption map.

To make a valid comparison, some constraints on the truck's dynamics need to be controlled:

1. The mass of the truck is approximated while it is in the collection zone. This approximation will add additional error to the comparison. To eliminate this error, the truck should be compared to the model before or after the collection zone, where the mass of the truck is known.
2. The truck contains a torque converter, which it a type of fluid coupling located between the engine crankshaft and the input to the transmission. The torque converter can act as a reduction gear, multiplying the engine's crankshaft torque into the transmission. Modelling a torque converter adds additional complexity to the model. To eliminate the need for a torque converter module, or an accurate one, the model and truck should be compared when the torque converter is *locked-up*, or when the transmission input shaft and engine crankshaft are rotating at the same speed. This occurs when the truck sustains higher speeds, such as in highway driving.
3. Road grade is estimated and is not directly measured. Road grade is a factor included in road load calculations and can add additional error to the comparisons. To reduce the amount of error, a cycle without high road grade variation will be investigated.

A scenario that meets all the above criteria is when the RE-RT urban truck is returning to the truck yard after the collection zone. A sample cycle is shown in Figure 6.6. With these constraints set, a simplified model of a conventional vehicle can be created. The conventional model is a similar *Simulink* structure compared to the BEV or REEV models discussed in future subsections, but with the added complexity of an engine and transmission sub-models.

6.5.1 Transmission Sub-Model

The transmission sub-model is responsible for the control of which transmission gear to choose while the truck is driving. This control logic is complex and is specific to each manufacturer. A simplified fuel cost control was implemented, where the fuel cost ($BSFC$) of each possible transmission gear ratio at a given engine torque (τ_i) and speed (ω_i) is calculated at each time step, and the gear ($gear_i$) corresponding to the minimum fuel cost is selected. If the engine has no tractive effort, or idling, the gear is set to zero, shown in Eq. 6.12.

$$gear_i = \begin{Bmatrix} \min\left(BSFC(\tau_i, \omega_i)\right) \\ IF\ idling, gear_i = 0 \end{Bmatrix} \quad \text{Eq. 6.12}$$

Additionally, the requested torque from the driver is compared to the maximum torque the engine can output at a given speed, using the torque-speed performance curve shown in Section 4.4.3. This performance curve was assumed to be the wide-open throttle (WOT) torque-speed curve.

To emulate realistic gear changing, the transmission control was limited to a single increase or decrease in gear per time step. Also, the accuracy of the transmission control was constrained further using a modified shifting schedule, extracted from the logged transmission data. A scatter plot of selected transmission gears versus vehicle speed was used to govern the upper limit on what gear should be chosen. This was required to prevent the truck from accelerating to a higher gear too quickly. The modified shifting map is shown in Figure 6.4.

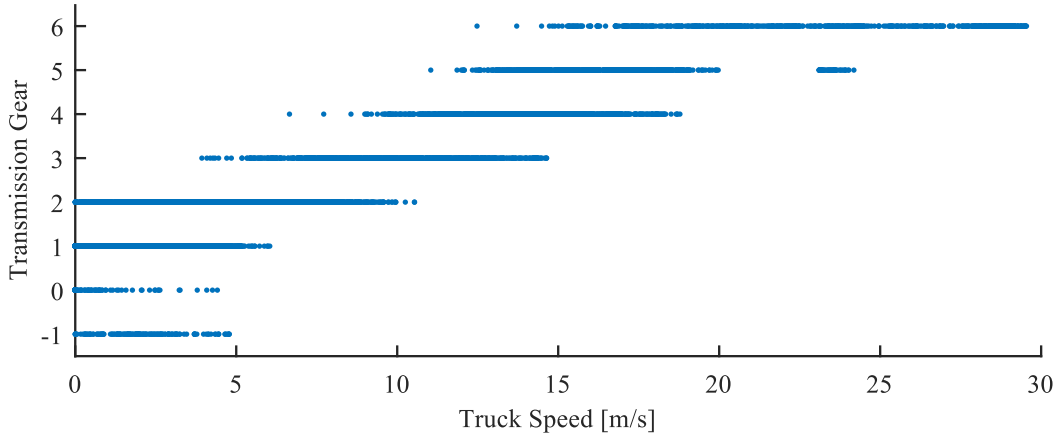

Figure 6.4: A shifting map generated for transmission gear versus truck speed.

The process described in how the conventional model calculates each gear per time step, and corresponding engine torque and speed to calculate the overall engine energy consumed, is illustrated in Figure 6.5.

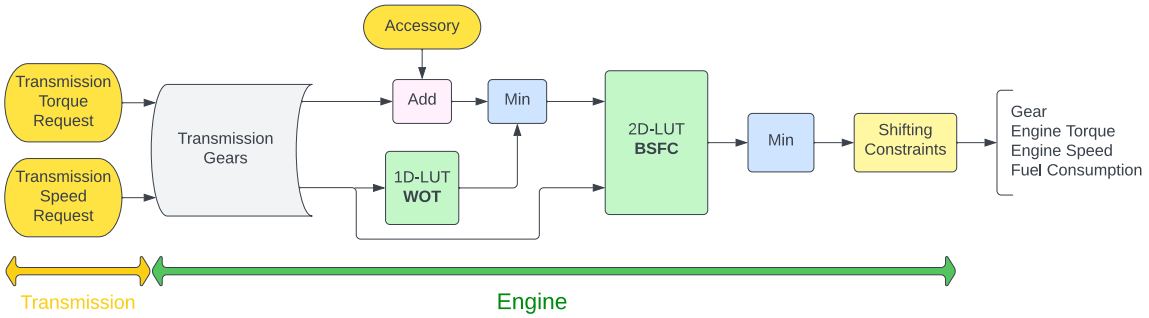

Figure 6.5: A simplified flow chart of the transmission and engine load estimator in the conventional truck model.

6.5.2 Road Load Validation Results

To validate the road loads while using a simplified conventional vehicle model, a drive and mass cycle had to be chosen that met the constraints outlined previously. The drive and mass cycle were isolated for when the truck was travelling between the collection zone and offloading sites. This is because the truck is highway driving and the torque converter ratio can be assumed as 1:1, and the mass of the truck at this time is known, eliminating the error of mass estimation while inside the collection zone. The drive and mass cycle for the road load validation segment are shown below. Here, the road grade variation is very small, there is no engine power from the hydraulic system and the payload is constant, as the truck is travelling back from the collection zone to the truck yard.

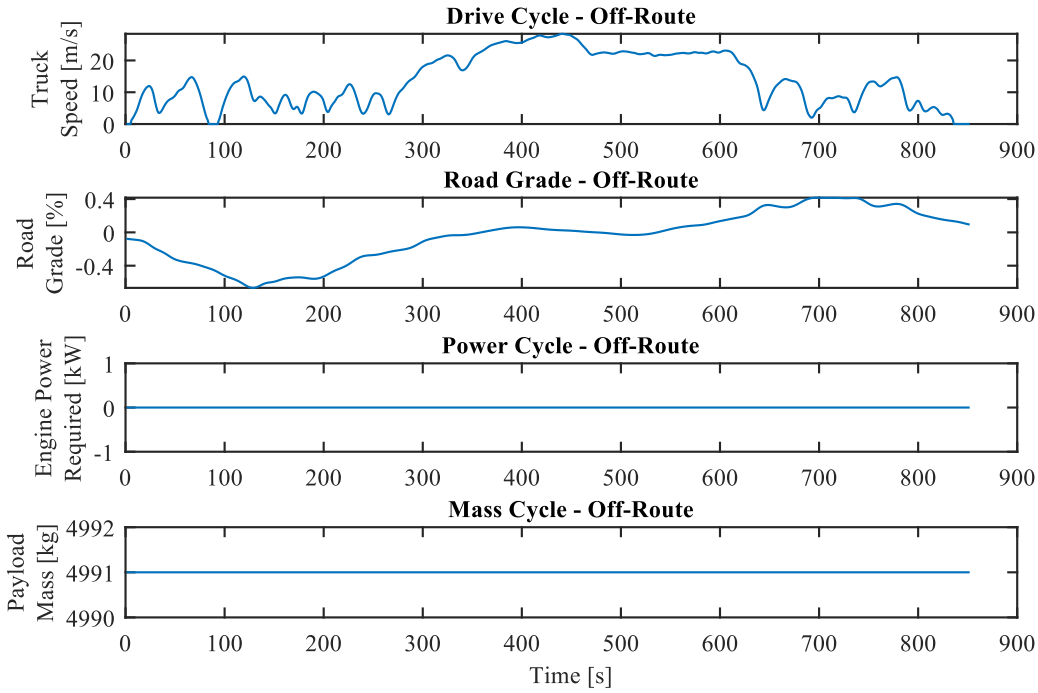

Figure 6.6: A sample drive and duty cycle for evaluating the road loads with the truck CAN data.

Some important parameters such as speed, gear and the loading on the engine for the corresponding cycle are shown in Figure 6.7 for the truck model versus the CAN data from the studied urban truck.

The trends between the engine loading from the CAN data and the model can be difficult to compare. This is because of the sampling rate of 1 Hz that the data logger records CAN data. This introduces some errors while interpreting engine behaviour. Since the sampling resolution of engine torque and speed are known per second, some information during transient behaviour may not be captured. An instance of transient behaviour is when the vehicle is accelerating, especially evident while the truck is within the collection zone.

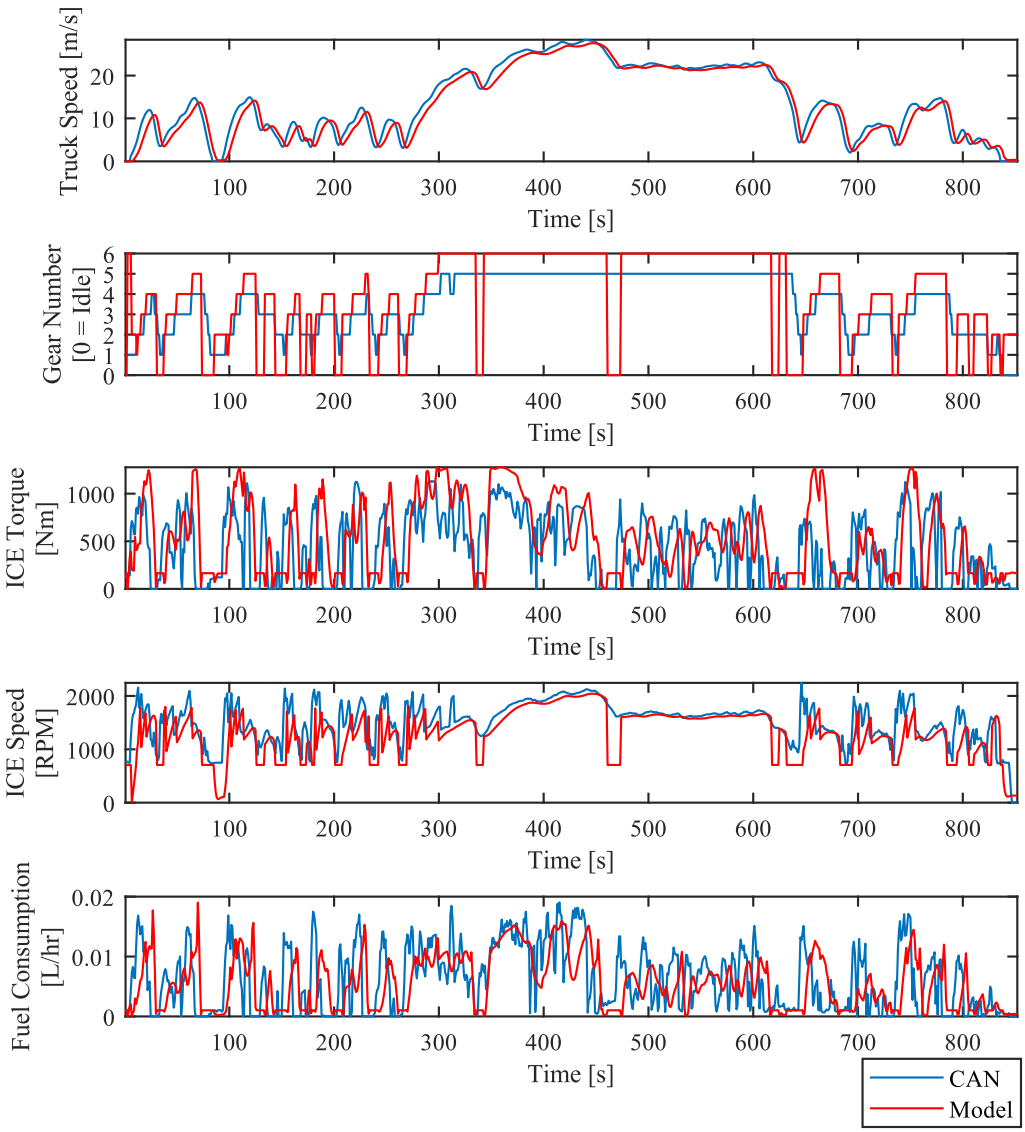

Figure 6.7: Operating trends from the conventional truck model and the truck's CAN.

The model uses a PI controller in the driver model to tune the torque request of the truck given the required speed and the truck's speed feedback from the chassis. The PI controller response to a given drive cycle may send torque commands that do not match what the CAN engine torque may be at that same time instance, as the CAN data is based on a real

driver, whereas the model is based on a driver model. This makes a second-by-second comparison of engine torque difficult to do so.

The comparison of cumulative engine energy from the CAN data and model are a more predictable indicator of model similarity. Looking at the cumulative engine energy provides a macro view of how the CAN and model trucks handled the given drive cycle, without considering the second-by-second dynamics. The cumulative engine energy usage from the collected CAN data and model are shown in Figure 6.8. The end cumulative engine energy consumed from the CAN data was 64.2 MJ and the model consumed 67.2 MJ, creating an absolute error of 4.7% between the model and the real truck.

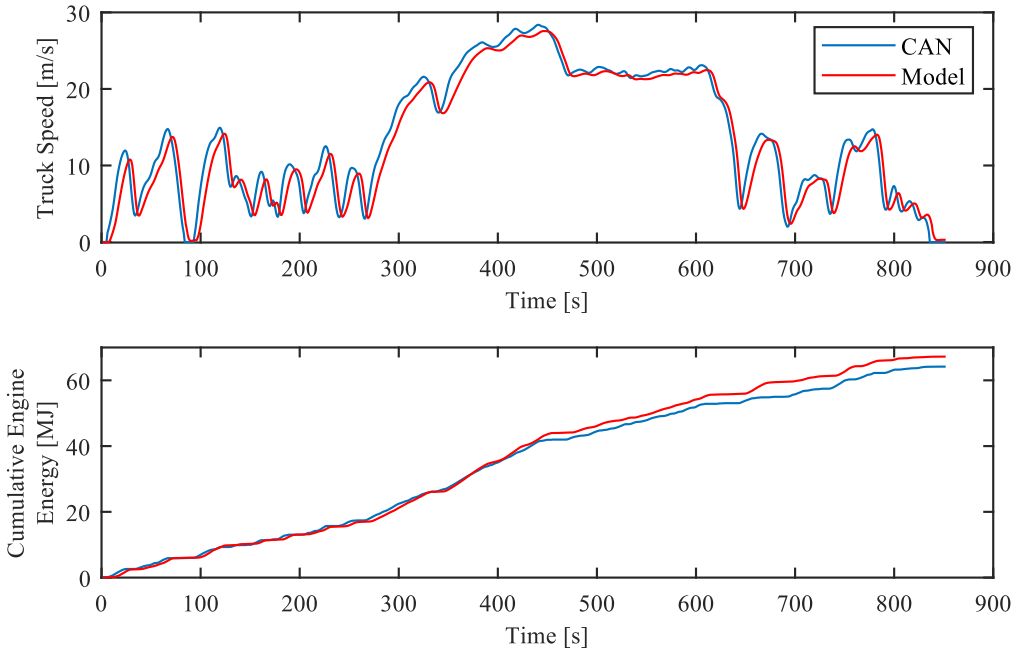

Figure 6.8: Truck speed and cumulative engine energy plots for the end-of-day off-route cycle.

The engine operating points were visualized using the WOT performance curve and the brake specific fuel consumption (BSFC) map of a similar sized diesel engine in Figure 6.9.

A significant portion of operating points lie within the 1000 to 1600 RPM range of engine speed. This can be expected because the truck spends a lot of time in gears one and two operating at low speeds, equating to this RPM range. Also, the trucks PTO operates at a target speed of 1200 RPM, which is also in this speed range.

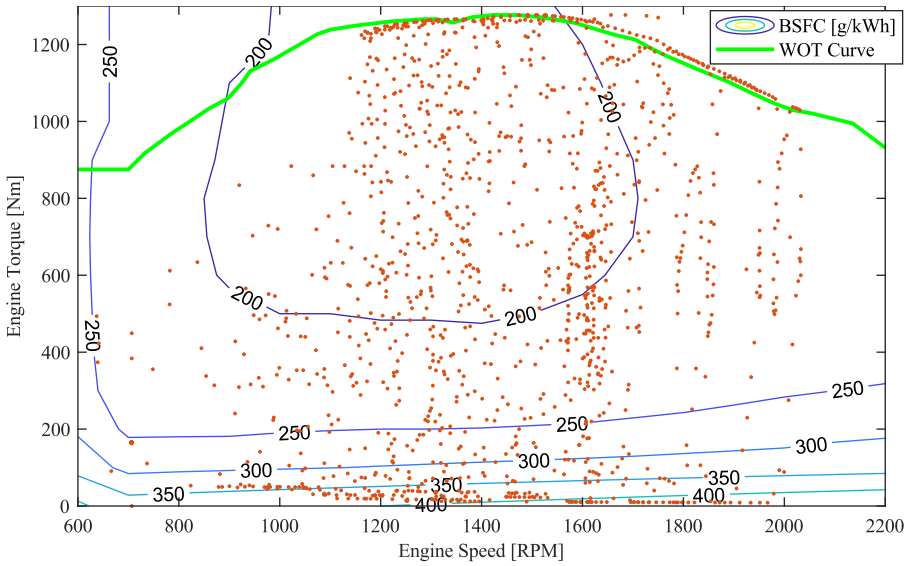

Figure 6.9: The engine operating points for the urban end-of-day cycle using a fuel map of a similar sized engine.

6.6 Refuse Truck Mass Characterization

The payload that the refuse truck can accommodate over the operational day is a significant factor to consider. An efficient refuse truck design should be able to gather all MSW along a specified route to reduce the number of trips required to offload if the capacity of the truck is reached prematurely before the end of the day. The refuse trucks in Hamilton are usually able to collect all MSW in a route without having to make more than one trip to

each respective drop off area for garbage and organics. On occasion, the truck will make more than one offload per category of MSW if large amounts of MSW are collected.

To meet the city of Hamilton's demand for waste collection, an alternative refuse truck configuration should match or exceed the current payload constraints. For the split side-loader, the total capacity of the garbage and organic sections are 15.1 m^3 and 10 m^3 respectively. The rear-loader truck has a capacity of 19.1 m^3. Based on information provided by the split SL-RT WCU manufacturer, garbage can be compacted to density of 386kg/m^3. A density for organics was not specified, a Canadian Government source was used for the typical density of household organics being 650 kg/m^3 [78]. Using these densities, the split SL-RT WCU can hold approximately 2540 kg and 5840 kg of MSW and organic respectively. The compacted garbage density of the RL-RT WCU manufacturer was not specified. As such, the maximum garbage payload collected by the truck over the data logging duration will be used as the maximum capacity, which was 12000 kg.

Given the total mass of the refuse truck, the mass of individual components can be added or subtracted to the overall truck mass, allowing accurate mass profiles of new powertrain configurations to be trialled. For example, when investigating an all-electric refuse truck, the masses of the conventional powertrain components should be removed, and the additional mass of the HV battery pack should be accounted for. The component masses of the studied split SL-RT and RL-RT are displayed in Table 6.3.

Table 6.3 categorizes a refuse truck's total mass into its chassis, WCU and payload potential. The major masses are outlined that may be of interest in approximating the

change of truck mass when trialling new powertrains. The remaining components on-board the truck will be assumed to carry across the different powertrains, where only the diesel tank and fuel, engine and transmission will be removed from the conventional powertrain. As defined early, the GVWR is the maximum possible weight the truck chassis can support and should not be surpassed when trialling new powertrain architectures.

Table 6.3: Refuse truck component masses.

Truck Component (kg)	Split SL-RT	RL-RT
Chassis		
Tare Mass	7020	7400
Diesel Fuel	159[6]	
Diesel Engine (dry)	740 [79]	
Transmission (dry)	330 [80]	
Fuel Tank	60 [81]	
WCU		
Tare Mass	6120	5500
Miscellaneous Mass[7]	2860	1500
Payload		
Garbage	5840	12000
Organic	2540	-
Truck Tare Mass	16000	14400
Truck GVWR	27216	27216

6.7 Battery Electric Refuse Truck

A battery electric refuse truck (BE-RT) is much more mechanically simplified compared to a conventional diesel truck, as the need for a complex transmission and torque converter

[6] Calculated using a diesel fuel density of 0.85 kg/L [104].

[7] Accounts for the remaining mass to equal to the trucks tare mass measured from the scale house.

is not required. The BE-RT's primary powertrain components include an electric traction motor responsible for propelling and regenerative braking, a HV battery pack, a rear differential, and wheels illustrated previously in Figure 3.1. In addition to the primary drivetrain, a secondary mechanical system must be available to meet the demands of the hydraulic WCU on-board. Traditionally, this is done with a PTO from a conventional truck's transmission. With a BE-RT, there are a few possible options to supply the necessary mechanical power to the hydraulic pump:

1. Configure a clutch on the main traction motor to divert mechanical power to the hydraulic pump. The hydraulic system on conventional trucks run on a constant speed of ~1200 RPM for compaction and offloading and ~700 RPM for operating an assistive loading arm. To simplify the powertrain, it will be assumed that the operation of the hydraulic system requires the truck to be stationary. This is how the conventional trucks operate. To allow the truck to move with the PTO clutch engaged, it would require a variable speed mechanical coupling to keep the hydraulic pump at the target speed, adding to the complexity of the model. Due to the traction motor operating at a variable torque at lower speeds, the traction motor will not be operating near best efficiency.
2. Use a smaller secondary electric motor or an electric hydraulic pump in addition to the traction motor. This configuration would allow the PTO system to operate separately from the powertrain. This configuration would allow the truck to be flexible with its PTO operation, allowing it to function whether the truck is

stationary or not. A smaller electric motor would allow it to operate closer to its best efficiency, though it would add additional weight to the vehicle.

3. Use an all-electric WCU instead of a hydraulic powered one. Having the input of a WCU as electric would allow a greater compatibility with a BE-RT. Hydraulic WCUs are the norm in current waste collection and because little information on the power requirements and energy consumption of electric WCUs are known, electric WCUs will not be considered in the model evaluation.

To simplify the consideration of the above options, only option one will be considered. Option two adds more complexity and cost to the model and the added functionality of driving while using the PTO is not an option the current refuse trucks use.

The BE-RT model was developed in *MATLAB* and *Simulink* and a top-level view of the vehicle plant is shown below.

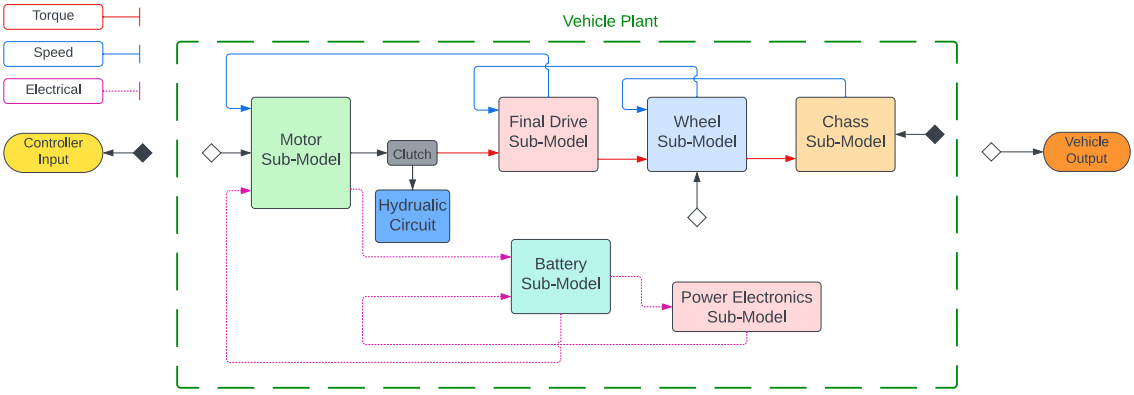

Figure 6.10: An overview of the vehicle plant for a battery electric refuse truck.

The vehicle plant evaluates each of the sub-models shown in Figure 6.10. Torque (red) is calculated from left to right, whereas chassis speed and rotational speed are calculated

backwards, right to left. There is a simplified clutch connecting the electric motor to the final drive or the hydraulic circuit. The chassis and wheel model calculate the road loads that the vehicle must overcome to accelerate. The final drive reduces the speed and multiplies the torque signals by the specified final drive ratio. The battery receives charge and discharge currents from the motor and power electronics allowing the change in battery SOC to be determined. The power electronics draw a constant power from the battery to account for electric loading from air conditioning and lighting.

The parameters for the BE-RT are shown below in Table 6.4. The parameters were obtained from credible sources or from model evaluation.

Table 6.4: Battery electric refuse truck parameters.

Parameter	Value	Unit	Parameter	Value	Unit
HTM-3500 Electric Motor [82]			Battery Pack [56]		
Max Power	400	kW	Capacity	360	kWh
Peak Torque	3500	Nm	Cell Type	LG 18650HG2	-
Max Speed	3500	RPM	Pack Configuration	223s120p	-
HPI-800 Inverter [83]			Pack Mass	2723	kg
Peak Output Current	800	A	Accessory Load	8.5	kW
DC Supply Voltage	400-800	V	Final Drive Ratio	5	-
Efficiency	0.98	-	Curb Mass	14030	kg
			Maximum Payload	12000	kg

Table 6.5: The LG 18650HG2 cell properties.

Parameter	Value
Nominal Capacity	3.0 Ah
Nominal Voltage	3.6 V
Cell Shape	Cylindrical
Cell Mass	0.047 g
Energy Density	240 Wh/kg
Power Density (discharge / charge)	0.30 kW/kg / 1.53 kW/kg

A final drive ratio of 5 was selected as the initial parameter value to closely match the conventional truck's ratio of 5.29. The final drive ratio will impact the operating points of the electric traction motor as it will simultaneously reduce the motors speed and multiply the motors torque to the wheels. A low final drive ratio will help obtain higher vehicle speeds at the cost of less usable wheel torque. Choosing an optimal final drive ratio involves trialling different ratios and quantifying the resultant in terms of motor and vehicle performance. The initial ratio of 5 yielded adequate traction motor operating points (torque, speed) shown in Section 6.7.3, thus the final drive ratio was not further optimized for the duration of this study. The results of the ratio on the motor operating points are adequate as a cluster of points can be seen accumulating near the most efficient regions of the motor's efficiency contour plot given a sample drive and duty cycle.

The battery pack mass was approximated using the number of cells required for the pack, the cell mass and a mass factor. A mass factor accounts for the battery management system (BMS), housing and pack temperature control. Determining the mass factor is difficult without doing analysis on the size of components required for a specific battery pack capacity. Further, literature on large battery pack sizes is limited as most literature is

focused on consumer level and light-duty vehicles that have smaller battery capacities of under 100 kWh.

A new vehicle from GMC called the *Hummer EV* is heavier vehicle that features a 210 kWh battery pack capacity, with a mass of 1326 kg [84], leading to a complete battery pack energy density of 158 Wh/kg. Little information is available about the battery cells used in this pack. It was assumed that the cells have a similar energy density to the LG 18650HG2 cell, which has an energy density similar to other popular types of battery cells used in electric vehicle applications. Therefore, if the energy density of a LG 18650HG2 cell is 240 Wh/kg ($\rho_{energy,cell}$), then the realized energy density of the entire pack ($\rho_{energy,pack}$) including housing, BMS and temperature control will be 158 Wh/kg, or an equivalent mass factor of 1.52 defined in Eq. 6.13.

$$\frac{\rho_{energy,cell}}{\rho_{energy,pack}} = \frac{240\ Wh/kg}{158\ Wh/kg} = 1.52 \qquad \text{Eq. 6.13}$$

Determining a mass factor to estimate additional mass added to the pack is important when considering less conventional energy dense cells, such as high-power cells that will be used in the range extended electric vehicle. The high-power cells will carry a large mass by themselves, and the mass factor will help approximate the remaining mass of the battery pack.

The size of the battery pack was incrementally adjusted during simulations to meet the needs of the most demanding drive and duty cycles. It was found that rural truck routes are the most demanding due to the long range and high variance in road grade compared to urban routes. Thus, the battery pack capacity was sized to ensure the truck could operate

on each of the rural routes given an initial battery state of charge (SOC) of 90% and a final SOC of at least 20%. An upper window of 90% and lower window of 20% were arbitrarily chosen to assume that the truck's battery would not be operating near the extremes of low or high capacity.

6.7.1 Battery Sub-Model

The battery model determines the HV battery terminal voltage (V_{term}) and SOC using the current demanded by the vehicle, an open circuit voltage (OCV) vs SOC relationship and discharging/chagrining resistances vs SOC relationships. The OCV is the electrical potential energy across the terminals of the battery cell while the circuit is open and without a load. To determine the voltage observed at the terminals under load, or the terminal voltage, the loss of electric potential energy inside the battery must be accounted for. Figure 6.11 shows a typical equivalent circuit model (ECM) of a battery, including V_{term}, OCV (V_{oc}) and dynamic voltage ($V_{dynamic}$), with the relationships between these variables defined in Eq. 6.14.

$$V_{term} = V_{oc} + V_{ohm} + V_{dynamic} \quad \text{Eq. 6.14}$$

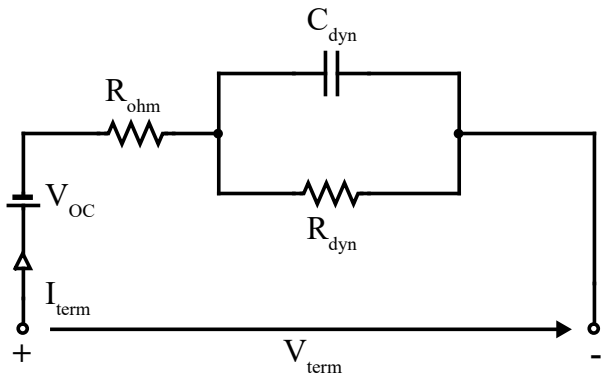

Figure 6.11: Equivalent circuit model of a battery cell.

To simplify the battery model, $V_{dynamic}$ and the dependency of the model on varying temperatures will not be considered. The battery model is assumed to be operating at 25ºC. With this simplification and substituting $V_{ohm} = R_{int}I$, the following relationship between V_{term} and V_{oc} is obtained in Eq. 6.16. R_{int} denotes the internal resistance of the battery cell

$$V_{term} = V_{oc} - R_{int}I \qquad \text{Eq. 6.15}$$

To estimate the battery SOC, a method called *Coulomb Counting* was used, where the current demanded from the battery is integrated over time to calculate the total sum of energy entering or leaving the battery. This SOC estimation is described in the following equation, where Cap_{Ah} is the initial battery in ampere-hours, $I(t)$ is the battery current in amperes and *sign* assigns a negative magnitude for charging and positive magnitude for discharging, defined by Eq. 6.16.

$$SOC(t) = SOC(t_i) + \frac{1}{Cap_{Ah} * 3600}\int_{t_i}^{t} I(t)\eta_{bat}\big(sign\big(I(t)\big), SOC\big)dt \qquad \text{Eq. 6.16}$$

Figure 6.12 shows how the Coulomb Counting technique was integrated into the *Simulink* model.

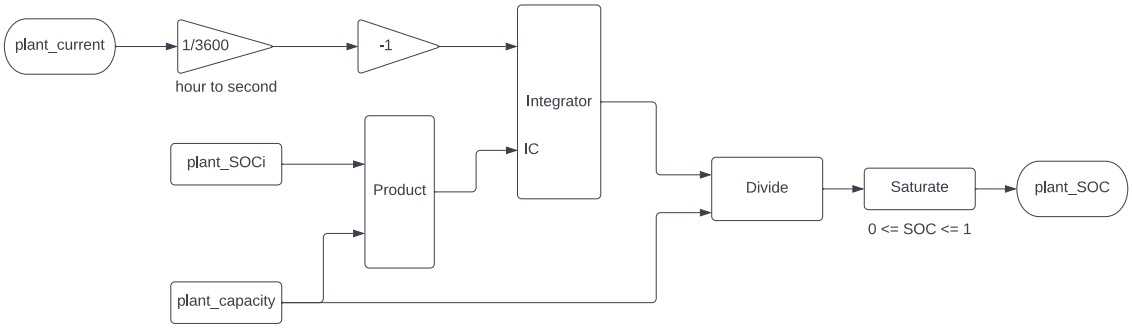

Figure 6.12: Battery state-of-charge estimation using the Coulomb Counting technique.

It should be noted that the divide block is configured to avoid dividing signals by zero. This block was used throughout the different vehicle models to divide signals. The formula used in the divider block is described in Eq. 6.17.

$$u_1/\big(u_1 + (u_2 = 0)\big) * (u_2 \neq 0) \qquad \text{Eq. 6.17}$$

Where u_1 is the numerator signal and u_2 is the denominator signal.

Once the SOC has been estimated, it can be used to calculate the corresponding V_{oc} given a V_{oc} vs SOC relationship. A V_{oc} vs SOC relationship is non-linear and an example of one for a LG 18650HG2 cell is shown in Figure 6.13.

To calculate the internal losses caused by the internal resistance of the battery pack, a discharge and charge resistance vs V_{oc} is required. Based on the current battery SOC and whether the battery is charging or discharging, different internal resistances can be approximated that will affect V_{ohm}. The corresponding charging (R_{chg}) and discharging (R_{dis}) resistance curves for a cell are shown in Figure 6.14.

The V_{oc}, R_{chg}, R_{dis} vs SOC curves are incorporated into the *Simulink* model as seen in Figure 6.15. Each curve is implemented as a 1-D lookup table. From here, the terminal voltage can be tracked throughout the simulation.

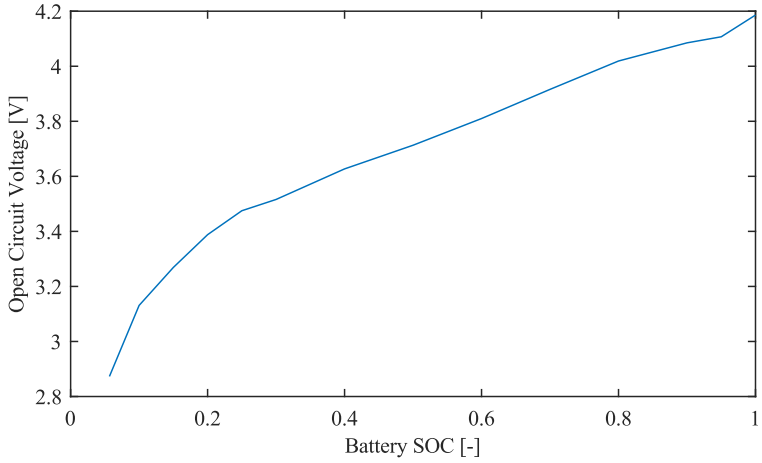

Figure 6.13: The open circuit voltage versus battery state-of-charge for the LG 18650HG2 cell.

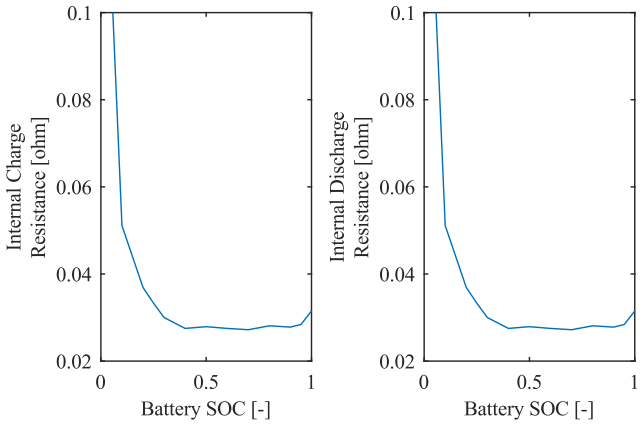

Figure 6.14: Internal charge resistance (left) and internal discharge resistance (right) for the LG HG2 18650 cell.

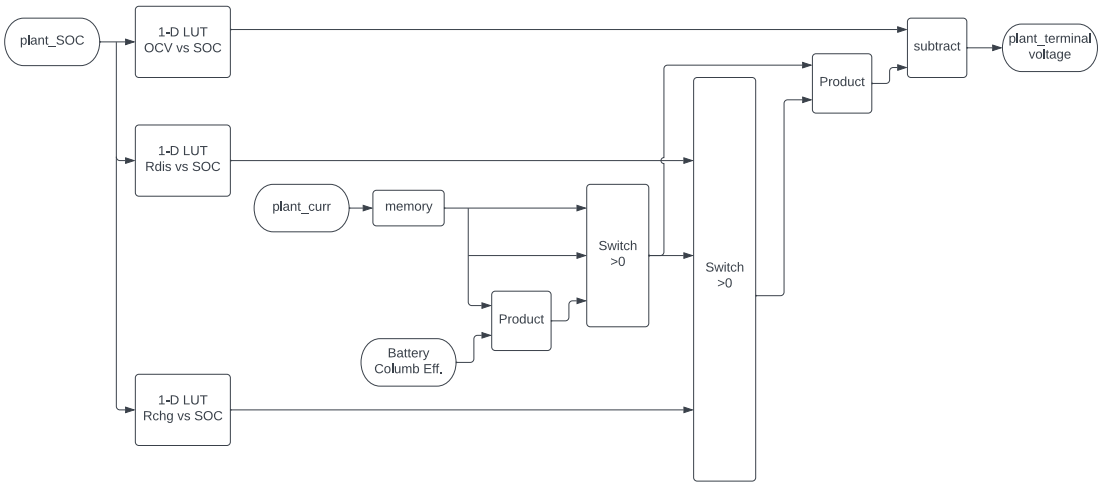

Figure 6.15: One-Dimensional look-up tables of open circuit voltage, internal charge and discharge resistance, as a function of battery state-of-charge.

6.7.2 Traction Motor Sub-Model

The HTM-3500 from *Equipmake* was selected as the traction motor due to its design for heavy-duty vehicle applications, including start and stop applications making it a good candidate for refuse trucks. The electric motor can be attached directly to the powertrain differential, eliminating the need for a multi-speed transmission. The torque-speed curve and efficiency map are shown in Figure 6.16. The efficiency map was obtained from *Equipmake* for the 400-kW variant of the electric motor [82]. To match a real-world scenario, the 340-kW variant was selected as it is similar to the motor used on the Lion8 BE-RT described in Section 3.1.2. The efficiency map for the 400-kW motor was scaled down appropriately to match the 340-kW.

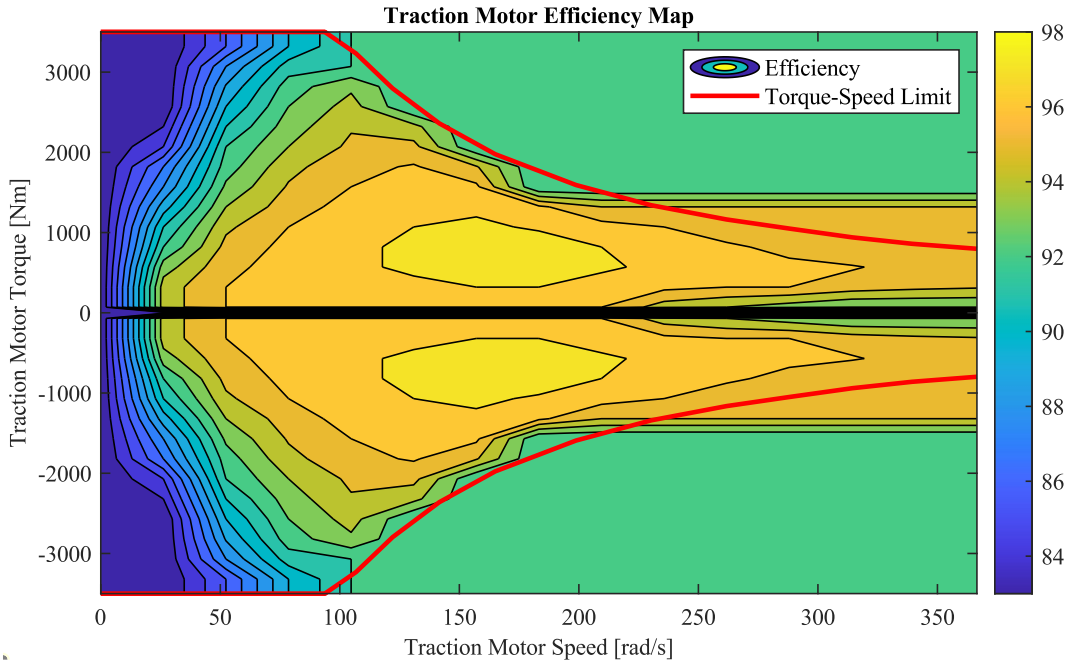

Figure 6.16: Traction motor efficiency map, digitized from *Equipmake's* publicly available efficiency specifications.

Equipmake also manufactures inverters that are compatible with their motors. The HPI-800 was selected due to its capacity to handle the high-power demand of the electric motor. The efficiency of the inverter was assumed to be a constant 98% [83].

The regenerative braking is controlled by a relationship between the fraction of regen that can be accepted for a specific vehicle speed, shown in Figure 6.17. For a given speed, the vehicle can recuperate a fraction of the braking torque. The fraction of braking torque that is dependent on the vehicle's speed must also be less than the maximum torque that the traction motor can accept. This is a simplified method of calculating the accepted regenerative braking energy, where a more accurate model is achievable through collaboration with the vehicle's original equipment manufacturer (OEM).

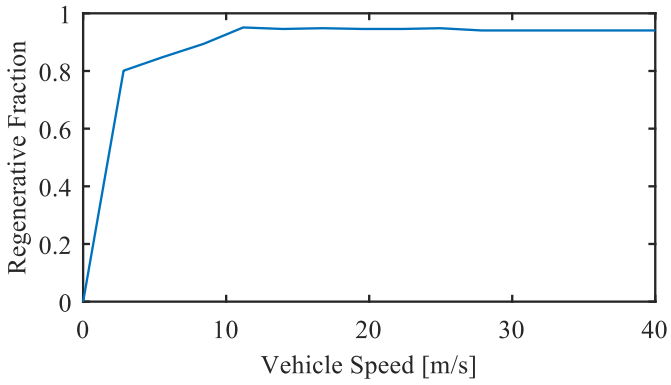

Figure 6.17: The fraction of braking torque that is accepted for regen for a specific speed [57].

6.7.3 Simulation Results

The BE-RT model was simulated for each operating day for both the urban RL-RT and urban/rural SL-RT. This allows for a comprehensive study to be completed to determine whether the BE-RT with the specified parameters would be able to meet the demands the city has for these truck routes.

A sample simulation running on a rural route will be investigated. In Figure 6.18 the model tracks the desired speed quite well, shown in the first quarter subplot. A magnified view between 25 and 30% of the operational day is shown, to see how the driver sub-model can react to the changes in desired speed. The remaining subplots show the entire operational day. The model initial SOC was set at 90% and depleted to 0.12% after this specific route. It should be noted that because this was a rural route, the battery SOC experiences the deepest total discharge, compared to urban routes due to the long route distances. The total battery consumption for the route was 225 kWh. The maximum charge and discharge powers of the battery were 413 and -310 kW respectively.

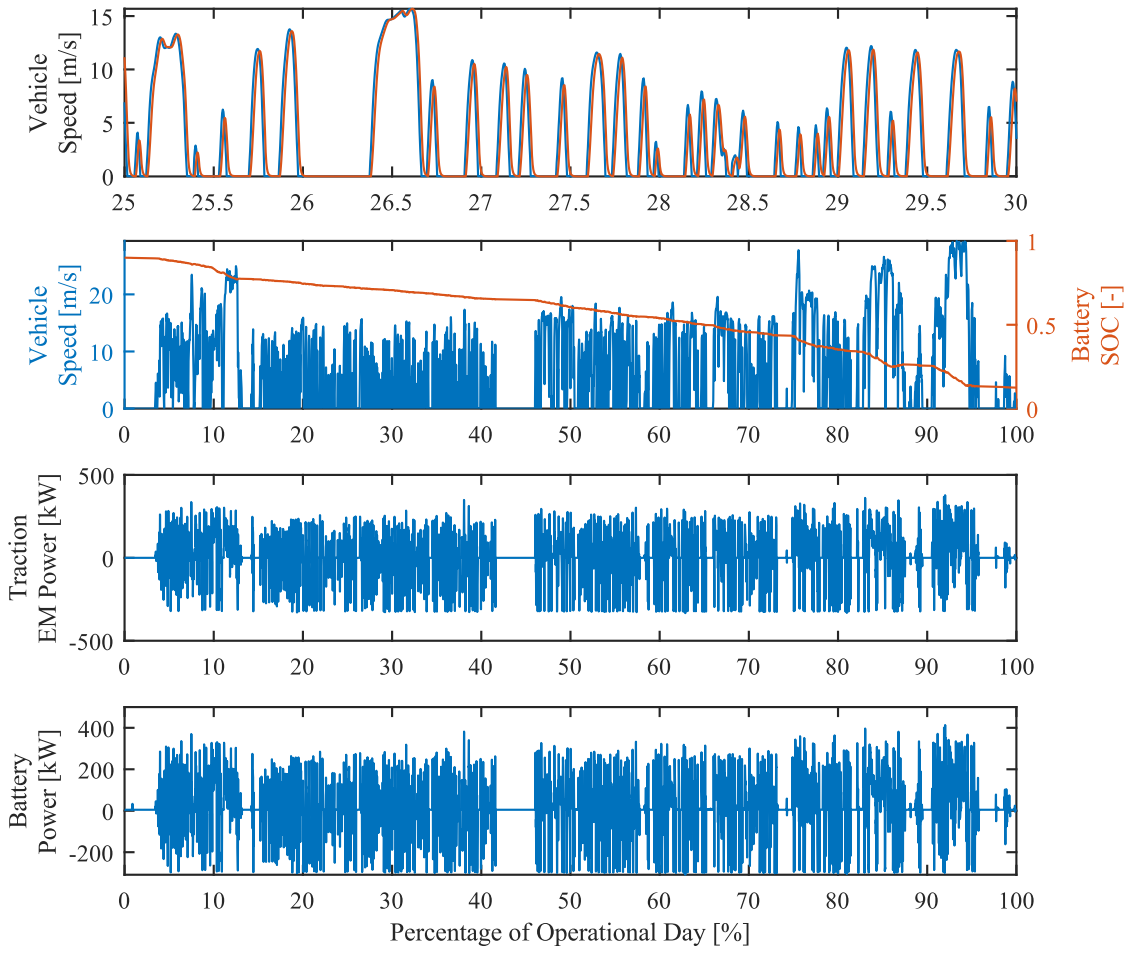

Figure 6.18: Battery electric refuse truck model trends for a sample rural cycle.

The operating points for the traction motor are shown in Figure 6.19, illustrating that the traction motor operates within the possible limits of the maximum torque. With a final drive ratio 5, a large portion of operation points land within the higher efficiency regions of the motor, except for high torques to accelerate the stationary truck, or deep regenerative braking torque commands.

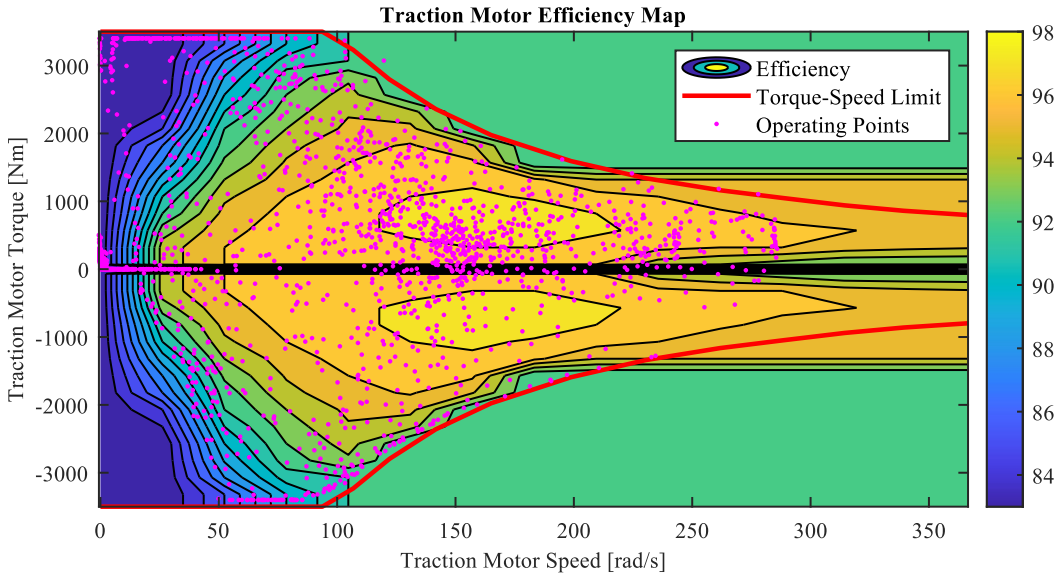

Figure 6.19: The operating points of the traction motor for a sample rural route.

Generalized trends for simulating all operational days for both the split SL-RT and RL-RT in the battery electric model are shown in the following boxplots in Figure 6.20. Due to the Monday route being rural and the longest distance for the SL-RT, it makes sense that the highest battery consumption occurs on this route. The Monday route also has the highest amount of road grade variation. This variation puts larger amounts of power requests on the driver which strains the driver sub-model leading to a larger RMSE between the desired vehicle speed and the model's speed. For both the SL-RT and RL-RT on urban routes, the typical battery consumption was under 100 kWh per day.

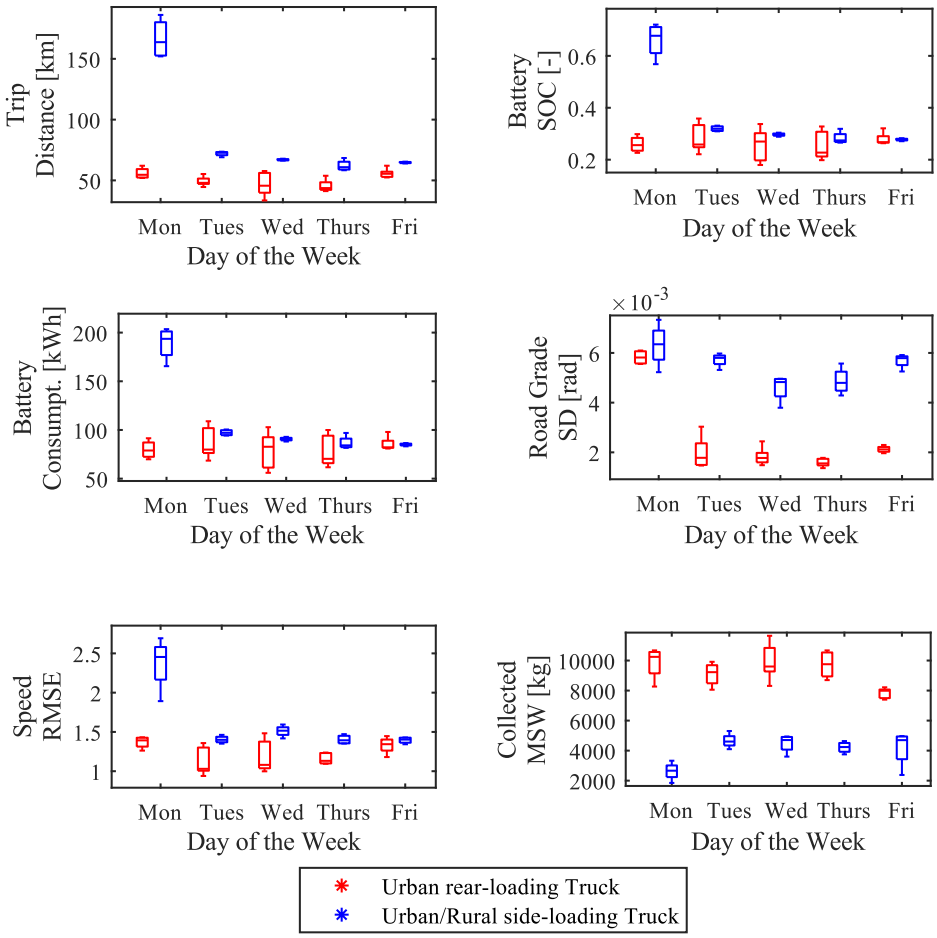

Figure 6.20: Battery electric model generalized operating trends for the urban rear-loading and urban/rural split side-loading refuse truck.

6.8 Range Extended Electric Refuse Truck

A promising alternative to BE-RT is the use of a REEV architecture in heavy-duty vehicles. As mentioned in Section 3.2, a REEV architecture allows the battery to be downsized, gives more range to the same battery capacity, or allows the battery pack to be more power dense. A common issue with current Li-ion battery cell technology is not being able to achieve both high energy and power density, where one is forfeited to achieve the other.

By adding extra range through a small engine and generator, battery cells that are more power dense at the expense of being less energy dense can be chosen. This allows the battery pack to supply higher current to the inverter and traction motor, while being able to accept larger regenerative currents when braking.

A range extended electric refuse truck (REE-RT) was modelled using the same driver, chassis and wheel sub-models as the previous models discussed. What changes is the vehicle's plant model, shown in Figure 6.21. In addition to the components in the BE-RT's plant model, a REE-RT has an engine and generator as well. The engine consumes gasoline fuel using a small spark-ignition (SI) engine, which produces mechanical power that the generator can convert to electrical energy. The generator is also used to supply mechanical power to the hydraulic pump, where it will operate as a motor. This is favourable over coupling the hydraulic pump to the main traction motor, as the generator is a smaller machine and will operate in more efficient regions than the traction motor, as the PTO power requests are smaller in magnitude than traction requests. The generator can be decoupled from the engine to turn the hydraulic pump, and vice versa to receive mechanical power from the engine.

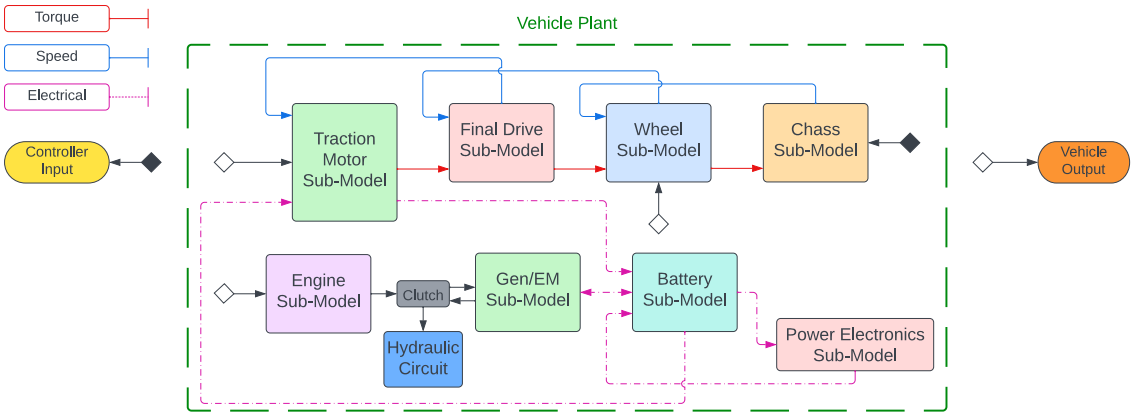

Figure 6.21: An overview of a vehicle plant for a range extended electric refuse truck.

The REE-RT parameters are displayed in Table 6.6. The traction motor and inverter are the identical to the components used in the BE-RT model.

Table 6.6: Range extended electric refuse truck parameters.

Parameter	Value	Unit	Parameter	Value	Unit
HTM-3500 Electric Motor[8]	-	-	Engine [85]		
HPI-800 Inverter[8]	-	-	Max Power	130	kW
HV Battery Pack			Peak Torque	230	Nm
Capacity	240	kWh	Max Speed	6300	RPM
Cell Type:	LTO	-	Mass [86]	97	kg
Pack Configuration	334s60p	-	Generator [87]		
Pack Mass	2520	kg	Max Power	130	kW
Accessory Load	12.5	kW	Peak Torque	450	Nm
Final Drive Ratio	5	-	Max Speed	9000	RPM
Curb Mass	17380	kg			
Maximum Payload	9840	kg			

[8] Each component has the same parameters as the BE-RT model.

The final drive ratio, battery pack size, motor and inverter for the REE-RT were chosen on a similar basis as the BE-RT described in Section 6.7. The optimum sizing of the engine and generator are critical to the vehicle's energy management system as these components are used to provide supplemental energy to the vehicles HV battery. Minimal information is available for sizing engines and generators for a REE-RT application. Information from the literature mentioned a generator size of 80 kW [42]. A higher power dense engine and generator combination of 130 kW was chosen.

The engine type was chosen first to match a power output of 130 kW and then a theoretical generator was developed to ensure operation in optimal efficiency regions given the output torque and speed of the engine at peak power output. Information on the engine and generator are described in Section 6.8.1.

6.8.1 Generator and Engine Selection and Maps

The generator and engine are responsible for supplying the REE-RT with supplemental energy to the HV battery pack. The selected 130 kW generator can accept most operating points from the engine. The generator is coupled to the engine at a 1:1 gear ratio. The properties of the generator were created using *Simcenter Amesim*, where inputs such as motor power, speed and torque can be used to size a theoretical motor. Below, is the efficiency plot of the generator.

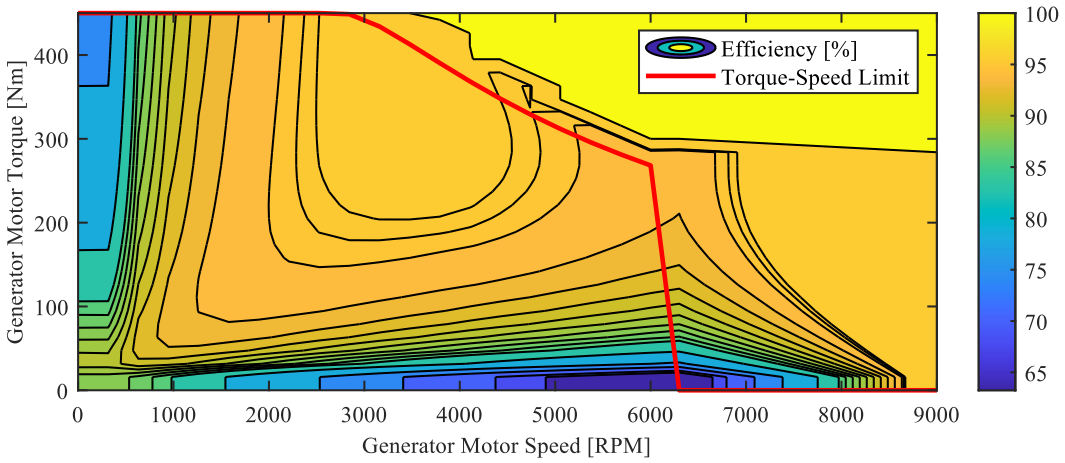

Figure 6.22: Range Extended Electric Vehicle generator efficiency map, in absolute torque [87].

The engine chosen was a Honda 1.5 L SI engine rated at 130 kW at 6000 RPM, to match the approximate power rating for the engine used in real world REEV scenarios [42]. The engine sub-model in a REE-RT is much simpler compared to a conventional vehicle as the engine is mechanically decoupled from the powertrain. The purpose of this engine sub-model is to track the fuel consumption of the engine given a power output that is required by the generator to give the HV battery additional range.

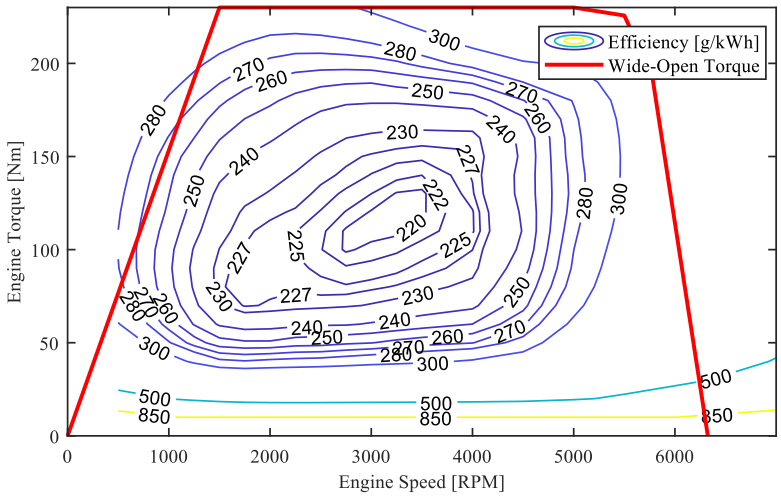

Figure 6.23: 1.5 L engine brake specific fuel consumption map [85].

6.8.2 Battery Cell Selection

The battery cell selection for a REE-RT can be designed to meet different requirements compared to a BE-RT. Because a REE-RT has an additional energy source, being the fuel tank, the battery pack can be optimized to be more power dense, compared to being more energy dense. Typically, a BEV battery pack is designed to be energy dense to maximize the vehicles range, so the battery cells that are chosen will be more energy dense at the expense of lowering the power density, due to the current battery cell technology. Energy and power density are balanced on opposite ends of the cell technology spectrum, where one is usually higher than the other.

The energy density of the cells used in the BE-RT have an energy density of 250 Wh/kg and a power density of 0.30 kW/kg and 1.53 kW/kg for charging and discharging respectively.

The battery cell chosen for the REE-RT was a lithium-titanate oxide (LTO) cell, with its properties shown below in Table 6.7 [54].

Table 6.7: The properties of a LTO battery cell.

Parameter	Metric
Nominal Capacity	2.9 Ah
Nominal Voltage	2.4 V
Cell Shape	Prismatic
Weight	150.8 g
Energy Density	45 Wh/kg
Power Density (discharge / charge)	3.2 kW/kg / 3.2 kW/kg

The LTO cell is much heavier than the LG 18650HG2 cell at 150.8 g compared to 0.047 g, and thus has a much lower energy density. Although, the power density of this cell is much higher compared to the LG 18560HG2 allowing the battery pack to handle higher power demand from either traction requests, regenerative braking or from the generator. The relationships between the cell's OCV and internal resistances versus SOC relationships are shown in Figure 6.24 and Figure 6.25 respectively.

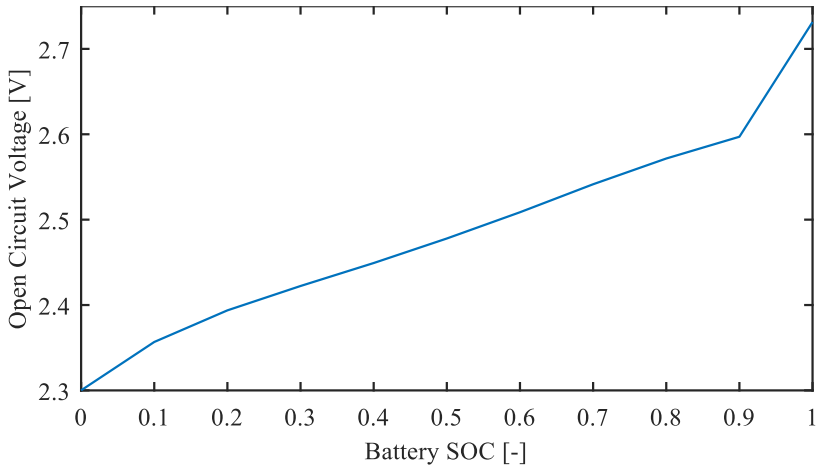

Figure 6.24: LTO battery open circuit voltage versus state-of-charge relationship.

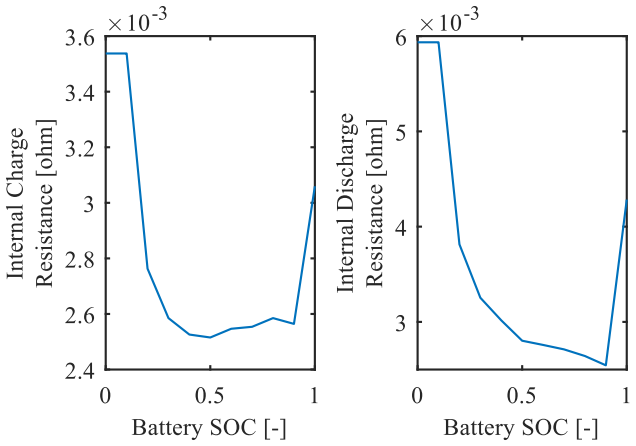

Figure 6.25: Internal charge resistance (left) and internal discharge resistance (right) for the LTO cell.

6.8.3 Dynamic Programming Optimization

The use of a REE-RT, or a series hybrid powertrain architecture introduces the additional complexity of an auxiliary ESS, where the storage system is an engine and fuel tank. Specifically, the control scheme for how to operate the engine can be challenging, as the engine is mechanically decoupled from the wheels. The engine can be turned on arbitrarily but should be done so only when necessary to minimize fuel consumption and tailpipe emissions.

Since the operation of the engine is arbitrary, finding an optimal sequence of engine usage events throughout each situation will be useful. A method to determine the most optimal engine usage is using a dynamic programmer (DP), which is a form of global optimization offline control technique. The workflow for a DP is shown in Figure 6.26.

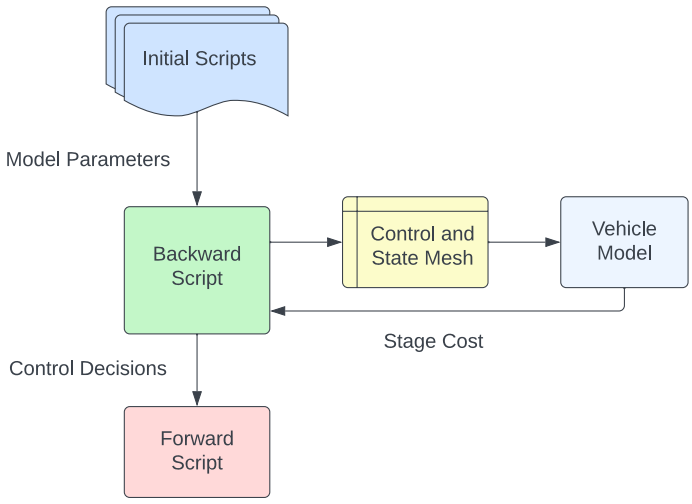

Figure 6.26: The workflow for implementing a DP.

An offline control technique is computationally expensive and cannot be done in real time, as the controller must know the entire drive cycle beforehand. In the case of a refuse truck, the duty cycle must be known beforehand as well. This makes an inadequate real-world solution, as the controller cannot adapt to changes in the drive and duty cycle in real time. The usefulness of a DP is to analyse the model's response to a drive and duty cycle and use this response to help tune the controls of a real-time controller to improve the fuel economy.

A DP finds the global optimization given a set of drive and duty cycles, by running backwards through the cycles. A set number of state and control variables are defined, which represent the problem the DP is attempting to optimize. The states define the environment that the DP attempts to optimize, whereas the controls dictate how the DP can switch between the available states. Given all possible combinations of states and controls defined within a mesh, the DP will find the path from the end of the cycle to the initial conditions that minimize an objective function at each stage. At each stage, the minimum

stage cost is evaluated given a combination of state and control variables as shown in Figure 6.27.

To apply the DP to a REE-RT, the states $X(i)$ and controls $U(j)$ are defined as the following in Eq. 6.18 and Eq. 6.19.

$$X(i) = \begin{bmatrix} T_{engine}(i) \\ \omega_{engine}(i) \\ SOC(i) \end{bmatrix} \quad \text{Eq. 6.18}$$

$$U(j) = \begin{bmatrix} \Delta T_{engine}(j) \\ \Delta \omega_{engine}(j) \end{bmatrix} \quad \text{Eq. 6.19}$$

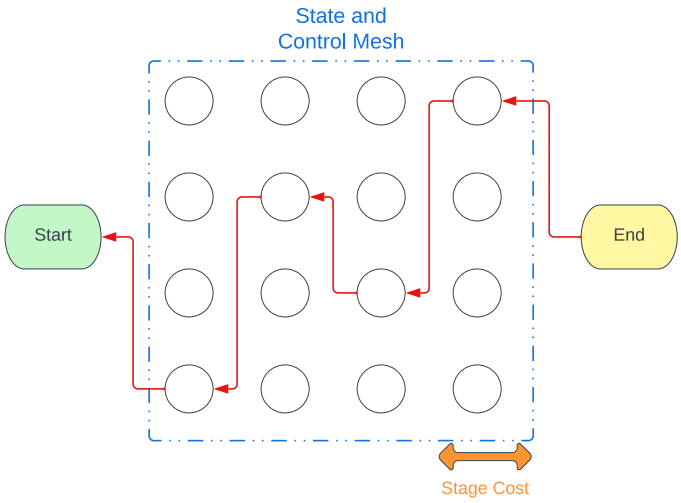

Figure 6.27: A simplified explanation of the backwards evaluation method of the DP.

The states and controls are carefully chosen to achieve an effective solution considering as much of the trucks operating environment as possible, while not adding unnecessary states or controls. This is because the addition of more states or control variables significantly increases the mesh size by many orders of magnitude, exponentially increasing the solving

time of the DP. The cost function (G_k) to evaluate each stage during the backwards evaluation is defined in Eq. 6.20 from the literature [88].

$$G_k(X_i, U_j) = \dot{m}_{fuel}(X_i, U_j) + \zeta * \Delta\text{Mode} + \Gamma * (\text{X}_\text{i}, \text{U}_\text{j}) \qquad \text{Eq. 6.20}$$

Where $\dot{m}_{fuel}$ is the instantaneous fuel consumption, ζ and Γ represent penalties applied to switching the engine on and infeasible operations, respectively. Infeasible operations carry a penalty of 10^6, whereas feasible operations are assigned a penalty of zero.

The DP solver that was utilized is called *DynaProg* [89], which is a *MATLAB* toolbox. This solver evaluates the backwards and forwards model given a problem defined by initial scripts.

To evaluate the operation of the engine, three scenarios will be considered:

1. Collection Zone operation on an urban route
2. Collection zone operation on a rural route
3. End-of-day off-route travel from collection zone to transfer station.

At any given moment, the truck can be operating in pure electric mode (EV), where the engine is off. Or the truck can operate in a hybrid mode (HEV) when the engine is on and supplying mechanical power to the generator. During each of these scenarios, the DP will evaluate whether the truck can operate in a charge-sustaining mode or a charge-depleting mode. A charge-sustaining mode means the engine and generator can supply enough energy to offset the energy consumed by the HV battery pack from tractive efforts and accessory loads. Charge-depleting mode means that the energy supplied by the engine and

generator does not completely offset the energy consumed by the HV battery and accessory loads.

The DP results for each scenario for urban and rural routes are shown below.

Urban Route: Collection Zone Trends

For the urban collection zone route segment shown in Figure 6.28, the trip distance was 0.58 km, the engine consumed 0.21 L of gasoline and the battery had a net energy consumption of -0.20 kWh. The net energy consumption is negative because the DP selected a final SOC slightly higher than the initial SOC while attempting to solve for charge sustaining, due to the resolution of selectable SOC points.

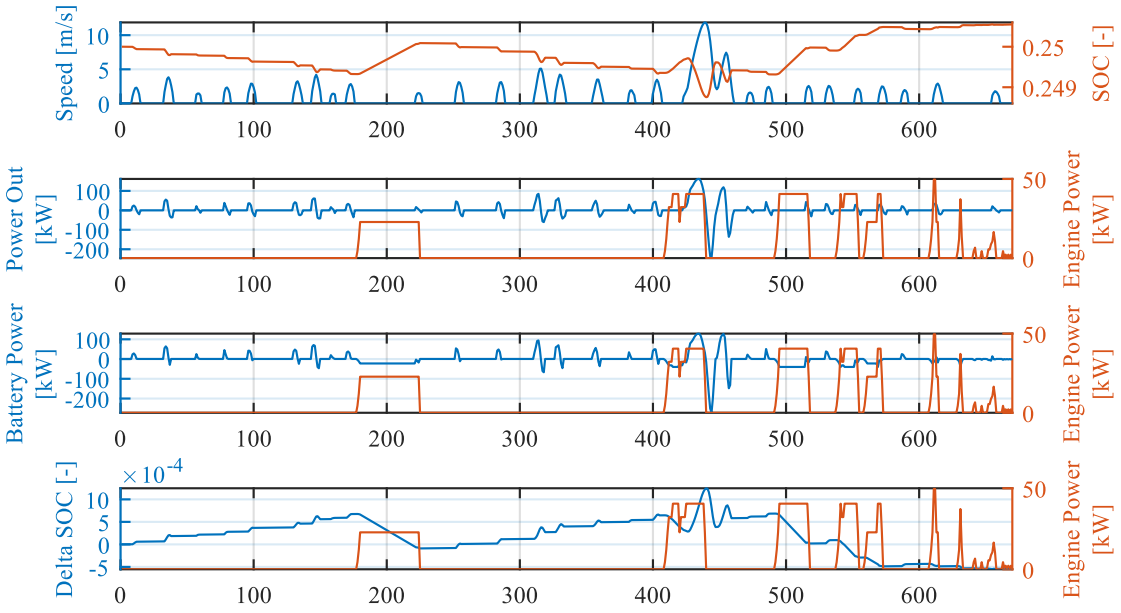

Figure 6.28: Dynamic programmer results of the split side-loader collection zone route in an urban area.

Urban Route: End-of-day Trends

The urban end-of-day route segment, shown in Figure 6.29, covered a trip distance of 26.1 km, the engine consumed 7.3 L of gasoline and the net battery consumption was 19.8 kWh operating in a charge-depleting mode. This route segment involves the truck travelling at highway speeds while under maximum payload. As such, the engine must be on a significant amount of time to reduce the rate of SOC discharge. During this segment, it is not possible to achieve charge-sustaining with the current engine and generator size. A large engine and generator must be used if charge-sustaining is desirable for this segment.

Rural Route: Collection Zone Trends

The rural collection zone route segment, shown in Figure 6.30, covered 4.6 km of distance, the engine consumed 1.0 L of gasoline and the net battery energy consumption was -0.70 kWh. The net energy consumption is negative because the DP selected a final SOC slightly higher than the initial SOC while attempting to solve for charge-sustaining, due to the resolution of selectable SOC points.

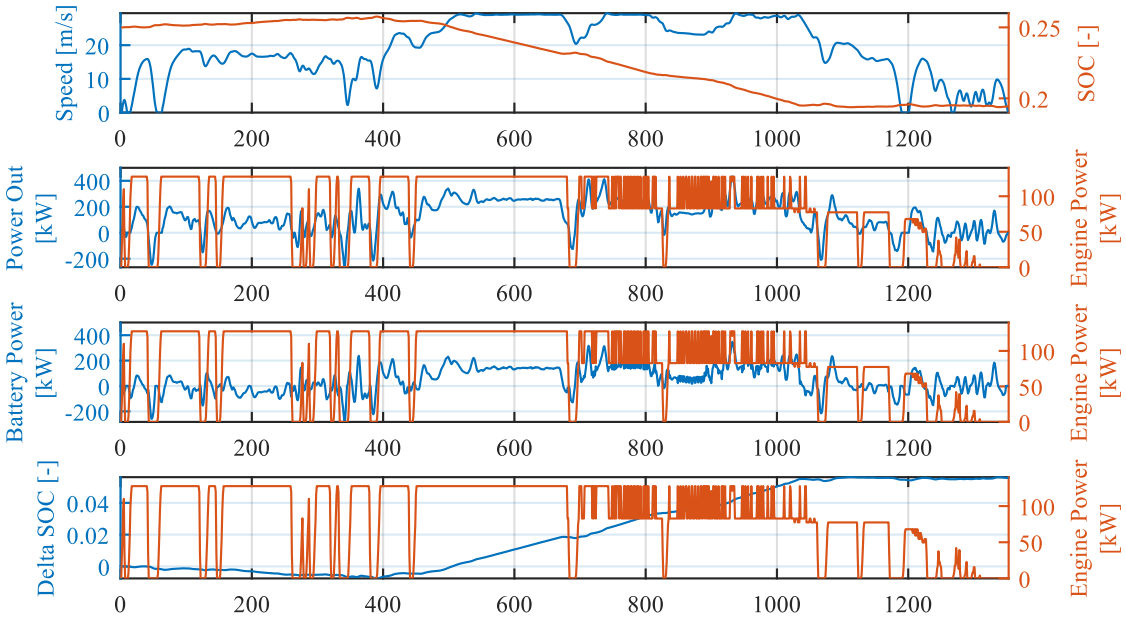

Figure 6.29: Dynamic programmer results of the split-side loader for an end-of-day trip from the collection zone to a transfer site.

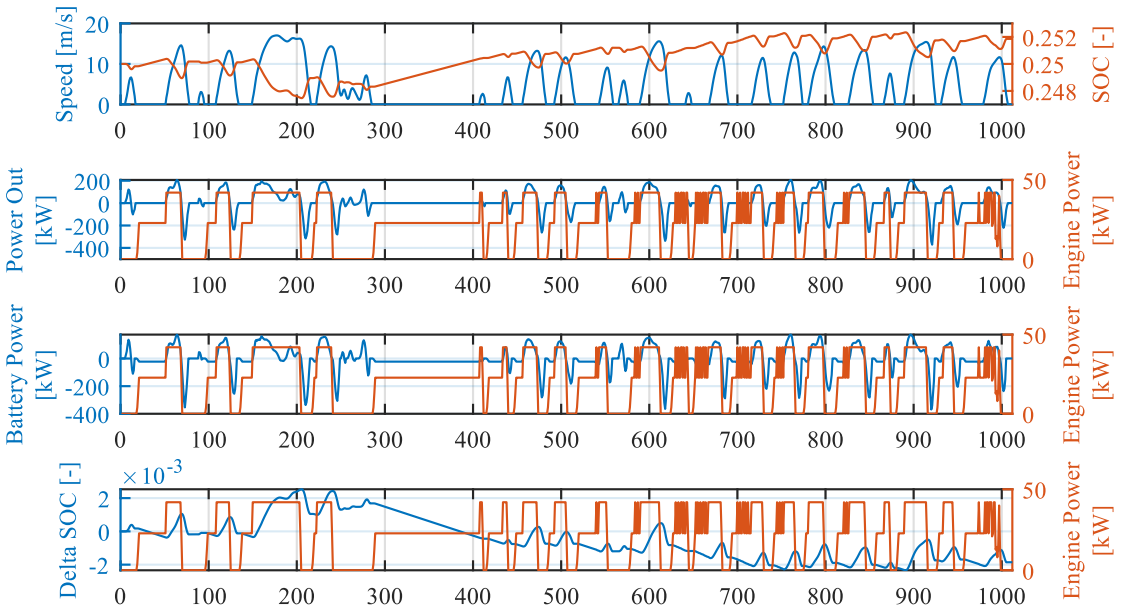

Figure 6.30: Dynamic programmer results of the split side-loader collection zone route in a rural area.

These situations were considered because together they cover a large range of typical refuse truck operation on a day-to-day basis. The urban collection zone operation typically has lower sustained power output from the wheels due to lower travel speeds and lower accumulated payload. The rural collection zone operation has similar characteristics to its urban counterpart, but sustained speeds tend to be higher as more rural highway driving occurs.

Both urban and rural scenarios were able to achieve charge-sustaining, which means that the engine and generator can supply supplemental energy to return the battery SOC to its initial value by the end of the cycle. This is an important observation as the online control scheme for a REE-RT can then assume that while the truck is operating in the collection zone on an urban or rural route, the energy management system (EMS) is capable of charging-sustaining. It is possible that when the truck's payload passes a certain threshold, that the current powertrain components could not sustain the battery SOC, and the EMS would need to operate in a charge depleting mode.

The end-of-day cycle operation for both urban and rural routes are quite similar, and thus only the end-of-day cycle for an urban route was considered. Here, the truck's payload is at the maximum amount for that day and the truck will experience highway driving. Power out at the wheels will be significant for sustained periods of time, resulting in a high-power draw from the battery and rapid decrease in battery SOC. With the current engine size, generator size and battery charge limits, it was not feasible to charge-sustain during the end-of-day cycle. The EMS can turn on the engine to reduce the rate at which the battery SOC decreases in a charge-depletion mode.

The operating points of the engine from each scenario are shown in Figure 6.31. Similar trends can be concluded as compared to the previously discussed plots. The urban end-of-day (EOD) cycle demands the highest engine operating points compared to the collection zone (CZ) cycles for rural and urban. The urban end-of-day cycle requests near maximum engine power which means if charge-sustaining is to be achieve during the end-of-day cycle, a larger engine and generator must be used in the truck's powertrain.

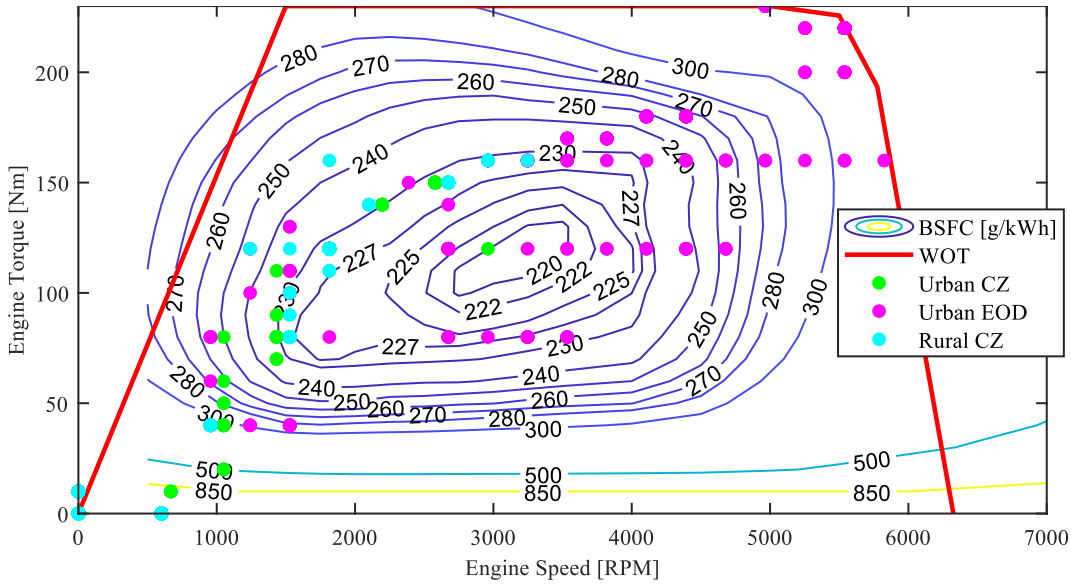

Figure 6.31: Engine operating points for all dynamic programmer scenarios. EOD is end-of-day and CZ is collection zone.

6.8.4 Real Time Control Strategy

Creating an online control strategy for a REE-RT is necessary for it to operate in real-time. Control decisions from the DP can be used to aid in the design of an online control strategy. Also, the daily routines of refuse trucks present the opportunity to design a control strategy

that can adapt to the route for a given day. It was found that whether a truck is on a rural or urban route, the kinematics are different when the truck is in the collection zone.

Given the trends seen in the previous section in terms of engine performance over urban or rural cycles, a simplified online controller can be implemented to utilize the engine to prevent the on-board battery pack from depleting too low. The initial battery SOC is set at 80% and an ideal final battery SOC is assumed to be above 20%.

The online controller must be capable of detecting whether the refuse truck is on an urban or rural route and whether it is within the collection zone or not on either route. To achieve this control logic, *StateFlow* was implemented into the *Simulink* model, as this allows the model to react to different conditions as they are met along a route. A flow chart is illustrated in Figure 6.32 to show how the *StateFlow* logic was placed into the *Simulink* model environment. The purpose of this block is to control when the engine turns on (HEV) or turns off (EV). Within this decision, there are two paths to consider. The blue path is when the truck is off-route, travelling between the truck yard, transfer station and collection zone. The red path is when the truck is in the collection zone for either a rural or urban route. This is determined using the GPS location of the truck and the geo-referenced bounds of each collection zone.

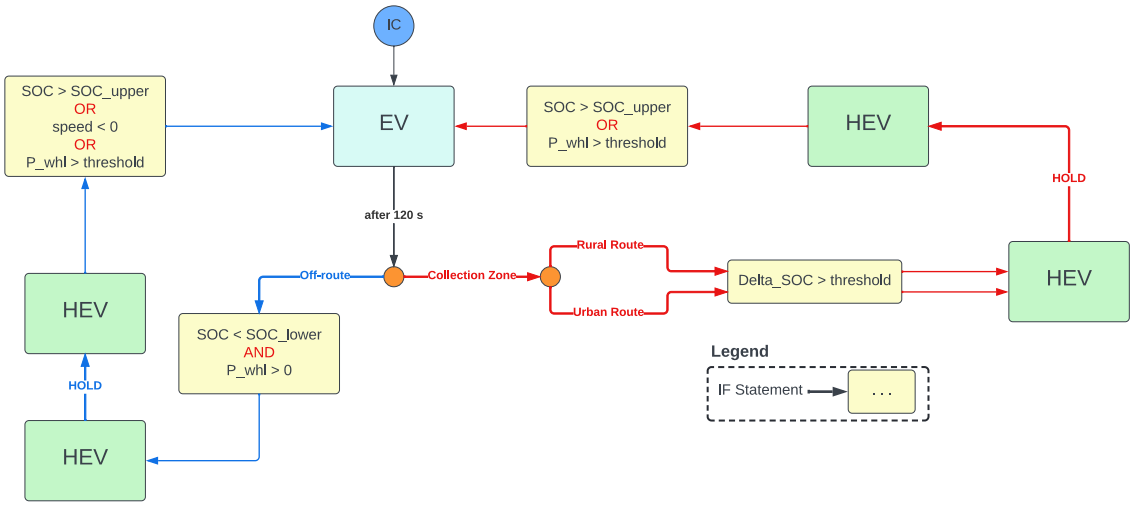

Figure 6.32: Online REEV control logic, produced in *Simulink StateFlow*.

Blue Path

When the truck is off-route, it experiences high sustained speeds and high magnitudes of battery power are requested for both tractive and regenerative efforts. On this path, the engine is only turned on if the wheel power (P_{whl}) is greater than zero and the battery SOC is below the lower threshold (SOC_{lower}). The engine is turned on when P_{whl} is above zero to prevent the engine turning on while the vehicle is stationary or braking, to reduce driver confusion. Once the truck is in HEV mode, it is held in HEV mode for a minimum duration. After the minimum duration has passed, the truck will switch to EV mode once the upper SOC threshold (SOC_{upper}) has been reached, or vehicle speed equals 0 or regenerative power at the wheels (P_{whl}) surpasses maximum battery charging power. The minimum durations are listed in Table 6.8. After the truck enters EV mode, it is kept in this mode for a minimum of 120 seconds. This prevents rapid switching between engine on and engine off events.

Red Path

When the truck is in collection zone and in an urban area, lower vehicle speeds are observed between 0 to 15 m/s, with low amounts of power draw from the battery. In a rural area, higher speeds are seen between 0 to 20 m/s. Within this operating period, battery SOC does not reduce rapidly, and charge sustaining can be achieved with proper engine control and lower accumulated payloads. The engine will turn on when the delta SOC in the collection zone (ΔSOC_{CZ}) increases past a threshold. When the truck enters the collection zone, the battery SOC at this time instance is stored as the initial collection zone ($SOC_{initial,CZ}$). The delta SOC is then defined by Eq. 6.21:

$$\Delta SOC_{CZ} = SOC_{initial,CZ} - SOC \qquad \text{Eq. 6.21}$$

When the ΔSOC_{CZ} is greater than a threshold, the truck enters HEV mode. The truck will be held in HEV mode for a minimum duration, then be switched to EV mode when the SOC is greater than the upper threshold (SOC_{uper}) or P_{whl} is greater than the maximum battery power charge limit. As with the off-route path, the truck will be kept in EV mode for 120 seconds before further control decisions are made.

The outputs of the *StateFlow* logic controller include the previously mentioned HEV holding periods and the HEV mode, listed in Table 6.8. The HEV mode describes 4 different scenarios where the engine is on, where each mode describes a different operating engine power, given if the route is rural or urban and whether the truck is in the collection zone or off-route.

Table 6.8: Input and output parameters for the *StateFlow* logic, implemented in *Simulink*.

Input	Value	Output	Value
SOC (Plant)	Model Dependent	HEV Hold Durations	
P_{whl}	Model Dependent	Off-route	Urban: 30 sec, Rural 60 sec
Speed (Plant)	Model Dependent	Collection Zone	Urban: 30 sec, Rural: 40 sec
SOC_{upper}	45%	HEV Mode	Urban, off-route = 1
SOC_{lower}	30%		Urban, collection zone = 2
Truck Mode	Off-route = 0, On-route = 1		Rural, off-route = 3
$SOC_{initial,CZ}$ (Start of Collection Zone)	Battery SOC when truck enters on-route.		Rural, collection zone = 4

6.8.5 Real Time Controller Comparison

The real time controller developed in the previous subsection was evaluated in the scenarios that the DP was exposed to, given the same constraints on battery SOC. A comparison between the two control strategies is shown in Table 6.9. The performance of the real-time controller on the urban collection zone was comparable to the DP for each compared metric. The real-time controller results for the rural collection zone and urban end-of-day routes deviated from the DP due to the rule-based controls on holding the engine on and off for specific time intervals. The results from the DP show that the engine can be turn on or off in quick succession.

Table 6.9: A comparative chart between the real time control strategy and the DP off-line control solution.

	Urban Collection Zone		Rural Collection Zone		Urban End-of-Day	
Parameter	DP	Real Time	DP	Real Time	DP	Real Time
Fuel Usage	0.21 L	0.25 L	1.04 L	0.63 L	7.25 L	6.60 L
Battery Consumption	-0.20 kWh	0.68 kWh	0.77 kWh	3.33 kWh	19.77 kWh	23.59 kWh
Final SOC	25.05 %	24.72 %	24.71 %	23.73 %	19.43 %	17.50 %

6.8.6 Simulation Results

Similar to the BE-RT, the REE-RT was simulated for each day that operational data was available for. A sample urban cycle is shown Figure 6.33. The REE-RT powertrain consumed 10.60 L of gasoline and used 78.28 kWh of battery capacity. As mentioned in the REE-RT control strategy, the engine operates at different powers depending on whether the truck is in the collection zone or not. Within the collection zone or between 15 to 75% of the operational day, the engine outputs 23 kW of power to the generator. At this power output, the battery SOC depletion rate is reduced. The magnitude of SOC depletion rate in the collection zone with the current control strategy is a function of the accumulated payload. A more complex control strategy could adapt to the accumulated truck payload, but this level of complexity will not be considered. Off-route or between 75 to 100% of the operational day, the engine outputs 94 kW of power to the generator. The maximum and minimum battery power observed was 400 and -402 kW respectively.

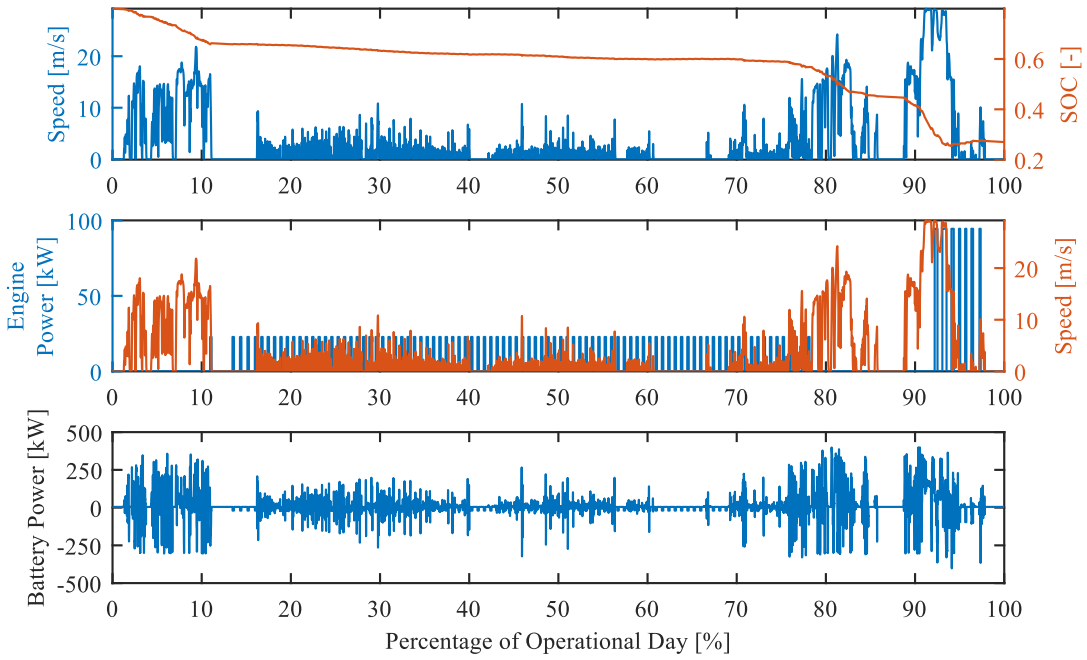

Figure 6.33: The range extended electric refuse truck model results for a sample urban route.

Figure 6.34 shows general simulation trends from all operational data logged from the study refuse trucks with regards to their routes. Similar to the BE-RT model, the highest battery consumption occurs during the rural route, or the Monday route shown in blue, corresponding to the split SL-RT. This route also corresponds to the highest fuel usage as well. Despite the rural route being an outlier, all urban routes have similar trends with regard to fuel usage and battery capacity usage. Like the BE-RT, the rural route puts the most strain on the vehicle, as the rural route is sometimes three times longer in distance than some urban routes. For each day and payload, the REE-RT was able to successfully service the route, while maintaining a final SOC of above 20%.

Fuel usage from the REE-RT typically ranged from 7 to 13 litres of fuel consumption for urban routes, and 28 to 39 litres for rural routes. The rate of fuel consumption increases as

the operational day progresses, due to the increasing truck payload. The fuel rate has the largest increase during the off-route end-of-day cycle, when the truck is travelling from the collection zone to a transfer station or truck yard under maximum payload for that day.

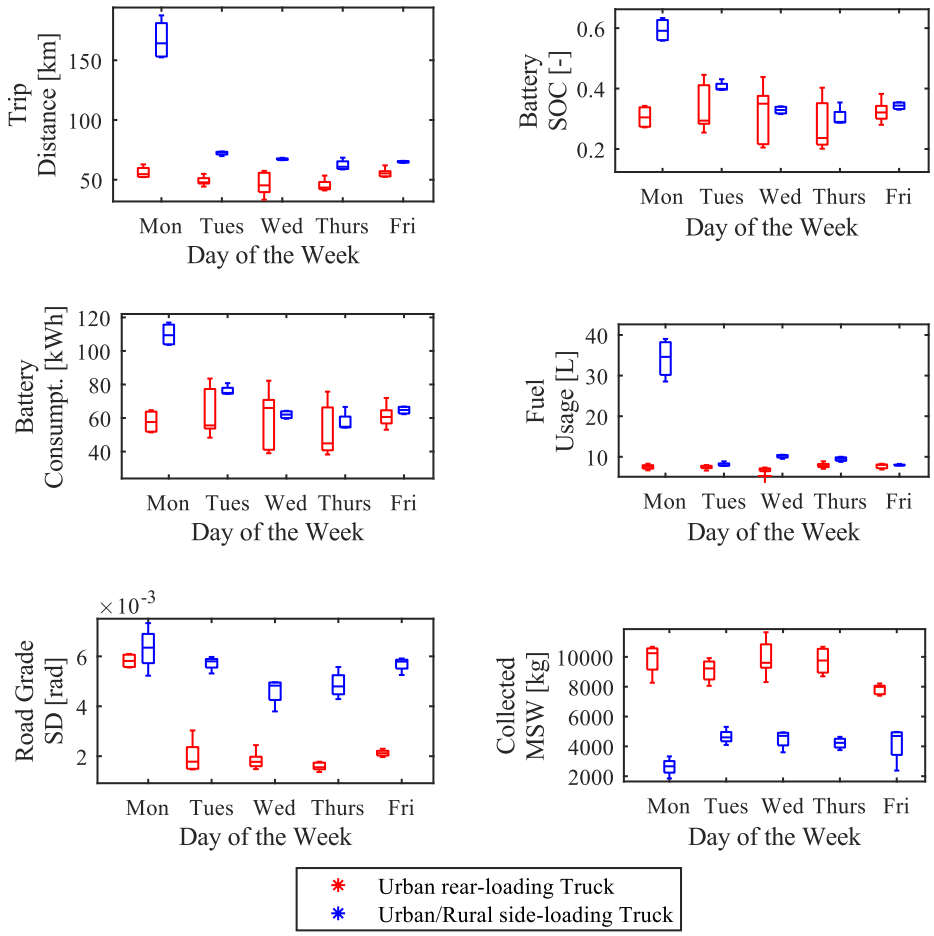

Figure 6.34: Simulation trends from the range extended electric refuse truck model.

6.9 Sources of Error in Modelling

While modelling the powertrains, there were assumptions and sources of error that may contribute to results deviating from their true values. The collected data from the refuse trucks operated during the winter, spring and summer months in Ontario, Canada. This

means the truck was exposed to low temperatures of -20 ºC to high temperatures of +30 ºC. Literature has shown that fuel economies of conventional trucks can change based on weather. For city driving, a gasoline car can have a 15% worse fuel economy in -6 ºC weather compared to 20 ºC weather [90]. The performance of electrified powertrains is also affected by changes in climate. HV batteries exposed to high operating temperatures can lead to faster battery state-of-health decay, whereas colder operating temperatures can lead to a reduction in range and power capabilities [91] [92]. The reduction in power capabilities in colder climates can reduce the amount of regenerative braking that can occur, further exacerbating the reduction in range.

The vehicle software models assumed a constant environmental temperature of 25 ºC and ideal operating temperatures of all internal components. The models operated independent of temperature. This meant that during extreme swings in weather, the actual refuse truck could be significantly affected and lead to higher amounts of fuel usage, whereas the models always operated in ideal scenarios. This introduces a source of error between the powertrain comparisons in chapter 7.

Road grade was approximated using knowledge from the literature and queried elevation data. The elevation data has a horizontal accuracy of 30 m which introduces error into the road grade calculations. Additionally, the smoothing and filtering used to achieve a realistic road grade profile will intermittently remove some data from the grade profiles. This is either from smoothing out noisy profiles or filtering infrequent spikes in data. This ultimately leads to road grade that may not be representative of the true roadway.

Measuring road grade directly requires costly instrumentation and the implementation of such instruments was not included in the scope of this thesis.

The comparison between the actual truck and the models involves comparing the drivers. The driver in the vehicle models are based on a PI controller, whereas the actual truck has a real driver. Given a specific drive cycle, the drivers may react differently and output different torque requests to the vehicle controller for either propelling or braking torque. The comparisons between models assumed that the different drivers operated similarly.

6.10 Summary

To summarize, the methodology for modelling each powertrain has been explained with specific areas of each model explained in detail. Effort was directed towards accurately accounting for a significant portion of energy usage from conventional refuse trucks such as selecting appropriate vehicle parameter and characterizing the truck mass.

Both the BE-RT and REE-RT models were simulated for each studied operational day, with general trends shown for each powertrain. These trends illustrate that both powertrains would be capable of servicing the urban or rural regions of the studied trucks.

Chapter 7

Powertrain Comparison and Emissions

This chapter covers general comparisons between the CAN data collected from the actual refuse trucks versus the modelled powertrains. Comparison metrics include powertrain efficiencies in terms of equivalent fuel economy, payload capacity and emissions. Emissions are quantified in terms of CO_2e and emissions that affect air quality. Finally, the energy costs to run each powertrain are examined for both urban and rural routes.

7.1 Powertrain Efficiency Comparison

The first comparison investigates the fuel economy of each proposed powertrain, compared with the baseline diesel truck, for both the rear and side-loader trucks. This fuel economy takes into account pump-to-wheel (PTW) fuel, meaning only fuel and energy consumed on-board the vehicle will be considered. Because each powertrain has unique energy consumption pathways, an equivalent fuel consumption must be considered. For instance, the fuel consumption of a diesel truck measured in L/100km cannot be directly compared to the energy consumption of an electric vehicle in kWh/100km.

The fuel consumptions of the diesel-powered trucks were used as a baseline to compare other energy consumption units with, in diesel litre equivalence. To convert the energy consumption of an all-electric vehicle to a diesel litre equivalence, the measured direct current (DC) power out at the battery terminals must be calculated first. The total energy consumption (E_{DC}) in Wh can be calculated using Eq. 7.1.

$$E_{DC} = \frac{\Delta T}{3600} * \sum_{i=1}^{N} \left(V_{term}(i) * I_{term}(i) \right) \qquad \text{Eq. 7.1}$$

Where ΔT is the sampling time, V_{term} and I_{term} are the terminal voltage and current of the HV battery. Next, the energy consumption is converted to an electric energy economy (E_M) in Wh/km, by using the route distance in km in Eq. 7.2.

$$E_M = \frac{Route\ Distance}{E_{DC}} \quad \text{Eq. 7.2}$$

To calculate a L_e/100km of diesel fuel, Eq. 7.3 was used in its imperial units of miles per gallon equivalent (MPGe):

$$mpge = \frac{E_D}{E_E * E_M} \quad \text{Eq. 7.3}$$

Where E_D and E_E are the energy content per gallon of diesel fuel or per watt-hour of electricity respectively. E_D is 128,488 Btu/gal and E_E is 3,414 btu/kWh [93]. Once the MPGe is calculated, it can be converted into metric units according to Eq. 7.4:

$$L_e/100km = \frac{235.215}{1\ mpge} \quad \text{Eq. 7.4}$$

For all-electric vehicles, the electrical energy consumption is straight forward to calculate using the previously defined equations. For a hybrid electric vehicle, the blended energy and fuel consumption must be considered. For a series hybrid, the vehicle is always consuming electrical energy while moving, as the engine does not drive the wheels. Intermittently, the engine will turn on to supply supplemental energy to the battery pack, adding a certain amount of fuel costs to the trip. To calculate the fuel economy equivalence for a series hybrid ($REEV_{FCe}$), the fuel consumption of the gasoline engine (HEV_{FC}) must

be converted to the diesel litre equivalent (HEV_{FCe}) first using Eq. 7.5, where the factor in denominator is taken from the literature [94].

$$HEV_{FCe} = \frac{Gasoline\ [L]}{1.155} \quad \text{Eq. 7.5}$$

HEV_{FC} is then added with the equivalent fuel consumption of electrical energy (EV_{FCe}) in diesel litres, shown in Eq. 7.6.

$$REEV_{FCe} = EV_{FCe} + HEV_{FCe} \quad \text{Eq. 7.6}$$

The fuel consumptions of the diesel-RT, BE-RT and REEV-RT are displayed in the following sub-sections.

7.1.1 Conventional Refuse Truck Fuel Economy

The fuel consumptions of the split SL-RT and RL-RT are shown in Figure 7.1. Typically, the fuel economies ranged between 80 – 110 L/100km for urban routes, and 50 – 60 L/100km for rural routes in terms of diesel fuel consumed.

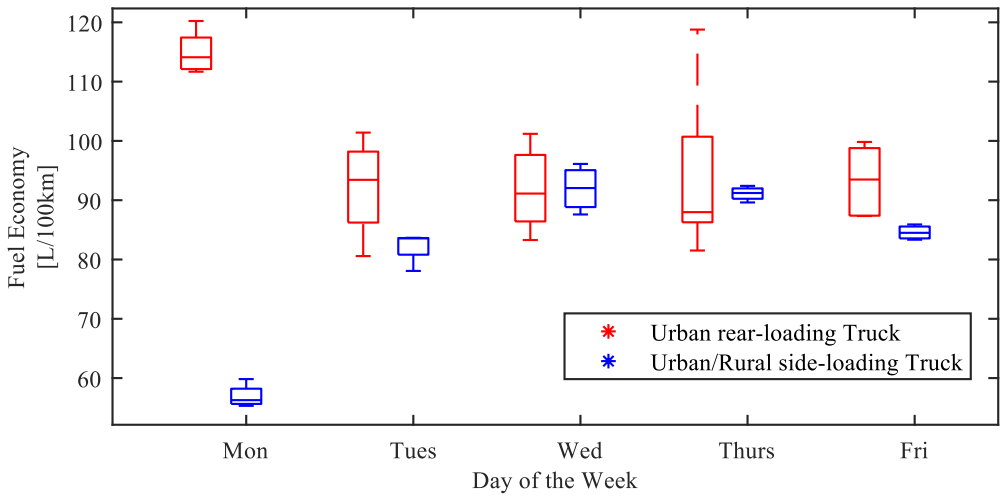

Figure 7.1: The fuel economies of the split side-loading refuse truck and the rear-loading refuse truck. Monday is a rural route, Tuesday – Friday are urban routes.

7.1.2 Battery Electric and Range Extended Refuse Truck Fuel Economy

The equivalent fuel economies in diesel litres for both the BE-RT and REE-RT were calculated on urban and rural routes, shown in Figure 7.2. Overall, the BE-RT had the lowest equivalent fuel economies for both urban and rural routes between 5 – 15 L_e/100km. The REE-RT equivalent fuel economy was comparable across all urban routes ranging from 16 – 24 L_e/100km. The equivalent fuel economy of the REE-RT on rural routes is substantially more than the other powertrains, ranging from 33 – 42 L_e/100km. The reason why the REE-RT consumes much more equivalent fuel on a rural route is primarily due to the long distance of these types of routes. The smaller battery compared to the BE-RT will lose capacity at a higher rate. This leads to the engine being on for a much longer period than the REE-RT operating on urban routes. Despite the high fuel usage for the REE-RT, it is still approximately one third of the diesel fuel consumed by the SL-RT on a rural route.

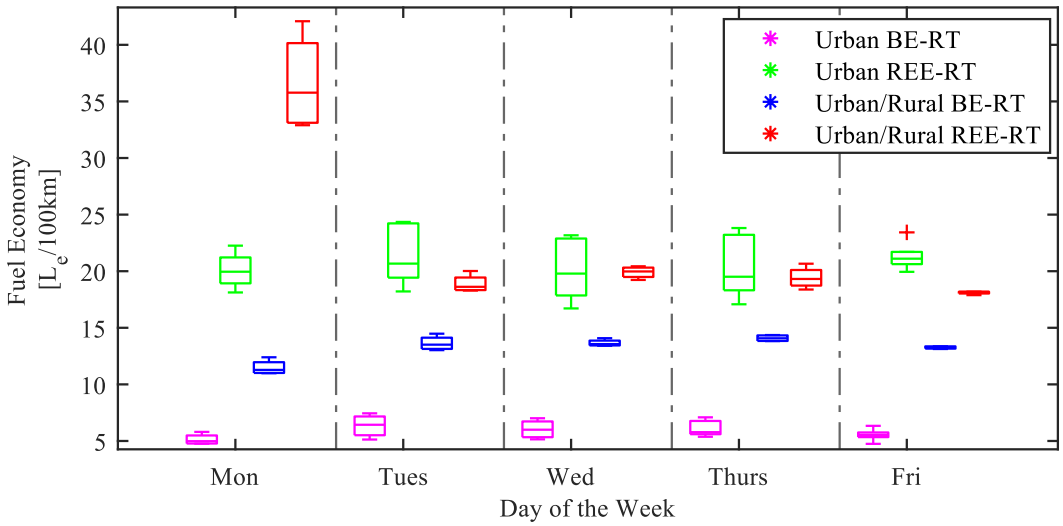

Figure 7.2: The fuel economies of the battery electric and range extended refuse truck powertrains. Monday is a rural route, Tuesday – Friday are urban routes.

7.1.3 Powertrain Payload Capacity

Another aspect of powertrain efficiency is the effectiveness of each powertrain's payload capacity, illustrated in Figure 7.3. The configuration of the RL-RT was used for this comparison, as the RL-RT demanded the highest payloads, reaching maximum values of 12 tonnes. It was found that after adding the HV battery to the BE-RT, while removing the mass of the conventional truck's transmission and engine, could sustain a slightly lower payload of 11.68 tonnes while operating under the truck's GVWR, of 27.2 tonnes.

Due to the low energy density of the REE-RT's battery pack, the pack's mass was approximately 5.3 tonnes. This led to a reduction of the truck's overall payload capacity from 12 tonnes to 8.33 tonnes. This means that the REE-RT would not be able to complete all the urban routes that request a high payload, in a single trip. It will need to make multiple trips on the busiest waste collection days.

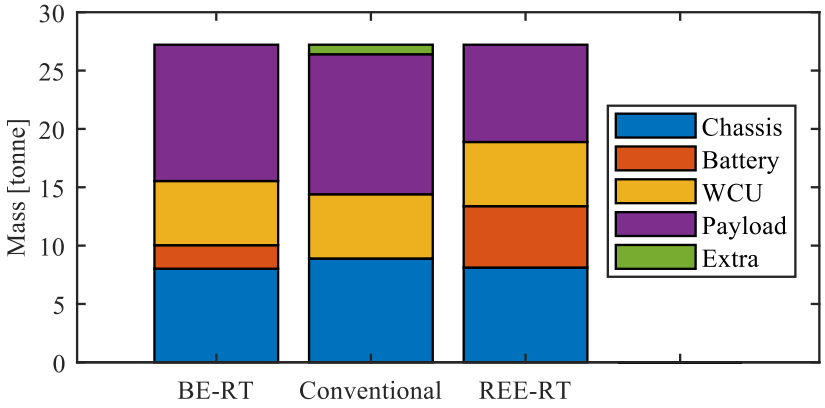

Figure 7.3: A breakdown of the significant mass components of each modelled powertain.

7.2 Powertrain Emission Comparison

Emissions were considered for the urban truck across 5 weeks of operation. The Well-to-Wheel (WTW) emissions are considered for all types of truck powertrain architectures discussed throughout the thesis. WTW includes WTP emissions and represent all emissions associated with the production, processing, distribution and usage in a vehicle [95]. The emissions are calculated using factors from the GREET database on a kg/mile basis. For a conventional refuse truck, diesel, biodiesel and LNG were considered. LNG emissions were approximated using a heavy-duty short-haul truck application, whereas diesel and biodiesel were approximated using a heavy-duty refuse truck application. CNG was not considered for a conventional refuse truck as the emission factors were not available from the database.

Additionally, the WTW emissions associated for the BE-RT are included as well. The associated emissions with electricity production, processing and distribution are based on an energy production mixture in the U.S. Lastly, the WTW emissions associated for a REE-

RT architecture are included with a variety of engine fuels including gasoline, biodiesel, CNG and LNG. For the engines, the emission consumption is based on a light-duty vehicle. This consideration is due to the engine being decoupled from the wheels mechanically and thus having a much smaller engine size compared to the conventional refuse truck.

For the conventional truck and BE-RT, the emission factors are based on a mean urban route distance of 51.9 km and a mean rural route distance of 167.1 km. For the REE-RT refuse truck, the emission factors are based on a blended combination of HEV or EV route travel. For the HEV mode, the truck travelled a mean of 5.6 km and 53.4 km for an urban and rural route respectively. These values are shown in Table 7.1.

Table 7.1: Mean distances for both ranges extended refuse truck operating modes for urban and rural routes.

Type of Powertrain	Mean Distance (km)
Urban Route	51.9
HEV Mode	5.6
Rural Route	167.1
HEV Mode	53.4

The WTW CO_2e emissions and the WTW air quality emissions were investigated for urban and rural routes, for units in kg. The air quality emissions are composed of $PM_{2.5}$, PM_{10}, CO, VOC and SO_x. The air quality emissions were selected based on their impact on lowering air quality based on qualitative knowledge from the literature [96].

More fuel types were considered in the emission analysis, as the emission amount is a function of vehicle trip distance. This means that different fuel types like CNG and LNG can be added to the comparison with little effort. The diesel, biodiesel and LNG HD

represent conventional vehicle architectures that use an engine to move the vehicle, given the fuel type. The gasoline, biodiesel, CNG and LNG REE-RT represent the same vehicle powertrain modelled in chapter 6, with the addition of looking at different fuel types consumed by the engine to extend range. The BE-RT represents an all-electric truck.

Figure 7.4 and Figure 7.5 show emission trends for different powertrains on an urban route. For the REE-RT hybrid architecture, the EMS control scheme primarily favours EV mode and as such the impact of CO_2e emissions from HEV mode are minuscule. It is evident that diesel and biodiesel have the most impactful CO_2e with LNG contributing with the third most CO_2e emissions. The LNG architecture contributes the most methane compared to the other powertrain architectures. The lowest impact on CO_2e was the BE-RT truck, with the REE-RT architectures being comparable as well.

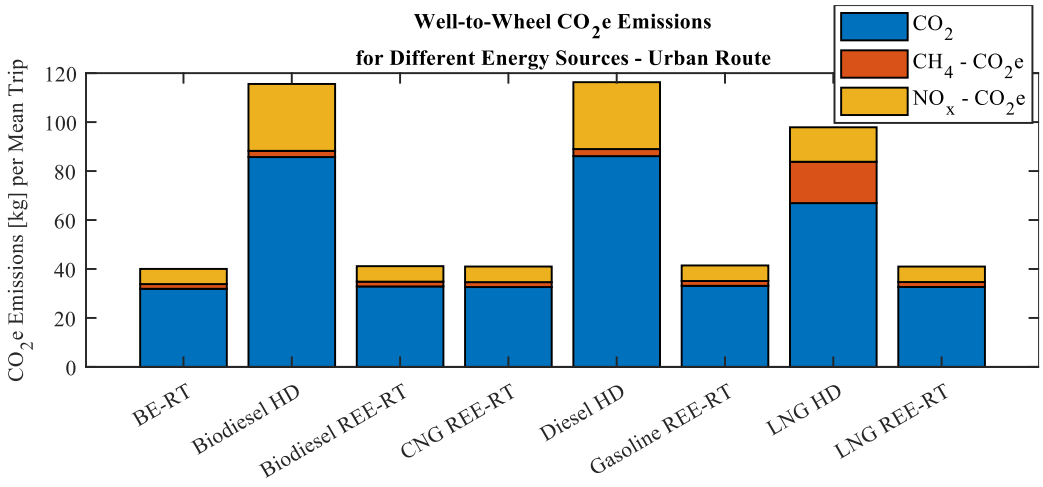

Figure 7.4: Well-to-Wheel CO_2e emissions for each refuse truck powertrain for an urban route.

In terms of air quality, the conventional truck consuming diesel and biodiesel contribute the most to lowering air quality, with the LNG fuel placing third. Similar to the CO_2e trends, the BE-RT and REE-RT powertrains rank in similar amounts of emissions released.

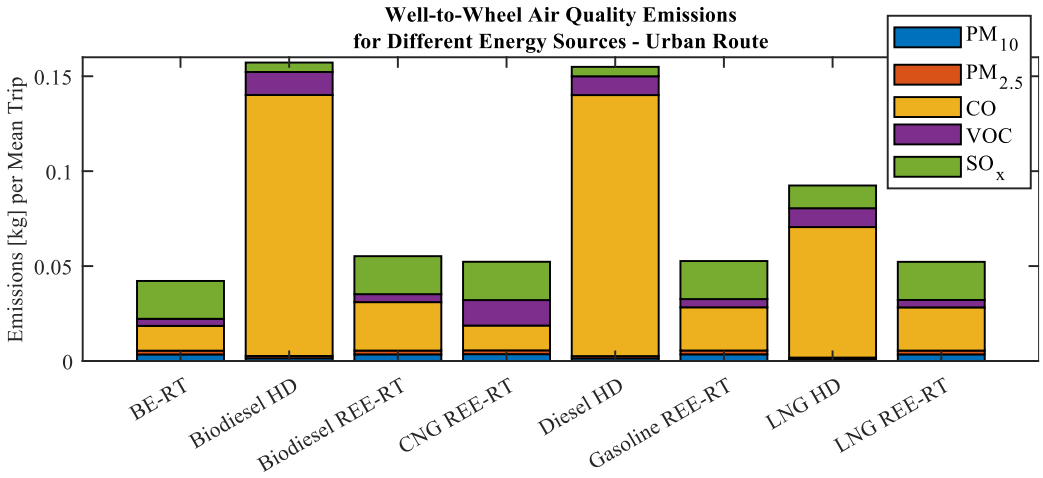

Figure 7.5: Well-to-Wheel air quality emissions for each refuse truck powertrain for an urban route.

Trends similar to the above plots are shown for a rural route as well in Figure 7.6 and Figure 7.7, given each type of powertrain architecture and fuel. The same conclusions can be drawn here as discussed previously with an urban route. Although, the magnitudes of emissions for both CO_2e and air quality are higher for a rural route, given that the truck travels much further distances, sometimes three times as far compared to an urban route in Hamilton.

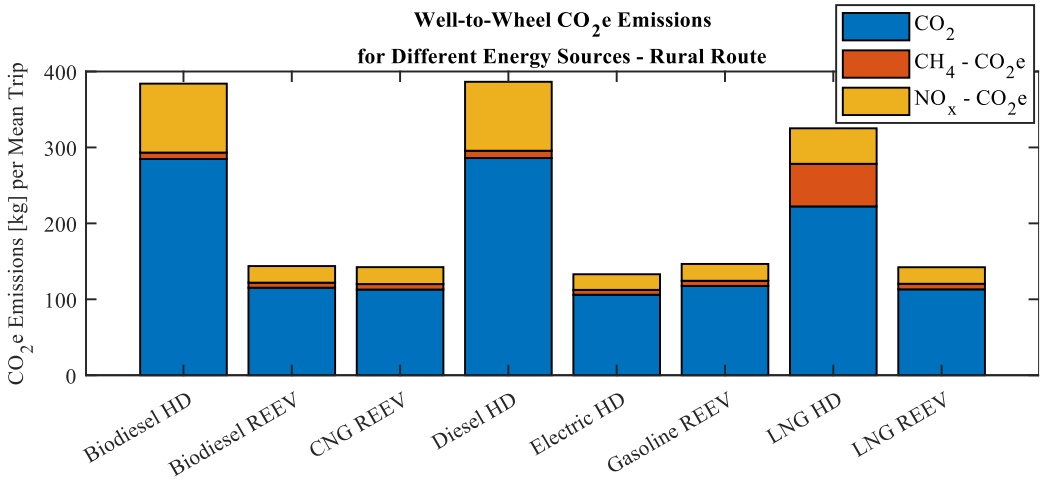

Figure 7.6: Well-to-Wheel CO_2e emissions for each refuse truck powertrain for a rural route.

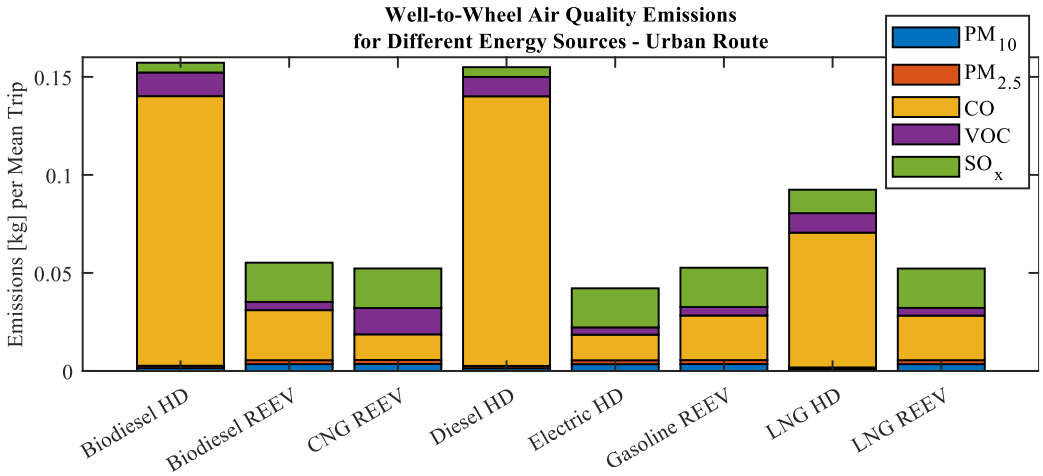

Figure 7.7: Well-to-Wheel air quality emissions for each refuse truck powertrain for a rural route.

7.3 Powertrain Energy Consumption Cost

The cost to supply the required energy in either litres of fuel or kWh of electricity was evaluated for each urban and rural route. As mentioned previously, the conventional powertrain represents the current powertrain technology that the City of Hamilton uses, which are diesel powered refuse trucks. The REE-RT consumes either electricity in EV mode, or electricity and gasoline fuel in HEV mode. The historical prices of gasoline and diesel in Ontario, Canada were averaged from the past two and a half years [97]. An average price of electricity in Ontario was referenced as well [98]. The prices of diesel, gasoline and electricity are displayed in Table 7.2.

Table 7.2: Prices for each respective energy type averaged from January 2020 to July 2022.

Energy Type	Price
Diesel	1.31 CAD/Litre
Gasoline	1.29 CAD/Litre
Electricity	0.13 CAD/kWh

Using the above energy prices, the respective trip cost for each powertrain on both urban and rural routes could be determined. These trends are illustrated below in Figure 7.8.

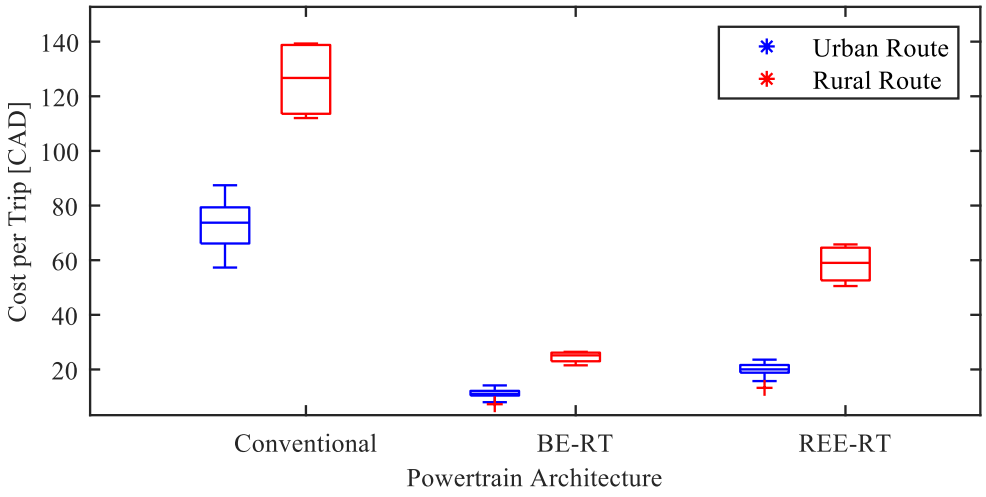

Figure 7.8: Cost per trip for each modelled powertrain, on rural or urban routes.

The conventional trucks than run solely on diesel fuel cost the most per trip, where rural routes are the most expensive. The REE-RT is less than half as expensive than the conventional truck in most cases, primarily due to the lower cost of electricity on a kWh/km basis compared to L/km of diesel fuel. The least expensive modelled powertrain was the BE-RT, where the cost of a rural route, or the most energy intensive route, is comparable to the cost of the REE-RT operating on an urban route. The BE-RT operates at an 80% less energy cost compared to the conventional truck on a rural route, and 86% less energy cost on an urban route.

On a yearly basis, using the averaged energy prices, the prices to operate each type of truck scenario are shown in Table 7.3. The scenario includes a truck that operates on an urban route 5 days a week or a truck that operates on a rural day once a week and the remaining

workdays are urban. The REE-RT was found to save about $13,500 to $14,000 annually per truck in energy usage costs compared to the diesel trucks. The BE-RT was found to save about $16,000 to $18,000 annually per truck in energy costs compared to diesel trucks.

Table 7.3: Yearly energy usage costs for each refuse truck powertrain, on a per truck basis.

Route Type	Urban	Rural / Urban
Day/Week	5	1 / 4
Diesel - $/year	$19,169.80	$21,924.24
REE-RT - $/year	$5,512.00	$7,737.60
BE-RT - $/year	$2,886.00	$3,619.20

7.4 Summary

This chapter covered a quantitative look at how each powertrain might perform in the City of Hamilton. It was found that diesel and biodiesel powered trucks produce the most amount of CO_2e and harmful air quality emissions for both urban and rural routes. LNG shows improvements in the reduction of these emissions. Future work should be done to see how CNG compares to LNG. The emissions from BE-RT slightly less than the REE-RT emissions for most fuel types.

Diesel powered trucks are the most expensive truck to operate on an energy usage basis. REE-RT powertrains are the second most expensive, though around two or more times less expensive than the diesel powertrain. BE-RT had the cheapest energy usage, significantly better than the diesel alternative and better than the REE-RT. The annual savings in energy costs to operate the alternative powertrains compared to diesel trucks are a promising factor to lead municipalities to consider purchasing new types of refuse truck technology to save in energy costs compounded over their entire truck fleet.

Chapter 8

Conclusions, Future Work and Publications

8.1 Summary of Work

The work described was completed over a span of 16 months. From the initial idea of using refuse trucks as an application, to the beginning of the research collaboration with the City of Hamilton's waste division, a wide range of topics have been investigated and evaluated.

The initial idea of electrifying refuse trucks came into conception by the natural characteristics of its route. Similar to delivery vehicles, these trucks operate on predetermined routes and return back-to-base at the end of the day. Additionally, these trucks are heavy polluters from both a GHG and local air quality point of view. Lastly, literature on vehicle electrification is heavily weighted towards consumer level vehicles and higher performance vehicles, where gaps in literature exist for heavy-duty vehicles. Even more gaps in literature are present for heavy-duty vehicles that utilize additional functionality such as refuse trucks, cranes, dump trucks and more.

To address the underrepresented heavy-duty trucks in vehicle electrification, a comprehensive study was focused on refuse trucks to shed light on what is required to electrify them, and how that might compare to what is currently available to customers. The creation of thesis follows the series of events involved with answering these comparative questions and the objectives stated in chapter one.

A review on current refuse truck technology and state-of-the-art refuse technology was completed to provide a foundation for innovative ideas to stem from. A solution to the underrepresented literature and open-source GPS and CAN data surrounding refuse trucks was addressed by collaborating with a municipality to use a purchased data logger in their

refuse truck fleet. Next, the process of decoding and organizing this data into useful is explained. Once decoded, the CAN and GPS data can be used to quantify the refuse truck's environment inside a software vehicle model. Here, various vehicle powertrains can be explored in terms of how they handle the loads, speeds and trip length that a refuse truck must meet to serve the City of Hamilton. Notably, the alternative powertrains that were explored were an all-electric vehicle and range extended hybrid vehicle.

Data from many operational days was captured, allowing the vehicle models to be simulated in many different environments to see the robustness of the component sizes and EMS control strategies. The control strategy for the REE-RT benefited the most from this, as the control strategy has many more layers of complexity over the BE-RT vehicle.

Overall, the scope of the thesis was outlined in chapter one and the process involved in answering questions posed by this thesis were answered.

8.2 Conclusions

A literature review on the current state of technology and state of the art trends provided a foundation of where refuse truck powertrain technology currently is and where it might be headed in the future. These trends were used in the latter chapters to assist in building a narrative on how refuse trucks in the City of Hamilton may function in the near and far future. The data collected from the truck's CAN port and GPS antenna paired with data processing techniques showed that information on the truck's hydraulic loading could be extracted without the need for invasive devices such as pressure transducers, speed or torque sensors. The accuracy of the extracted CAN signals was assumed to be accurate but

comparisons to the actual loads should be considered. As for example, the CAN data was used to extract engine torque, engine speed and the PTO activation switch, to approximate the additional loading that the hydraulic pump has on the engine. This approximation should be compared with data collected from pressure transducers installed in the hydraulic circuit of the truck, to verify that the loading on the engine from the collected CAN data is correct.

Drive and duty cycles reflective of refuse truck operation in the City of Hamilton have been created for each day that data was logged for. This creates many environments that the vehicle software models can be exposed to, leading to more robust results with respect to energy consumption and power requirements.

Simulating the BE-RT and REE-RT with the given drive and duty cycles yielded promising results compared to a diesel truck. Each electrified powertrain alternative was able to complete the routes outlined by the cycles defined in chapter 5, indicating that these types of trucks could be used by the city. Due to the low energy density of the REE-RT HV battery, the REE-RT has a reduced payload capacity compared to the BE-RT and conventional vehicle.

Rural routes lead to the most energy consumed by the powertrains, due to longer periods of higher traveling speeds and longer route distances. This type of route provides the most barriers for an electrified powertrain to replace the conventional trucks, due to the lack of energy density available in electrified ESS's. The REE-RT can utilize an onboard engine to extend the HV battery's range, whereas the BE-RT must have a large HV battery pack as the observed battery energy consumption surpassed 120 kWh. Fuel cells acting as a

range extender may offer a better solution to more energy intensive routes such as rural routes.

Rural areas also require a lesser load on truck payload capacity. This leads to possible optimization to be done to use smaller trucks, or move to a bi-weekly pickup schedule, depending on the waste collection requirements of individual regions.

Urban routes are typically closer to the truck yard and have much shorter route distances than rural routes, up to three times as short. These routes offer great opportunities for electrified powertrain alternatives to replace diesel powered trucks. If a range extender is preferred, an engine configured to consume a favourable fuel could be configured. Municipalities are beginning to use different fuels for their heavy-duty truck fleets including busses and refuse trucks. These fuels are typically natural gas in either gaseous or liquefied form.

Both the BE-RT and REE-RT benefit from the low and steady cost of electricity, compared to the rising and volatile costs of diesel fuel in recent years. Using BE-RT and REE-RT architectures allows adaptation of further innovation in WTP efficiencies and emissions. If electricity generation can be made more sustainable in Ontario, refuse trucks powered partially or solely be electricity will amplify these sustainability efforts.

8.3 Future Work

Through the process of writing this thesis and observing insightful directions of refuse truck technology, future work could be focused in numerous promising areas. A trend with refuse trucks or other heavy-duty vehicles is the barrier to entry for powertrain

electrification due to the energy density constraints on battery cell technology. To address this issue, a range extender refuse truck was explored that has gasoline fuel on-board to supplement the energy usage from the HV battery. This powertrain proved to handle most of the drive and duty cycles, though with the heavier payloads the vehicle's mass would surpass the limits that the chassis can support. Future work could be done to investigate how alternative fuels would perform in the range extender such as CNG or LNG.

Also, a powertrain with an ESS composed of a fuel cell and HV battery could be explored. The powertrain architecture of the REE-RT allows for multiple solutions to supply supplemental energy to the HV battery. A REE-RT is not constrained to solely a diesel engine, the engine could use alternative fuels or be swapped with a fuel cell system instead. Key findings would include how much payload the truck could still support given these powertrain changes. A more energy dense HV battery cell could be considered, as the battery pack accounts for a significant amount of mass added to the chassis.

Since the HV battery capacity was sized to meet the demands of a rural route, the HV battery was found to be oversized for urban routes. Optimizing a refuse truck for an urban route is an area to explore as this would allow a smaller HV battery to be used, allowing a higher payload potential to be considered.

All vehicle software models were temperature independent and assumed to have an operating ambient temperature of 25 ºC. The studied refuse trucks operated in an ambient temperature range of -20 ºC to +30 ºC. Future work could involve making the vehicle software models temperature dependent, allowing for a more accurate energy analysis assessment.

It was assumed that the CAN data from the truck was accurate, as the data comes from on-board sensors or in-house calibration tables from the control units on-board the truck, such as the engine control unit or the transmission control unit. To verify how accurate the data and derivatives of the collected data such as stop estimation, road grade and hydraulic loading on the engine, work to install sensors to accurately measure these metrics should be completed. This will allow a comparative analysis to be done, verifying whether the techniques used to create the drive and duty cycles using CAN data are representative of the actual loads the truck experiences.

8.4 Publications

1. **J. Toller**, A. Biswas and A. Emadi, "The Development of a Drive and Duty Cycle for a Refuse Truck in the City of Hamilton using Non-Invasive Sensors", in 2022 IEEE/AIAA Transportation Electrification Conference and Electric Aircraft Technologies Symposium (ITEC+EATS), pp. 249 - 254, July 2022.
2. P. Anselma, A. Biswas, A. Rathore, Y. Wang, **J. Toller**, and J. Roeleveld, "A Computationally Lightweight Dynamic Programming Formulation for Hybrid Electric Vehicles", in SAE International, March 2022.
3. Y. Wang, P. Anselma, A. Biswas, A. Rathore, **J. Toller**, et.al., "Adaptive Real-Time Energy Management of a Multi-Mode Hybrid Electric Powertrain", in SAE International, March 2022.

4. A. Biswas, O. Rane, A. Rathore, P. Anselma, Y. Wang, **J. Toller**, et.al., “Energy Management System for Input-Split Hybrid Electric Vehicle (Si-EVT) with Dynamic Coordinated Control and Mode-Transition Loss”, in SAE International, March 2022.

References

[1] "HEIL Bodies," [Online]. Available: https://www.heil.com/. [Accessed 8 October 2021].

[2] R. H. Haunton, "Heart of the Valley: A History of Knoxville, Tennessee," *Journal of American History,* vol. 64, no. 4, pp. 1128-1129, 1979.

[3] "Garwood Load Packer," Internet Archive, [Online]. Available: https://web.archive.org/web/20181216095735/http://www.tigerdude.com/garbage/rearload/garwood/loadpacker.html. [Accessed 20 June 2022].

[4] Government of Canada, "Municipal solid waste: a shared responsibility," Enviroment and Natural Resources, [Online]. Available: https://www.canada.ca/en/environment-climate-change/services/managing-reducing-waste/municipal-solid/shared-responsibility.html.

[5] L. Wiginton, C. Smith, M. Ewing and G. Battista, "Fuel savings and emissions reductions in heavy-duty trucking: A blueprint for fruther action in Canada," *Pembina Institute,* 2019.

[6] O. Wysocki, T. Zajdzinski and J. Kropiwnicki, "Evaluation of the efficiency of the duty cycle of refuse collection vehicle based on real-world data," *International Automotive Conference,* 2018.

[7] N. Dembski, G. Rizzoni, A. Soliman, J. Fravert and K. Kelly, "Development of Refuse Vehicle Driving and Duty Cycles," *SAE World Congress & Exhibition,* 2005.

[8] J. Toller, A. Biswas and A. Emadi, "The Development of a Drive and Duty Cycle for a Refuse Truck in the City of Hamilton using Non-Invasive Sensors," *2022 IEEE Transportation Electrification Conference & Expo (ITEC),* pp. 249-254, 2022.

[9] C. Chalkias and K. Lasaridi, "Optimizing municipal solid waste collection using GIS," *Energy, Environment, Ecosystems, Development and Landscape Architecture,* pp. 45-50, 2009.

[10] "Waste Generation," The Conference Board of Canada, 2012. [Online]. Available: https://www.conferenceboard.ca/hcp/provincial/environment/waste.aspx.

[11] Environment Canada, "Canadian Environmental Protection Act, 1999," Canada Gazette, 3 March 2013. [Online]. Available: https://canadagazette.gc.ca/rp-pr/p2/2013/2013-03-13/html/sor-dors24-eng.html.

[12] Freightliner, "108SD," Freightliner, 2021. [Online]. Available: https://freightliner.com/trucks/108sd/.

[13] Natural Resources of Canada, "Energy Use Data Handbook Tables," Government of Canada, 2018.

[14] Canadian Environmental Protection Act Registry, "Discussion paper on heavy-duty vehicles and engines in Canada: transitioning to a zero-emission future," Government of Canada, December 2021. [Online]. Available: https://www.canada.ca/en/environment-climate-change/services/canadian-environmental-protection-act-registry/heavy-duty-vehicle-engines-zero-emission-future-discussion-paper.html.

[15] Statistics Canada, "More vehicles on the road in 2019," 10 September 2019. [Online]. Available: https://www150.statcan.gc.ca/n1/daily-quotidien/200910/dq200910d-eng.htm.

[16] S. Gurdas S., F. H. Christopher, B.-H. Shannon and J. Elizabeth, "In-use activity, fuel use, and emissions of heavy-duty diesel roll-off refuse trucks," *Air & Waste Management Association,* vol. III, no. 65, pp. 306-323, 2015.

[17] Parker, "PowerShift (Hydraulic) 10-Bolt Power Take-Off (PTO) - 280 Series," [Online]. Available: https://ph.parker.com/us/en/280-series-powershift-hydraulic-10-bolt-power-take-off-pto. [Accessed 13 July 2022].

[18] United Nations Human Settlements Programme (UN-Habitat), Collection of Municipal Solid Waste in Developing Countries, Malta: Gutenberg Press, 2010.

[19] U.S. Environmental Protection Agency, Office of Resource Conservation and Recovery, "Volume-to-Weight Conversion Factors," April 2016. [Online]. Available: https://www.epa.gov/sites/default/files/2016-04/documents/volume_to_weight_conversion_factors_memorandum_04192016_508fnl.pdf.

[20] Dillon Consulting, "City of Hamilton - Collection Route Review - Route Optimization," Kitchener, 2021.

[21] S. Gurdas S., F. H. Christopher, B.-H. Shannon and J. Elizabeth, "In-use measurement of the activity, fuel use, and emissions of front-loader refuse trucks," *Atmospheric Environment,* no. 92, pp. 557-565, 2014.

[22] S. Gurdas, F. Christopher, B.-H. Shannon and J. Elizabeth, "Real-world activity, fuel use, and emissions of diesel side-loader refuse trucks," *Atmospheric Environment,* vol. 129, pp. 98-104, 2016.

[23] Galbreath, "Hoists, Container Handlers & Trailers," [Online]. Available: https://www.galbreathproducts.com/. [Accessed 3 July 2022].

[24] Energy Efficiency & Renewable Energy, "Alternative Fuels Data Center," U.S. Department of Energy, [Online]. Available: https://afdc.energy.gov/fuels/. [Accessed 23 June 2022].

[25] "Compressed Natural Gas (CNG)," Unitrove, [Online]. Available: https://www.unitrove.com/engineering/gas-technology. [Accessed 23 June 2022].

[26] A. Soukhov and M. Mohamed, "Occupancy and GHG emissions: thresholds for disruptive transportation modes and emerging technologies," *Transportation Research Part D,* 2022.

[27] M. Brander, "Greenhouse Gases, CO2, CO2e, and Carbon: What Do All These Terms Mean?," August 2012. [Online]. Available:

https://ecometrica.com/assets/GHGs-CO2-CO2e-and-Carbon-What-Do-These-Mean-v2.1.pdf.

[28] "Greenhouse Gas Emissions," United States Environmental Protection Agency, 2020. [Online]. Available: https://www.epa.gov/ghgemissions/overview-greenhouse-gases.

[29] "Greenhouse Gas (GHG) Emissions and Removals," United States of Environmental Protection Agency, [Online]. Available: https://www.epa.gov/ghgemissions. [Accessed 5 July 2022].

[30] "Climate Change Indicators: Greenhouse Gases," United States Environmental Protection Agency, [Online]. Available: https://www.epa.gov/climate-indicators/greenhouse-gases. [Accessed 5 07 2022].

[31] "Global Warming Potential Values," Greenhouse Gas Protocol, 2014.

[32] "GREET Model 2021," Argonne National Laboratory, [Online]. Available: https://greet.es.anl.gov/. [Accessed 23 6 2022].

[33] G. S. Sandhu, C. H. Frey, S. Bartelt-Hunt and E. Jones, "Real-world activity, fuel use, and emissions of heavy-duty compressed natural gas refuse trucks," *Science of the Total Environment,* no. 761, 2021.

[34] "EPA Emission Standards for Heavy-Duty Highway Engines and Vehicles," United States Environmental Protection Agency, [Online]. Available: https://www.epa.gov/emission-standards-reference-guide/epa-emission-standards-heavy-duty-highway-engines-and-vehicles. [Accessed 24 06 2022].

[35] National Renewable Energy Laboratory, "Project Startup: Evaluating the Performance of Hydraulic Hybrid Refuse Vehicles," September 2015. [Online]. Available: https://www.nrel.gov/docs/fy15osti/65013.pdf.

[36] MACK, "MACK LR Electric," 2022. [Online]. Available: https://images.info.macktrucks.com/Web/MackTrucks/%7B70ffbb1f-513b-4bda-

9fd5-ffab07279d60%7D_Mack_Electric_LR_SellSheet_0222_web.pdf. [Accessed 10 July 2022].

[37] MACK Trucks, “Mack Trucks Introduces Next Generation Mack LR Electric with Improved Range and Capacity,” Cision PR Newsire, 3 March 2022. [Online]. Available: https://www.prnewswire.com/news-releases/mack-trucks-introduces-next-generation-mack-lr-electric-with-improved-range-and-capacity-301495195.html.

[38] MACK, “LR Electric,” [Online]. Available: https://www.macktrucks.com/trucks/lr-electric/specs/. [Accessed 2 2022 April].

[39] Lion, “Urban Class 6 & 8 Trucks,” Lion, [Online]. Available: https://thelionelectric.com/en/products/electric_truck_class8.

[40] J. Rory, “Lion8 refuse truck,” E-Mobility Engineering, [Online]. Available: https://www.emobility-engineering.com/lion8-refuse-truck/.

[41] A. Deshpande, D. Nagaraj, G. Varma, M. Narendrakumar and V. Vishnu, “Simulation of Conventional and Series Hybrid Electric Refuse Collection Truck using ADVISOR,” *Academia,* 1999.

[42] Wrightspeed, “ROUTE™ POWERTRAIN,” Wrightspeed, [Online]. Available: https://www.wrightspeed.com/the-route-powertrain.

[43] P. Kelly-Detwiler, “Electric Garbage Trucks: Huge Energy Savings And They Won't Wake You Up In The Morning,” Forbes, 4 March 2015. [Online]. Available: https://www.forbes.com/sites/peterdetwiler/2015/03/04/electric-garbage-trucks-huge-energy-savings-and-they-wont-wake-you-up-in-the-morning/?sh=1c1e3aee6368.

[44] J. Hitch, “Stealthy Wrightspeed ready to make noise in refuse,” FleetOwner, 19 May 2021. [Online]. Available: https://www.fleetowner.com/emissions-efficiency/article/21164594/stealthy-wrightspeed-ready-to-make-noise-in-refuse.

[45] M. Masih-Tehrani, M.-R. Ha'iri-Yazdi, V. Esfahanian and A. Safaei, "Optimum sizing and optimum energy management of a hybrid energy storage system for lithium battery life improvement," *Power Sources,* 2013.

[46] P. G. Anselma, P. Kollmeyerc, J. Lempertc, Z. Zhaoc, G. Belingardia and A. Emadi, "Battery state-of-health sensitive energy management of hybrid electric vehicles: Lifetime prediction and ageing experimental validation," *Applied Energy,* 2021.

[47] J. M. Miller, P. J. McCleer, M. Everett and E. G. Strangas, "Ultracapacitor Plus Battery Energy Storage System Sizing Methodology for HEV Power Split Electronic CVT's," *IEEE International Symposium on Industrial Electronics,* 2005.

[48] J. M. Miller and . Sartorelli, "Battery and ultracapacitor combinations—Where should the converter go?," *IEEE Vehicle Power and Propulsion Conference (VPPC),* 2010.

[49] A. W. tienecker and C. A. T. Stuart, "A combined ultracapacitor-lead acid battery storage system for mild hybrid electric vehicles.," *IEEE Vehicle Power and Propulsion Conference,* 2005.

[50] M.-E. Choi, S.-W. Kim and S.-W. Seo, "Energy Management Optimizationin a Battery/Supercapacitor HybridEnergy Storage System," *IEEE TRANSACTIONS ON SMART GRID,* vol. 3, no. 1, pp. 463 - 472, 2012.

[51] J. Sen, "Energy Management Of A Battery-Ultracapacitor Hybrid Energy Storage System In Electric Vehicles," *Department of Electrical and Computer Engineering,* 2016.

[52] J. Bauman, "ECE 724 Class Slides," McMaster University, 2021.

[53] B. Andrew and M. Marshall, "Performance Characteristics of Lithium-ion Batteries of Various Chemistries for Plug-in Hybrid Vehicles," *UC Davis Institute of Transportation Studies,* 2009.

[54] T. Nemeth, P. J. Kollmeyer, A. Emadi and D. U. Sauer, “Optimized Operation of a Hybrid Energy StorageSystem with LTO Batteries for High PowerElectrified Vehicles,” *IEEE Transportation Electrification Conference,* 2019.

[55] F. G. J. G. H. El Fadil, “Lyapunov Based Control of Hybrid Energy Storage System in Electric Vehicles,” in *2012 American Control Conference*, Montreal, Canada, 2012.

[56] P. Kollmeyer, C. Vidal, M. Naguib and M. Skells, “LG 18650HG2 Li-ion Battery Data and Example Deep Neural Network xEV SOC Estimator Script,” Mendeley Data, 5 05 2020. [Online]. Available: https://data.mendeley.com/datasets/cp3473x7xv/3. [Accessed 13 04 2022].

[57] W. Liu, Hybrid Electric Vehicle System Modeling and Control, John and Wiley Sons, 2017.

[58] X. Yu, N. S. Sandhu, Z. Yang and M. Zheng, “Suitability of energy sources for automotive application – A review,” *Applied Energy,* vol. 271, 2020.

[59] H. Xuebing, O. Minggao, L. Languang, L. Jianqiu, Z. Yuejiu and L. Zhe, “A comparative study of commercial lithium-ion battery cycle life in electrical vehicle: Aging mechanism identification,” *Journal of Power Sources,* vol. 251, pp. 38-54, 2014.

[60] Jelly Bros., “https://www.jellybrothers.com/products/hamilton-municipalities,” [Online]. Available: https://www.jellybrothers.com/products/hamilton-municipalities. [Accessed 6 June 2022].

[61] CSS Electronics, “CAN Bus Data Loggers,” [Online]. Available: https://www.csselectronics.com/.

[62] CSS Electronics, “CANedge2 Intro and Tools,” 8 2022 June. [Online]. Available: https://canlogger.csselectronics.com/canedge-getting-started/CANedge2Intro.pdf. [Accessed 27 June 2022].

[63] SAE International, “SAE J1939 Standards Collection on the Web: Content,” [Online]. Available: https://www.sae.org/standardsdev/groundvehicle/j1939a.htm.

[64] S. Mahmud, “CAN Extended Format and CAN FD (Flexible Data Rate),” 2018. [Online]. Available: http://webpages.eng.wayne.edu/~ad5781/ECECourses/ECE5620/Notes/CAN_Extended_CAN-FD.pdf.

[65] J. Hua, Z. Songb, J. Lia, Z. Hua, L. Xua and M. Ouyanga, “Energy Management of a Dual-engine System for Hybrid Heavy-duty Vehicles,” *IEEE Transportation Electrification Conference and Expo (ITEC),* 2019.

[66] D. B. Gesch, M. J. Oimoen and G. A. Evans, “Accuracy Assessment of the U.S. Geological Survey National Elevation Dataset, and Comparison with Other Large-Area Elevation Datasets—SRTM and ASTER,” 2014. [Online]. Available: https://pubs.usgs.gov/of/2014/1008/pdf/ofr2014-1008.pdf.

[67] Adam Schneider, “GPS Visualizer,” 2019. [Online]. Available: https://www.gpsvisualizer.com/.

[68] Samuel Pfrommer, “Terrain Elevation,” GitHub, 2022. [Online]. Available: https://github.com/spfrommer/terrain-elevation/releases/tag/v1.1.3. [Accessed 3 July 2022].

[69] “NREL DriveCAT - Chassis Dynamometer Drive Cycles,” Laboratory, National Renewable Energy, 2021. [Online]. Available: www.nrel.gov/transportation/drive-cycle-tool.

[70] M. Jaunich, J. Levis, J. Decarolis and E. Gaston, “Characterization of Municipal Solid Waste Collection Operations,” *Resources, Conservation and Recycling,* vol. 114, pp. 92-102, 2016.

[71] E. Wood, E. Burton, A. Duran and J. Gonder, “Appending High-Resolution Elevation Data to GPS Speed Traces for Vehicle Energy Modeling and Simulation,” June 2014. [Online]. Available: https://www.nrel.gov/docs/fy14osti/61109.pdf.

[72] Excel Truck Group, “Freightliner 108SD,” 13 February 2020. [Online]. Available: http://ncsheriffs.org/Bid%2021-05-

0506/Draft%20Bid%20Package/Equipment%20Additions/Excel%20Truck%20Group/FREIGHTLINER%20108SD%20DD8%20DETROIT%20ENGINE.pdf. [Accessed 14 05 2022].

[73] L. S. Mojtaba, An examination of heavy-duty trucks drivetrain options to reduce GHG emissions in British Columbia, Victoria: University of Victoria, 2020.

[74] "MOVES2010 Highway Vehicle Population and Activity Data," November 2010. [Online]. Available: https://cfpub.epa.gov/si/si_public_file_download.cfm?downloadID=504596.

[75] I. Kulikov, A. Kozlov, A. Terenchenko and K. Karpukhin, "Comparative Study of Powertrain Hybridization for Heavy-Duty Vehicles Equipped with Diesel and Gas Engines," *Energies,* pp. 1-23, 2020.

[76] N. PETTERSSON and K. H. JOHANSSON, "Modelling and control of auxiliary loads in heavy vehicles," *International Journal of Control,* vol. 79, no. 5, pp. 479-495, 2006.

[77] Idaho National Laboratory, "EV Auxiliary Systems Impacts," [Online]. Available: https://avt.inl.gov/sites/default/files/pdf/fsev/auxiliary.pdf. [Accessed 8 July 2022].

[78] Enivronment Canada, "Technical Document on Municipal Solid Waste Organics Processing," 2013. [Online]. Available: https://www.ec.gc.ca/gdd-mw/3E8CF6C7-F214-4BA2-A1A3-163978EE9D6E/13-047-ID-458-PDF_accessible_ANG_R2-reduced%20size.pdf. [Accessed 20 April 2022].

[79] DieselIQ, "8.3 Cummins Engine," 15 April 2021. [Online]. Available: https://dieseliq.com/8-3-cummins-diesel-engine-problems-reliability-specs/.

[80] Allison Transmission, "3000/3200 Seriees," [Online]. Available: https://www.allisontransmission.com/docs/default-source/specification-sheets/int3000_sa5341(201306)blk.pdf?sfvrsn=2. [Accessed 2022 22 April].

[81] "FREIGHTLINER FUEL TANK 48 GALLON MILGRADE," FleetTruckParts, [Online]. Available: https://www.fleettruckparts.com/Freightliner-Fuel-Tank-48-

Gallon-Milgrade-Aluminum-18-x-18-x-38-Passenger-Side-by-Alumitank. [Accessed 19 May 2022].

[82] Equipmake, "HTM-3500," [Online]. Available: https://equipmake.co.uk/products/htm-3500/. [Accessed 30 05 2022].

[83] Equipmake, "HPI-800," [Online]. Available: https://equipmake.co.uk/products/hpi-800/. [Accessed 30 05 2022].

[84] C. Hoffman, "2022 GMC Hummer EV EPA Documents Reveal MPGe, Weight, Other Details," Car and Driver, 15 February 2022. [Online]. Available: https://www.caranddriver.com/news/a39049358/2022-gmc-hummer-ev-pickup-epa-specs/.

[85] M. Stuhldreher, J. Kargul, D. Barba, J. McDonald and e. al., "Benchmarking a 2016 Honda Civic 1.5-Liter L15B7 Turbocharged Engine and Evaluating the Future Efciency Potential of Turbocharged Engines," *SAE International,* pp. 1-34, 2018.

[86] "GM 1.4 Liter I4 Ecotec L2Z Engine," GM Authority, [Online]. Available: https://gmauthority.com/blog/gm/gm-engines/l2z/. [Accessed 20 June 2022].

[87] Siemens, "Simcenter Amesim," [Online]. Available: https://www.plm.automation.siemens.com/global/en/products/simcenter/simcenter-amesim.html. [Accessed 8 July 2022].

[88] J. Lempert, B. Vadala, K. Arshad-Aliy, J. Roeleveld and A. Emadi, "Practical Considerations for the Implementation of Dynamic Programming for HEV Powertrains," *2018 IEEE Transportation Electrification Conference and Expo (ITEC),* pp. 755-760, 2018.

[89] F. Miretti, D. Misul and E. Spessa, "DynaProg: Deterministic Dynamic Programming solver for finite horizon multi-stage decision problems," *Spessa,* vol. 14, SoftwareX.

[90] Office of Energy Efficiency and Renewable Energy, "Fuel Economy in Cold Weather," United States Department of Energy, [Online]. Available: https://www.fueleconomy.gov/feg/coldweather.shtml#:~:text=Cold%20weather%

20and%20winter%20driving,to%204%2Dmile)%20trips.. [Accessed 13 June 2022].

[91] D. Jie, C. Bae, A. Denlinger and T. Miller, "Electric Vehicles Batteries: Requirements and Challenges," *Joule,* vol. 4, no. 3, pp. 511-515, 2020.

[92] G. Zhang, S. Ge, X. Yang and Y. Leng, "Rapid restoration of electric vehicle battery performance while driving at cold temperatures," *Journal of Power Sources,* vol. 371, pp. 35-40, 2017.

[93] U.S. Department of Energy, "Fuel Properties Comparison," [Online]. Available: https://afdc.energy.gov/fuels/properties. [Accessed 14 July 2022].

[94] "Fuel Conversion Factors to Gasoline Gallon Equivalents," United States Department of Energy, [Online]. Available: https://epact.energy.gov/fuel-conversion-factors. [Accessed 25 08 2022].

[95] Energy Efficiency & Renewable Energy, "Alternative Fuels Data Center," U.S. Department of Energy, [Online]. Available: https://afdc.energy.gov/vehicles/electric_emissions.html. [Accessed 5 July 2022].

[96] "Progress Cleaning the Air and Improving People's Health," United States Environmental Protection Agency, [Online]. Available: https://www.epa.gov/clean-air-act-overview/progress-cleaning-air-and-improving-peoples-health#:~:text=Clean%20Air%20Act%20programs%20have,the%20six%20common%20pollutants%20(PM2.. [Accessed 1 08 2022].

[97] Government of Canada, "Transportation fuel prices," [Online]. Available: https://www.nrcan.gc.ca/our-natural-resources/domestic-and-international-markets/transportation-fuel-prices/4593. [Accessed 15 07 2022].

[98] Energy Hub, "Electricity Prices in Canada 2021," [Online]. Available: https://www.energyhub.org/electricity-prices/. [Accessed 15 July 2022].